Nano-Micro Letters

e-ISSN 2150-5551
CN 31-2103/TB

REVIEW

https://doi.org/10.1007/s40820-024-01430-4

MXene Key Composites: A New Arena for Gas Sensors

Yitong Wang[1], Yuhua Wang[1] ✉, Min Jian[1], Qinting Jiang[2], Xifei Li[2,3] ✉

Cite as
Nano-Micro Lett.
(2024) 16:209

Received: 10 March 2024
Accepted: 22 April 2024
© The Author(s) 2024

HIGHLIGHTS

- With its layered structure, abundant functional groups, and excellent electrical conductivity, MXene is of great research interest in the field of gas sensing.
- The preparation technology of gas sensors is constantly being optimized, opening up avenues for the development of gas sensing.
- MXene-based composite materials (MXene/graphene, MXene/metal oxides, MXene/MOF, and MXene/polymer) are applied in various gas sensors.

ABSTRACT With the development of science and technology, the scale of industrial production continues to grow, and the types and quantities of gas raw materials used in industrial production and produced during the production process are also constantly increasing. These gases include flammable and explosive gases, and even contain toxic gases. Therefore, it is very important and necessary for gas sensors to detect and monitor these gases quickly and accurately. In recent years, a new two-dimensional material called MXene has attracted widespread attention in various applications. Their abundant surface functional groups and sites, excellent current conductivity, tunable surface chemistry, and outstanding stability make them promising for gas sensor applications. Since the birth of MXene materials, researchers have utilized the efficient and convenient solution etching preparation, high flexibility, and easily functionalize MXene with other materials to prepare composites for gas sensing. This has opened a new chapter in high-performance gas sensing materials and provided a new approach for advanced sensor research. However, previous reviews on MXene-based composite materials in gas sensing only focused on the performance of gas sensing, without systematically explaining the gas sensing mechanisms generated by different gases, as well as summarizing and predicting the advantages and disadvantages of MXene-based composite materials. This article reviews the latest progress in the application of MXene-based composite materials in gas sensing. Firstly, a brief summary was given of the commonly used methods for preparing gas sensing device structures, followed by an introduction to the key attributes of MXene related to gas sensing performance. This article focuses on the performance of MXene-based composite materials used for gas sensing, such as MXene/graphene, MXene/Metal oxide, MXene/Transition metal

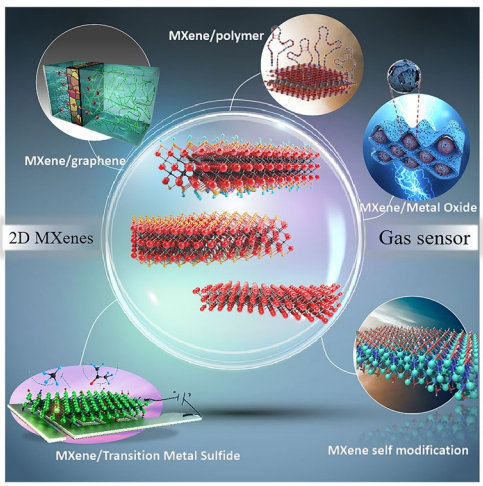

✉ Yuhua Wang, wangyuhua@wust.edu.cn; Xifei Li, xfli@xaut.edu.cn
[1] Hubei Province Key Laboratory of Systems Science in Metallurgical Process, Wuhan University of Science and Technology, Wuhan 430081, People's Republic of China
[2] Key Materials and Components of Electrical Vehicles for Overseas Expertise Introduction Center for Discipline Innovation, Institute of Advanced Electrochemical Energy and School of Materials Science and Engineering, Xi'an University of Technology, Xi'an 710048, People's Republic of China
[3] College of Materials Science and Engineering, Fuzhou University, Fuzhou 350108, Fujian, People's Republic of China

Published online: 06 June 2024

sulfides (TMDs), MXene/Metal–organic framework (MOF), MXene/Polymer. It summarizes the advantages and disadvantages of MXene composite materials with different composites and discusses the possible gas sensing mechanisms of MXene-based composite materials for different gases. Finally, future directions and inroads of MXenes-based composites in gas sensing are presented and discussed.

KEYWORDS MXene; Compound material; Gas sensor; Gas sensitive preparation; Gas sensitivity performance

1 Introduction

As a key component in information acquisition and signal conversion, sensors play an irreplaceable role in Internet of Things technology [1–4]. Among them, gas sensing can convert gas molecular signals over optical signals, electrical signals, etc., widely applicable to aerospace, industrial production, agricultural planting, and human health monitoring, to realize monitoring, forecasting, and automatic control of toxic and harmful gases, as well as prediction of human respiratory system diseases [5]. Sensors are mainly classified into electrical (resistive/capacitive), electrochemical, mass-sensitive, and optical types [6]. Electrical gas sensors are widely studied due to their simple structure and easy processing of output signals. Gas sensing materials in electrical sensor components can adsorb gas molecules through physical/chemical interactions and undergo charge transfer, thereby causing changes in the electrical signal of the device. Currently, electrical gas-sensitive materials include metal oxide semiconductors (MOSs), precious metals, carbon materials, organic materials, and two-dimensional materials. Since the discovery of graphene, two-dimensional materials, such as transition metal chalcogenides (TMDs) [7], boron nitride (BN) [8], layered double hydroxides (LDHs) [9], black phosphorus (BP) [10], and transition metal carbon/nitrides (MXenes) [11], have also been applied in the field of gas sensing. MXenes have become an emerging gas sensing material due to their unique layered structure, significant physical, optical, and electrical properties, as well as active surfaces [12, 13].

MXenes was proposed in 2011 by the Gogotsi group at Drexel University, USA [14]. Within the passed-century, MXenes and its composites have been receiving quite a lot of attraction in the field of energy storage and conversion [15, 16], electromagnetic shielding [17], and sensitive electronics [18]. Two-dimensional MXenes present a promising class on sensitive properties and a wide variety of structures, tunable structures, and controllable surface terminations [19]. In 2017, Lee et al. [20] found for the first time experimentally that Ti_3C_2 MXene has good gas-sensitive properties and exhibits gas-sensitive properties at room temperature [21–28]. Because common semiconductor gas-sensitive materials operate at high temperatures of 200–400 °C [29–32], MXene with room temperature gas-sensitive properties has the following advantages as a gas-sensitive material: (1) energy saving and simplification of the gas sensor structure [33, 34]; (2) painted on suitable matrix materials to develop portable and flexible gas sensors [35–41].

In recent years, the rapid development of MXenes has led to their rapid application in the field of gas sensing (Fig. 1) [1, 35, 38]. MXenes-based gas sensors are expected to achieve efficient and rapid detection of gases such as ammonia (NH_3), nitrogen dioxide (NO_2), and volatile organic compounds (VOCs) at room temperature [42–44]. However, due to its excellent electron transfer performance, two-dimensional layered structure, and abundant terminal groups, MXenes are not only sensitive to inorganic gases prone to electron loss or capture, but also highly sensitive to volatile organic compounds such as alcohols, ketones, and aldehydes [45]. This results in poor selectivity and specificity of MXenes in gas detection. Therefore, researchers often use surface modification, doping, and composite methods to enhance the gas sensing characteristics of MXenes [46–52]. Among them, compounding is an important strategy [53, 54]. The gas-sensitive composite phases of MXenes mainly include graphene and its derivatives, metal oxides, TMDs, MOFs, and polymers [55–57].

The current paper reviews the recent research progress of MXenes-based composites for gas sensors. Figure 2 shows an overview of the review article, highlighting the preparation of gas sensors, with a focus on the synthesis, advanced performance, and gas sensing behavior of MXenes composite materials (MXene/graphene, MXene/metal oxides, MXene/transition metal sulfides (TMDs), MXene/metal–organic framework (MOF), MXene/polymer). Finally, the (potential) advantages and challenges related to the development of MXenes were systematically discussed.

© The authors https://doi.org/10.1007/s40820-024-01430-4

Fig. 1 A significant research schedule of MXene compounded with other materials for gas sensors includes MXene self-modification, MXene/graphene, MXene/metal oxide, MXene/transition metal sulfide, MXene/MOF, MXene/polymer, etc. Reproduced with permission from Refs. [1, 35, 38, 42–44]

2 Preparation of Gas Sensors

Electrical gas sensors are sensors that convert gas composition and concentration into electrical signals [58–61]. In today's highly digitized and intelligent world, the increasingly deteriorating environmental and personal health issues have attracted widespread attention [27, 62–66]. In this regard, the development and design of gas sensors have

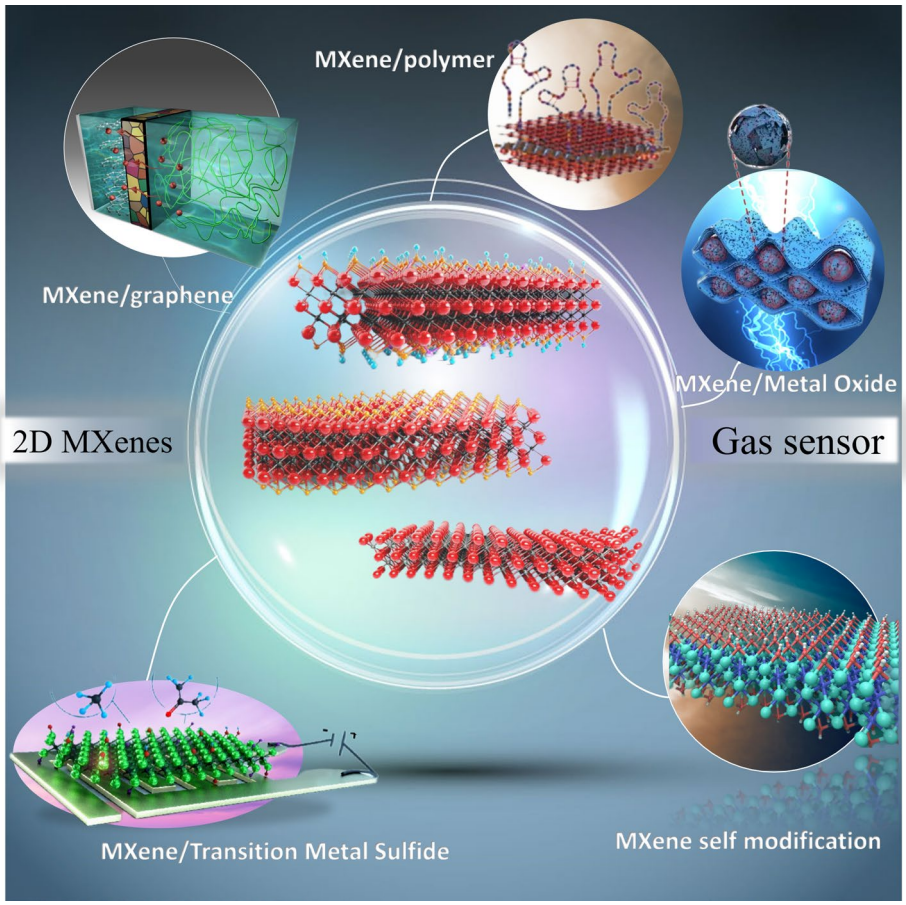

Fig. 2 The structural diagram of MXene and the selection of high sensitivity MXene composite materials for gas sensing devices (MXene self-modification, MXene/graphene, MXene/metal oxide, MXene/TMDs, MXene/MOF, MXene/polymer). Reproduced with permission from Refs. [55–57]

received attention and favor from researchers [67, 68]. Gas sensors can detect various gases, such as gas composition detection in chemical production, coal mine gas concentration detection and alarm, environmental pollution monitoring, gas leakage, fire alarm, combustion detection, etc. With the continuous development of social technology, the types of substrates continue to increase. However, traditional methods for preparing gas sensing devices are not suitable for many substrates, and traditional methods require high preparation conditions, low production efficiency, and extremely high preparation costs [69–74]. Therefore, innovative manufacturing technologies for gas sensors are very important [75]. Appropriate manufacturing methods for gas sensors have provided strong support for the wide application of gas sensors by not only improving the performance of the sensors, effectively simplifying the process steps and reducing the cost of production [76–78].

At present, the existing technologies for preparing sensors include: coating technology [77–82], printing technology [83–87], rotating technology [88–93], transfer technology [94–96] (Fig. 3). These technologies have led to enormous efforts in manufacturing optimization, resulting in impressive advances in gas sensors [97–113]. Table 1 summarizes the advantages and limitations of these specific technologies [114].

Coating technology is a simple and efficient way to prepare sensitive soluble materials into thin-film structures at the surface of a substrate [115, 116]. The preparation process of this technique is not demanding in terms of equipment and fabrication conditions, making it suitable for many substrates, including many flexible substrates, especially if the boundary range of the sensitive material film is not strictly required [76, 117]. Therefore, the coating technique is also one of the most prevalent methods for the fabrication of

© The authors https://doi.org/10.1007/s40820-024-01430-4

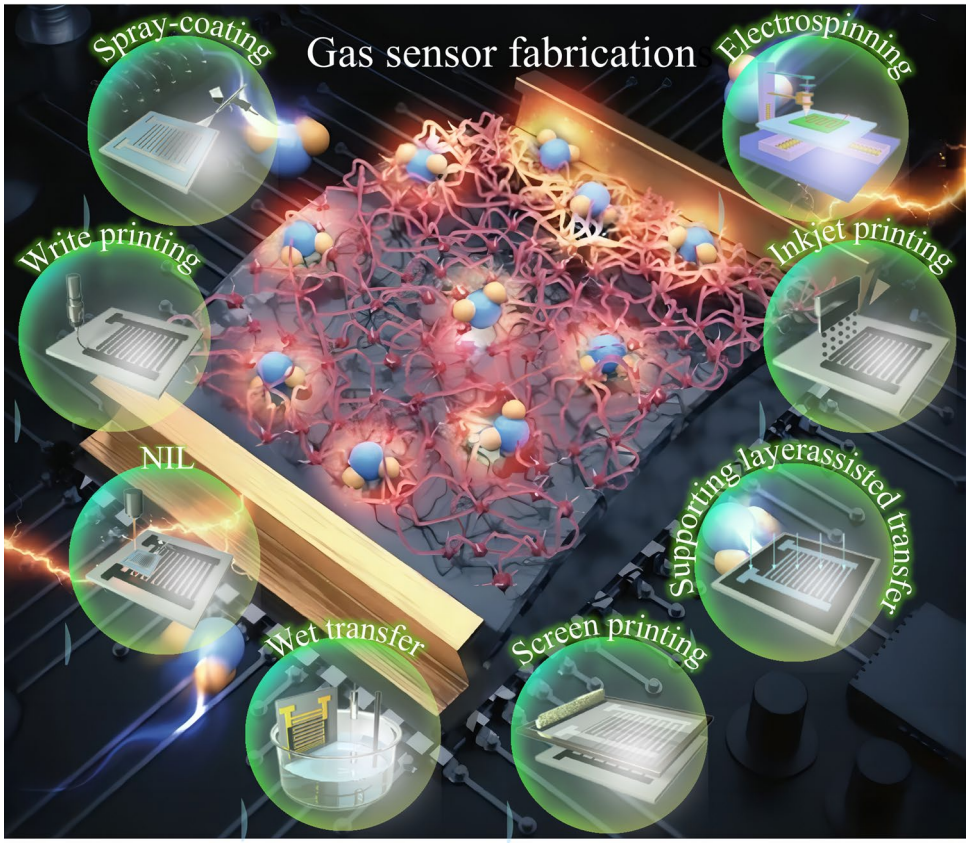

Fig. 3 Preparation methods for gas sensors: application of coating technology (trickle coating, spinner coating, sprays, soap coating); imprinting technology (inkjet printing, silk screen printing, writing printing, nano-imprinting (NL)); transfer technology (electrospinning, other spinning); assignment technology (drying transfer, humid transfer, support layer-assisted transfer)

gas sensors today. Specific methods of coating technology include trickle coating, spin coating, spray coating, and dip coating. Trickle-coating method is one of the simplest ways to prepare gas sensors by selecting a soluble sensitive material and applying the material solution dropwise onto the substrate via a pipette, which is simple to operate; spin-coating is an alternative and convenient method of making sensitive films, in which a soluble material is dripped onto a rotating substrate, which is then dried so that the substrate vaporizes the solvent and a sample of the substrate containing a thin film of the sensitive material is obtained; spray-coating method can be assisted by ultrasound and combines the hydrophilic and hydrophobic properties of the materials adhered to prepare a homogeneous and sensitive film, and it is a cost-effective method [79, 80, 118]. However, its shortcoming is that for films with specific needs (e.g., specific requirements for shape and location), a concealment procedure had to be applied to the areas that did the coating not need to be applied; dip coating is a versatile and cost-effective method of preparing gas-sensitive sensors, which proceeds by dipping the substrate into a solution of sensitive material, then adjusting the speed to lift the substrate out of suspension, and finally drying to eliminate any residual solvent on the substrate surface.

Printing technology is an innovative and modern manufacturing technology that enables the preparation of functional material suspensions based on substrates using the appropriate printers and finds its application in a wide range of electronic manufacturing applications [81, 119, 120]. Pre-designed gas sensors, such as specific patterns, film thicknesses, and boundary ranges, can be prepared on a massive scale by printing technology. Printing technologies can be categorized into four main types, which are inkjet printing, screen printing, writing printing, and nano-imprinting. Inkjet printing is an intriguing digital method for contactless spraying of ink and functional materials onto a variety of

Table 1 Summarized the technology for preparing gas sensing equipment, summarized its advantages and disadvantages, as well as the demand for materials

Technique	Classification	Advantage	Limitation	Requirement for sensitive material
Coating techniques	Trickle-coating	Facile High-efficient	Geometry-uncontrolled	Soluble or in solvent suspension
	Spinner-coating	Facile Thickness uniformity	Sensing material-waste	Soluble or in solvent suspension
	Sprays	Geometry-controlled	Nozzle-blockage Mask-relied	Soluble or in solvent suspension
	Soap-coating	Facile Versatile	Geometry-uncontrolled	Soluble or in solvent suspension
Imprinting techniques	Inkjet printing	Digital controllable backup	Nozzle-blockage	Soluble or in solvent suspension
	Screen printing	High-efficient Digital controllable backup	Mesh-relied	Soluble or in solvent suspension
	Write printing	Facile	Low-efficient	No special
	Nanoimprinting (NIL)	High resolution	Complicated	Soft
Transfer techniques	Electrospinning	High degree of efficiency Low cost	Irregular shape Blockage of nozzle	Soluble or in solvent suspension
	Other spinning yarn	High degree of efficiency Low cost	Geometry-irregular Nozzle-blockage	Soluble or in solvent suspension
Assignment technology	Drying transfer	Facile	Geometry-fragmentary	No special requirement
	Humid transfer	Facile	Low-efficient Location-uncontrolled	Low density
	Supporting layer-assisted transfer	Versatile	Complicated	No special requirement

substrates through micron-sized nozzles; screen printing is recognized as a highly attractive and competitive manufacturing technology compared to inkjet printing for the rapid mass fabrication of microelectronic devices due to its predesigned grid pattern and ease of manufacturing process; writing printing on a substrate is a familiar and practical printing technique in which a combination of a functional material solution is deposited on the substrate to form a structure by combining it with a pen or any other writing instrument; nanoimprint lithography (NIL) is a lithographic technique that offers the advantages of high productivity, low cost, and simplicity of the process to fabricate nanostructures in high volume, high resolution (< 5 nm), and lower cost. Simply put, NIL technology uses high-resolution electron beams and other methods to pattern complex nanostructures on a stamp, and then deforms the sensitive material with the patterned stamp to form the patterned material. Unlike traditional photolithography (where the direction or energy of the ions of the sensitive material is altered by photons or electrons to achieve pattern production), NIL technology mechanically deforms the sensitive material through direct contact, thus avoiding the resolution limitations of traditional techniques such as light diffraction or beam scattering.

Spinning is the process of extracting a precursor functional solution (e.g., polymer solution or melt) from a nozzle and depositing it on a collector to create long, continuous, one-dimensional fibers with micron/nanometer diameters [121–123]. Textiles can be coated with sensitive materials to form gas sensors. In addition, electronic devices based on sensitive optical fibers can be directly fabricated for gas detection via incorporating gas-sensitive materials into the precursor solution, which is a straightforward and effective method. Of the various spinning technologies, the electrospinning technology is of great interest and is widely utilized for the preparation of a wearable device.

Many substrates are incompatible given that in particular conventional fabrication techniques (e.g., chemical vapor deposition (CVD)), certain substrates cannot withstand drastic fabrication conditions (e.g., high temperatures, chemical

© The authors
https://doi.org/10.1007/s40820-024-01430-4

etching reagents). The optimum way to resolve these incompatibilities lies in the transfer of nanostructures or thin films on rigid/donor substrates (e.g., silicon, glass) prepared by conventional fabrication techniques to acceptor substrates (e.g., PET, PMDS), which is defined as a transfer technique [124, 125]. Effective transfer techniques are critical to the fabrication of flexible gas sensors, which will enable many traditional fabrication processes that are only applicable to hard substrates to be used in the manufacture of wearable/flexible sensors [114]. Transfer techniques consist of dry transfers, wet transfers, and support coatings-assisted transfers. Dry transfer utilizes the adhesion gap between the film layer and the underlying substrate to transfer the film from the primary substrate to the intended substrate; wet transfer is available for transferring a mono sensitive layer to a variety of substrates in service media; and support layer-assisted transfer is a prominent transfer technique that utilizes an elastomeric impression as a support layer to retrieve a material with micro/nanostructures back from the supplier substrate and attach it to a non-natural substrate [126].

However, most of the aforementioned widely practiced techniques (e.g., coating, printing, and spinning) rely on the sensing material being in the liquid phase, this restricts the amount of gas sensing materials available because some types of materials with excellent sensing capabilities are harder to realize in the bulk of the liquid phase. Spin-coating and screen-printing methods result in ink waste due to the use of solution-phase materials, while inkjet printing and electrospinning processes both require the use of nozzle devices, with the risk of nozzle clogging. Moreover, technology of transfer, particularly transfer with the assistance of a supporting layer where at least two etching cycles are involved, is partly complex and time-consuming. Hence, a long way lies ahead in commercializing the product for the exploitation of gas sensors with enhanced performance and large-scale production.

3 Structure and Properties of MXene

3.1 Structure of MXene

MXene material is a type of metal carbide or metal nitride material with a two-dimensional layered structure. It is a two-dimensional transition metal group carbon/nitride obtained by selectively etching the A atomic layer in the ternary conductive ceramic MAX phase. The phase structure of MXene is shown in Fig. 4a, and the general formula of MXene structure is $M_{n+1}X_nT_x$, where M is a transition metal (such as Ti, V, and Mo), X represents C or N, n = 1, 2, or 3, T_x represents surface terminal groups (-OH, =O, and/or -F) [127]. Due to the hexagonal crystal structure formed by the interlacing of the M layer and X layer with the A layer in the precursor MAX phase of MXenes, the MXene phase also has a similarly symmetrical hexagonal lattice (Fig. 4b). The M atoms in MXenes are arranged in a tight structure, while the X atoms fill the gap positions of the octahedron. There are three arrangements in the MXenes structure: $B_\gamma A\text{-}A_\gamma B$ ($M_2X\text{-}M_2X$), $B_\gamma A_\beta C\text{-}C_\beta A_\gamma B$ ($M_3X_2\text{-}M_3X_2$) and $B_\alpha C_\beta A_\gamma B\text{-}B_\gamma A_\beta C_\alpha B$ ($M_4X_3\text{-}M_4X_3$) [128]. As shown in Fig. 4c, the two-dimensional MXene consists of a thin sheet that has hexagonal cells, with an X layer sandwiched between two M transmission metal layers.

3.2 MXene Characteristics for Gas Sensing

In the aqueous environment of chemical etching solutions, the outer surface of the detached MX layer is usually functionalized by -F, -OH or =O functional groups. These surface rich functional groups (-F, -OH or =O) can become attachment sites for the direct growth of other nanostructured materials or functional molecules [129, 130], which can be modified to provide feasibility for improving the selectivity of gas sensors. In addition, this surface functionalization has a significant impact on the electronic and ion transport properties of MXenes, namely, the conductivity of MXenes is directly related to the electron transfer process that occurs on their surface [131]. MXenes have certain metal properties and narrow bandgap semiconductor properties, which give them the inherent advantage of good conductivity. For example, $Ti_3C_2T_x$ has a room temperature conductivity of up to 10,000 S cm^{-1} [132, 133].

Many theoretical calculations have shown that the ideal MXene is located near the Fermi level, with a considerable electron density and a cash property [128, 130]. Lane et al. calculated the ideal single-layer defect free MXene nanosheets using density functional theory, and the results showed that MXene exhibits metal conductivity, with Fermi levels higher than its precursor MAX phase [131]. However, when its surface is functionalized,

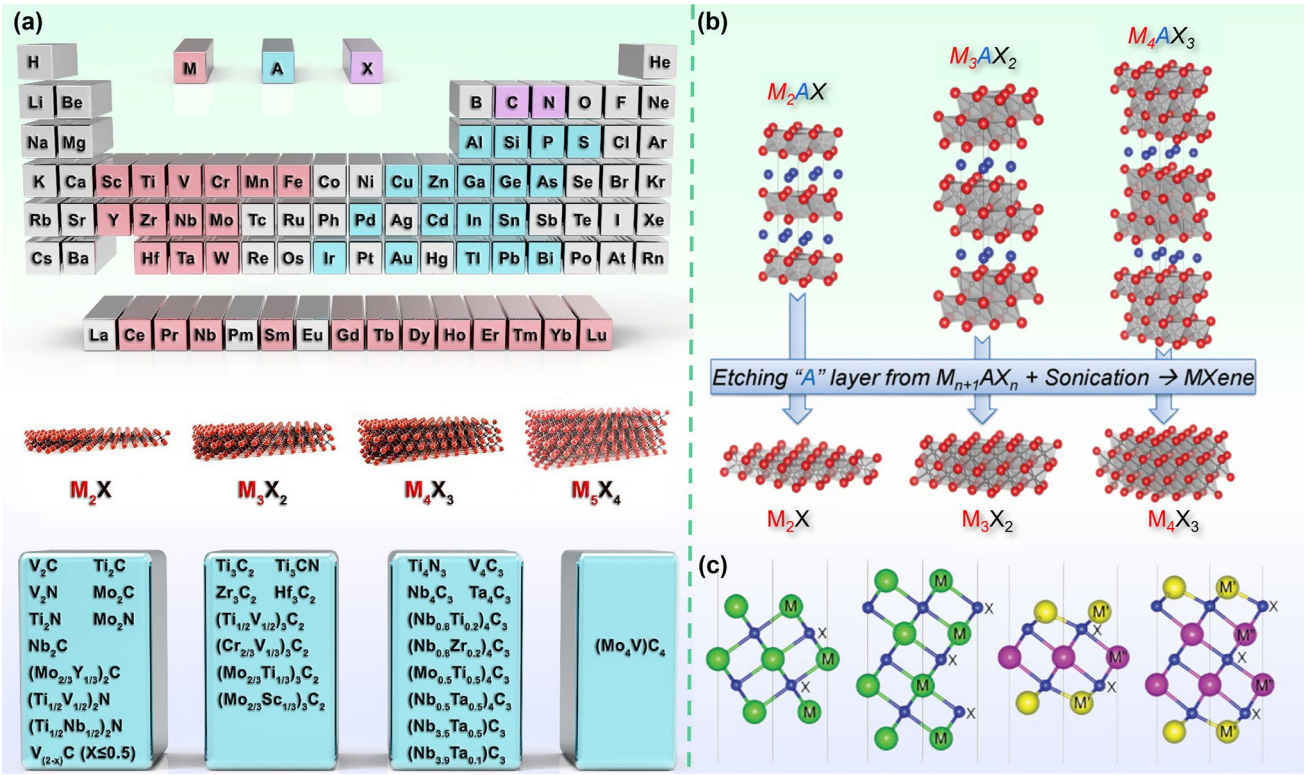

Fig. 4 **a** Explain the "M," "A," and "X" elements of MAX phase through the periodic table, as well as the schematic diagram of MXenes structure and the currently reported MXenes. Reproduced with permission from Ref. [127]. b Crystal structure of MXene generated from MAX phase. c Side views of pristine M_3X_2, M_4X_3, $M'_2M''X_2$, and $M'_2M''_2X$ MXenes, where M, M', and M'' denote transition metals, and X represents C or N. Reproduced with permission from Ref. [128]

some MXenes exhibit semiconductor properties. In addition, due to the different number of electrons received by different surface groups (-F, -OH, or = O) in equilibrium states, different surface groups have different effects on the electronic properties of MXene, and the orientation of the end groups also affects the electronic properties of MXene [132]. Table 2 lists the bandgap widths of some MXenes. MXenes with different bandgap widths can be used to prepare gas sensing arrays, achieving specific recognition of industrial raw gas, exhaust gas, and human exhaled gas. In summary, using MXenes as a gas sensing material has certain inherent advantages.

4 MXenes Composite in Gas Sensing Applications

In recent years, MXene composite materials containing graphene, semiconductor metal oxides, transition metal sulfides, organic metal frameworks, polymers, and other materials have received increasing research in gas sensing

Table 2 Bandgap width of some MXenes

MXenes	Functional group	Bandgap (eV)	References
Ti_2C	–F	0.72	[134]
	–OH	1.07	[134]
	=O	0.24	[135]
Ti_3C_2	–F	0.39	[134]
	–OH	1.35	[134]
Nb_2C	–F	0.96	[134]
	–OH	1.29	[134]
V_2C	–F	0.24	[134]
	–OH	1.09	[134]
Cr_2C	–F	3.49	[136]
	–OH	1.43	[136]
Cr_2TiC_2	–F	1.35	[137]
	–OH	0.84	[137]
Sc_2TiC_2	–F	1.03	[135]
	–OH	0.45	[135]
	=O	1.8	[135]
Hf_2C	=O	1.0	[135]
Hf_3C_2	=O	0.16	[138]
Zr_2C	=O	0.88	[135]

© The authors
https://doi.org/10.1007/s40820-024-01430-4

applications. Due to the more metallized nature and narrow band gap of MXenes, the addition of metal oxides, graphene derivatives, and chalcogenides provides more activated adsorption sites, defects, and modulation of working functions, thereby improving gas sensing performance. Table 3 summarizes the performance of gas/VOC/humidity sensors for MXene-based composites.

4.1 MXene/Graphene

Graphene is widely used in various fields because of its excellent thermal conductivity, high specific surface area, and easily modified structure [139–143]. MXenes are an excellent sensing material with a very narrow bandgap, but when pure MXenes are used in gas sensing devices, critical potential barriers are generated during the gas reaction process, which hinders their further sensitive response. Subsequently, researchers found that combining the two can effectively overcome this problem. For example, Liu et al. prepared three-dimensional (3D) hybrid aerogel [140] (Fig. 5a) from MXene ($Ti_3C_2T_x$), reduced graphite oxide (rGO) nanosheets, and ultrafine CuO nanoparticles. From the obtained 3D MXene/rGO/CuO aerogel, high pyruvic sensing performance was demonstrated at ambient temperature (Fig. 5b). Response of the sensor to 100 ppm of acetone was 52.09% (RT) (Fig. 5b), with a response time of ~ 6.5 s and a recovery time of ~ 7.5 s (Fig. 5c), demonstrating excellent reproducibility and selectivity. In 2020, Lee et al. [139] developed a $Ti_3C_2T_x$ MXene/graphene hybrid fiber wearable gas sensor without a metal binder through a wet spinning process (Fig. 5d). The bandwidth capacity of the composite material has increased from 1.05 to 1.57 eV, while the fiber properties of the composite material enhance flexibility and response to NH_3. A moderate response (6.8% at 50 ppm NH_3) was displayed by the composites (Fig. 5e), with this being 7.9 and 4.7 times more responsive than that of pure MXenes and rGO, respectively (Fig. 5f).

Wang et al. [141] proposed an ionic conductive composite film, which is composed of reduced graphite oxide (rGO), nitrogen doped MXene $Ti_3C_2T_x$ (N-MXene), and titanium oxide (TiO_2) (Fig. 5g), and detects 4–40 ppm formaldehyde HCHO vapor at room temperature (20 °C) and humidity. In various humidity conditions toward 4 ppm HCHO, the ternary sensor achieved an average reversible response of 26% at 54% RH (Fig. 5h). In addition, it also shows good repeatability, long-term stability, and selectivity (Fig. 5i). The excellent gas sensing performance of rGO nanosheets can be attributed to three aspects: firstly, in humid environments, rGO nanosheets serve as a good conductive platform for transporting and collecting charge carriers; second, the layered N-MXene facilitates the co-sorption and spreading of HCHO and water moieties; third, the TiO_2 nanoparticles provide abundant resorption sites, which promote decomposition of the sorbed water.

In the wet CO_2 sensing process of composite materials, few rGO nanosheets serve as a good conductive platform for transferring and collecting load carrier. The layered N-MXene provides further reactive sites to co-adsorb carbon dioxide and water, thus facilitating reactions involving water. The abundant amino groups in PEI polymers facilitate the binding of CO_2 molecules, leading to significant changes in charge carrier density through proton conduction behavior [98, 168–173]. However, MXene composite material sensors with graphene or graphene derivatives are mostly subjected to multi gas testing, with no targeted detection of a single gas, and there is little research on humidity sensing [128, 174–184].

4.2 MXene/Metal Oxide

Metal oxides represent the oldest and most widely used sensing material and can be used in a variety of applications due to the high specific surface area, ease of fabrication, ease of functionalization, and extremely high sensitivity to a broad range of gases/volatile organic compounds. The sensing mechanism of metal oxides is mainly due to the changes in resistance caused by pre adsorbed oxygen species (oxygen molecules (O_2), lattice oxygen < including surface lattice oxygen and bulk lattice oxygen > (O^{2-}), atomic adsorption of oxygen (O^-), molecular adsorption of oxygen (O_2^-)), and surface reactions of gas molecules [185]. Due to the high dependence of oxygen ionization on operating temperature, this mechanism typically requires metal oxide gas sensors to operate at relatively high temperatures, which is also the main drawback of metal oxide gas sensors [53, 145–147, 186]. However, research data suggests that the mixture of metal oxides with 2D MXenes has a more robust gas/volatile organic compound sensing response, and the emergence

Table 3 Gas/VOC/humidity sensor based on MXene-composite

Classification	MXene-based composite	Target gas	Test range	Carrier gas	Sensitivity	Response time ($t_{Res.}$)	Recovery time ($t_{Rec.}$)	Operating temperature	References
MXene/rGO	$Ti_3C_2T_x$/rGO fibers	NH_3	10–500 ppm	Dry air	6.77% (50 ppm)	> 10 min	> 25 min	RT	[139]
	$Ti_3C_2T_x$/rGO/CuO aerogel	Acetone (CH_3COCH_3)	10–500 ppm	Dry air	52.09% (100 ppm)	6.5 s	7.5 s	RT	[140]
	rGO/N-MXene/TiO_2 film	Formaldehyde (HCHO)	4–40 ppm	Wet air	26% (4 ppm)	27.6 s	4.8 s	20 °C	[141]
	rGO/N-MXene/PEI film	CO_2	8–3000 ppm	Wet air	1.3% (8 ppm)	8.8 min	9 min	20 °C	[142]
	$Ti_3C_2T_x$/TiO_2-spaced rGO	NO_2	0.05–20 ppm	Wet air	165% (1 ppm)	180 s	260 s	RT	[143]
MXene/metallic oxide	TiO_2/$Ti_3C_2T_x$ bilayer film	NH_3	0.5–10 ppm	Wet air	3.1% (10 ppm)	33 s	277 s	25 °C	[144]
	CuO/$Ti_3C_2T_x$ MXene hybrids	Toluene ($C_6H_5CH_3$)	10–50 ppm	Wet air	11.4% (50 ppm)	270 s	10 s	250 °C	[145]
	Co_3O_4@PEI/$Ti_3C_2T_x$	NO_x	0.03–100 ppm	Wet air	27.9% (100 ppm)	< 2 s	73 s	RT	[146]
	MXene sphere/ZnO	NO_2	5–100 ppm	Wet air	41% (100 ppm)	34 s	103 s	25 °C	[53]
	MXene/Co_3O_4	HCHO	0.01–10 ppm	Wet air	9.2% (10 ppm)	83 s	5 s	25°C	[147]
	$W_{18}O_{49}$/$Ti_3C_2T_x$	CH_3COCH_3	0.17–20 ppm	Wet air	11.6% (20 ppm)	5.6 s	6 s	200–400 °C	[45]
	partially oxidized $Ti_3C_2T_x$	Organic analytes	2 ppm	Dry air	40% (ethanol), 110% (methanol, 100% (isopropyl alcohol), and 180% (acetone)	–	–	20–350 °C	[148]
	$Ti_3C_2T_x$//TiO_2	Ethanol (C_2H_5OH)	10–800 ppm	Dry air	22.47% (100 ppm)	–	–	RT	[149]
	TiO_2/Ti_2CT_x	NH_3	1–100 ppm	Dry air	~0.4% (0.1 ppm)	–	–	RT	[150]
	$Ti_3C_2T_x$/WO_3	NH_3	1–5 ppm	Wet air	22.3% (1 ppm)	119 s	228 s	RT	[151]
	MXene/SnO_2	NH_3	0.5–100 ppm	Wet air	40% (50 ppm)	36 s	44 s	RT	[152]
	TiO_2/$Ti_3C_2T_x$	NO_2	0.125–5 ppm	Dry air	~37% (5 ppm)	–	–	RT	[44]
	SnO-SnO_2/$Ti_3C_2T_x$	CH_3COCH_3	10–100 ppm	Dry air	12.1 (100 ppm)	18 s	9 s	RT	[153]
	$Ti_3C_2T_x$-TiO_2	Hexanal	10–40 ppm	Dry air	~3.4% (10 ppm)	293 s	461 s	RT	[154]
	α-Fe_2O_3/$Ti_3C_2T_x$	CH_3COCH_3	5–200 ppm	Wet air	16.6% (5 ppm)	5 s	5 s	RT	[155]
	In_2O_3/$Ti_3C_2T_x$	CH_3OH	5–100 ppm	Wet air	29.6% (5 ppm)	6.5 s	3.5 s	RT	[156]
	ZnO/$Ti_3C_2T_x$	NO_2	5, 10 ppm	Wet air	54% (10 ppm)	–	–	RT	[157]
	$ZnSnO_3$/MXene	HCHO	5–100 ppm	Wet air	62.4% (5 ppm)	6.2 s	5.1 s	RT	[158]
	Ti_3C_2/TiO_2 nanowires	Humidity	7%–97% RH	Wet air	280 PF%RH	2 s	0.5 s	RT	[159]
	$Ti_3C_2T_x$/$K_2Ti_4O_9$	Humidity	11%–95%RH	Wet air	1.49% (95%RH)	65.2 s	84.8 s	RT	[160]
MXene/TMDs	MoS_2/$Ti_3C_2T_x$	NO_2	10, 20 ppm	Wet air	40.1% (20 ppm)	525 s	155 s	RT	[161]
	$Ti_3C_2T_x$/WSe_2	C_2H_5OH	1–40 ppm	Wet air	~9% (40 ppm)	9.7 s	6.6 s	RT	[162]
MXene/MOF	$Ti_3C_2T_x$/Cu MOF	NH_3	1–100 ppm	Dry air	24.8% (100 ppm)	45 s	29 s	RT	[163]
	Co-TCPP(Fe)/$Ti_3C_2T_x$	NO_2	10 ppm	Dry air	2.0% (10 ppm)	95 s	15 s	RT	[164]
MXene/polymer	Polyanline/$Ti_3C_2T_x$	NH_3	0.5–50 ppm	Wet air	1.7% (10 ppm)	–	–	20 °C	[165]
	cationic polyacrylamide (CPAM)/$Ti_3C_2T_x$	NH_3	50–200 ppm	Dry air	4.7% (200 ppm)	12.7 s	14.6 s	RT	[166]

© The authors
https://doi.org/10.1007/s40820-024-01430-4

Table 3 (continued)

Classification	MXene-based composite	Target gas	Test range	Carrier gas	Sensitivity	Response time ($t_{Res.}$)	Recovery time ($t_{Rec.}$)	Operating temperature	References
	PEDOT:PSS/MXene	NH_3	10–1000 ppm	Dry air	36.6% (100 ppm)	116 s	40 s	27 °C	[103]
	MXene/polyaniline/bacterial (MXene/PANI/BC)	NH_3	2.5–12.5 ppm	Dry air	56.63% (7.5 ppm)	–	–	RT	[101]
	PANI/$Ti_3C_2T_x$	C_2H_5OH	50–200 ppm	Dry air	27.4% (150 ppm)	0.4 s	0.5 s	RT	[105]
	$Ti_3C_2T_x$/PEDOT:PSS	CH_3OH	180–500 ppm	Dry air	36.6% (100 ppm)	116 s	40 s	27 °C	[104]
	$Ti_3C_2T_x$/polyurethane (PU)	CH_3COCH_3	0.05–50 ppm	Dry air	0.25% (50 ppb)	148 -190 s	164 -240 s	RT	[102]
	MXene/polyelectrolyte	Humidity	20%–70% RH	Wet air	39.5%	110 ms	220 ms	RT	[100]
	poly(vinyl alcohol)/$Ti_3C_2T_x$(PVA/MXene)	Humidity	11%–97% RH	Wet air	40% (90% RH)	0.9 s	6.3 s	RT	[99]
	$Ti_3C_2T_x$/chitosan (CS)	Humidity	14%–73% RH	Wet air	~0.16% (73% RH)	–	–	RT	[113]
	$Ti_3C_2T_x$/chitosan (MCQMS)	Humidity	1%–98% RH	Wet air	317% (90% RH)	0.75 s	1.6 s	RT	[112]
Others	Ti_3C_2/Ag	Humidity	35%–95% RH	Wet air	106,800%	80 ms	120 ms	RT	[111]
	$Ti_3C_2T_x$/Ag NWs	Humidity	57% RH	Wet air	~3%	5 s	80 s	20°C	[108]
	$Ti_3C_2T_x$-K/Mg	Humidity	0%–85% RH	Wet air	~8% RH	–	–	27°C	[110]
	$TiOF_2$@$Ti_3C_2T_x$	Humidity	11%–95% RH	Wet air	39.5%	16 s	20 s	RT	[98]
	$Ti_3C_2T_x$@Pb CNC	H_2	0.5%–40%	Dry air	23.0 ± 4.0% (4%)	(37 ± 7)s	(161 ± 23) s	RT	[167]
	$Ni(OH)_2/Ti_3C_2T_x$	NH_3	1–80 ppm	Wet air	6.2% (10 ppm)	78 s	~500 s	RT	[106]
	$Ti_3C_2T_x$/flfluoroalkylsilane (FOTS)	C_2H_5OH	5–120 ppm	Wet air	14% (120 ppm)	39 s	139 s	RT	[109]
	$Fe_2(MoO_4)_3$@MXene	n-butanol	100 ppm	Wet air	43.1%	18 s	24 s	120 °C	[107]

of this complex greatly overcomes the low selectivity and high operating temperature limitations of pure metal oxide sensing (Fig. 6).

Titanium dioxide (TiO_2) is an ideal material for gas sensor preparation due to its pollution-free properties, ability to generate photogenerated electrons when stimulated, and simple preparation process. However, TiO_2-based gas sensors also have some drawbacks, such as poor sensing performance, long response time, and recovery time. In 2019, Tai [144] designed a gas sensing element based on a $TiO_2/Ti_3C_2T_x$ bilayer film (Fig. 7a). According to the results, when compared with the pure $Ti_3C_2T_x$ sensor, this $TiO_2/Ti_3C_2T_X$ sensor exhibited a larger recognition value (1.63 times) with shorter response/recovery time (0.65/0.52 times) compared to the pure $Ti_3C_2T_X$ sensor for 10 ppm NH_3 at room temperature of 25 °C (60.8% relative humidity) (Fig. 7b, c). Choiet et al. [44] covered the amplification and inductive properties against NO_2 by Ti_3C_2 through the modulation of the introduction of the Schottky barrier (SB) (Fig. 7d), which combines TiO_2 into conducting MXenes to form a heterogeneous structure. The TiO_2/Ti_3C_2 composite sensor shows a NO_2 sensitivity 13.7 times higher than the original Ti_3C_2 MXene (Fig. 7e), while the response of the reducing gas is almost unchanged, the reason for this is the highest charge density of NO_2 in other interfering VOCs due to the formation and movement of SB inside caused by the adsorption of NO_2 molecules, together with other interfering VOCs, and as explained in the mechanisms of sensing (Fig. 7f, g). Kuang et al. [154] successfully prepared $Ti_3C_2T_x$-TiO_2 nanocomposites with regular morphology using $Ti_3C_2T_x$ as the titanium source through a simple one-step hydrothermal synthesis method (Fig. 7h). Due to the formation of interface heterojunctions and modulation of carrier density, the detection response of $Ti_3C_2T_x$-TiO_2 sensors to various VOCs at room temperature

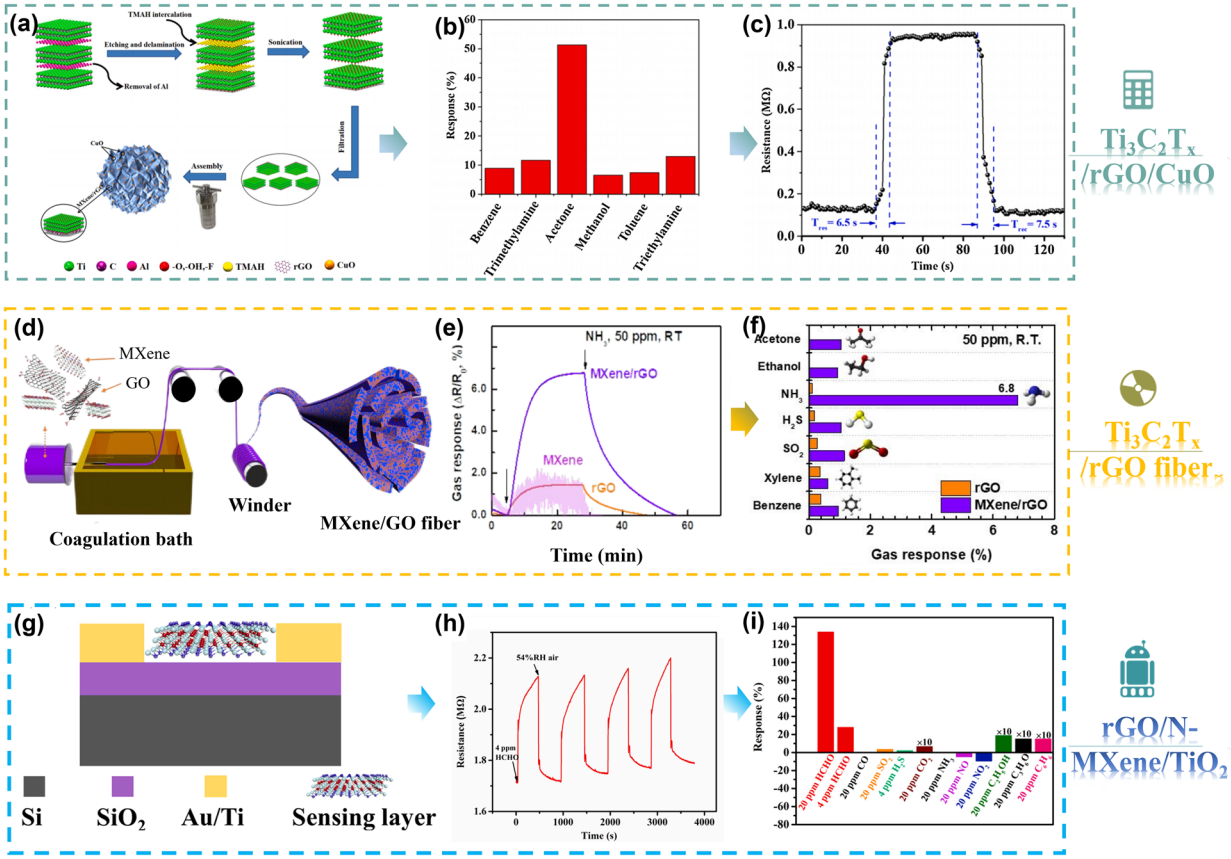

Fig. 5 **a** Schematic illustration of fabrication process of 3D MXene/rGO/CuO aerogel. **b** The selectivity for 3D MXene/rGO/CuO aerogel-based sensor to different gases of 100 ppm at RT. **c** Resistance changes of 3D MXene/rGO/CuO aerogel when exposed to 100 ppm acetone at RT. Reproduced with permission from Ref. [140]. **d** Schematic illustration of the spinning process for MXene/GO hybrid fiber. **e** Comparison of the gas response of MXene film, rGO fiber, and MXene/rGO hybrid fiber (40 wt% MXene). **f** Gas selectivity comparison of rGO fiber and MXene/rGO hybrid fiber (40 wt% MXene) to various testing gases at concentrations of 50 ppm. Reproduced with permission from Ref. [139]. **g** Schematic images of IDEs sensor. **h** Sensing performance of the ternary sensor toward HCHO vapor under 54%RH at 20 °C. **i** Selectivity investigation among a series of interference gases under 54%RH at 20 °C. Reproduced with permission from Ref. [141]

is enhanced by about 1.5–12.6 times compared to pure MXene sensors. In addition, this nanocomposite sensor has a better response to hexanal (the $Ti_3C_2T_x$-TiO_2 sensor has a gas response of approximately 3.4% to 10 ppm hexanal).

In addition to the hydrothermal partial oxidation of $Ti_3C_2T_x$ mentioned above, researchers have also prepared partially oxidized $Ti_3C_2T_x$ by heat treatment at 350 °C [148] (Fig. 8a–g) and microwave-activated oxygen plasma [149] treatment (Fig. 8h). Sun et al. [150] investigated the processing-dependent sensing behavior of Ti_2CT_x (LiF/HCl), Ti_2CT_x (HF), and TiO_2/Ti_2CT_x (LiF/HCl) at room temperature under 365 nm ultraviolet light (Fig. 9a, b). In addition, the results indicate that TiO_2/Ti_2CT_x (LiF/HCl) exhibits better sensing performance than other samples (Fig. 9c). Since it contains abundant oxygen functional groups (-O_x, -$(OH)_x$ and Ti–O-Ti), providing more NH_3 molecular interactions. Li et al. [159] developed a humidity sensor by in situ growth of TiO_2 nanowires on two-dimensional (2D) Ti_3C_2 MXene using alkaline oxidation method (Fig. 9d). They found that the sea urchin-like Ti_3C_2/TiO_2 composites have an order of magnitude larger surface area when compared to pure Ti_3C_2 or TiO_2 materials (Fig. 9e) and exhibit documented high sensitivity at environments with low thermal relative humidity (RH) (from 7% RH to 33% RH, approximately 280 pF/% RH) (Fig. 9f).

CuO exhibits the advantage of wide range response to VOCs, but has the drawbacks of small response values, slow response/recovery speed, and low durability. For this reason, Angga Hermawan et al. [145] reported a simple method to prepare CuO-$Ti_3C_2T_x$ MXene hybrid by self-assembling

© The authors https://doi.org/10.1007/s40820-024-01430-4

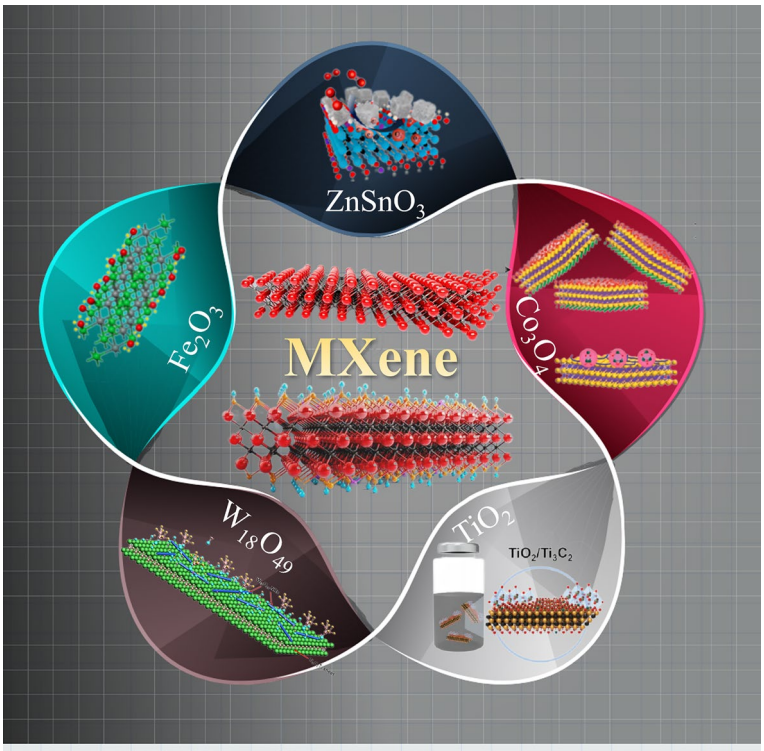

Fig. 6 MXene/metal oxide for gas sensors. Reproduced with permission from Refs. [44, 146, 155, 158, 187]

electrostatically (Fig. 10a). CuO-$Ti_3C_2T_x$ MXene showed a better methane gas sensing response (R_g/R_a) of 11.4 than pristine CuO nanoparticles at 250°C for 50 ppm toluene gas sensing response nearly five times higher than that of pristine CuO particles for 50 ppm toluene at 250 °C. (Fig. 10b). In addition, due to the high conductivity of the metal phase in $Ti_3C_2T_x$ MXene, the hybridization of CuO with $Ti_3C_2T_x$ MXene not only improves the response time, but also improves selectivity, response (270 s), and recovery time (10 s) (Fig. 10c, d).

Sun et al. [146] used simple noncovalent chemical methods and hydrothermal methods to effectively rivet Co_3O_4 nanocrystals onto functionalized $Ti_3C_2T_x$ MXene sheets of branched polyethylene imine (PEI), and prepared Co_3O_4@PEI/$Ti_3C_2T_x$ MXene composite material (Fig. 10e). Sun et al. examined the sensing performance of nitrogen oxides (consisting of NO_2 and NO) using Co_3O_4@PEI/$Ti_3C_2T_x$ (CoPM) complexes and found that CoPM-24 complexes exhibited 27.9% response when added at 2.4 mg $Ti_3C_2T_x$ along with high selectivity and very weak detection limits (30 ppb-NO_x) (Fig. 10f, g). In 2021, Zhang et al. [147] as a high-performance self-powered formaldehyde (HCHO) sensor based on MXene/Co_3O_4 composite was prepared. Electricity was supplied through piezoelectric nanogenerators (PENGs) of ZnO/MXene nanowire arrays. p-type metal oxide Co_3O_4 provided more active sites for formaldehyde interactions, thus the MXene/Co_3O_4 composite exhibited good response at room temperature with 9.2% response at 10 ppm HCOH and low detection limit—0.01 ppm.

In 2019, Sun et al. [187] used a simple solvothermal method to grow one-dimensional $W_{18}O_{49}$ nanorods in situ on the $Ti_3C_2T_x$ surface. The $W_{18}O_{49}$/$Ti_3C_2T_x$ composites exhibited a high response to low concentrations of acetone (11.6–20 ppm) (Fig. 11a), as well as high selectivity, long-term stability, and also a fast response and recovery response to very low of acetone (170 ppb) can also be detected (Fig. 11b). Physical properties of NH_3 sensing were improved by forming heterojunctions and enhancing the number of active sites, relative surface area, and pore size of pristine $Ti_3C_2T_x$ by functionalizing $Ti_3C_2T_x$ with WO_3 nanoparticles by a simple ultrasonic method, as shown in Fig. 11c. The resulting $Ti_3C_2T_x$/WO_3-50% (weight percent of WO_3) sensor exhibited excellent response to NH_3 (22.3% at 1 ppm), which was 15.4 times that of the pristine $Ti_3C_2T_x$

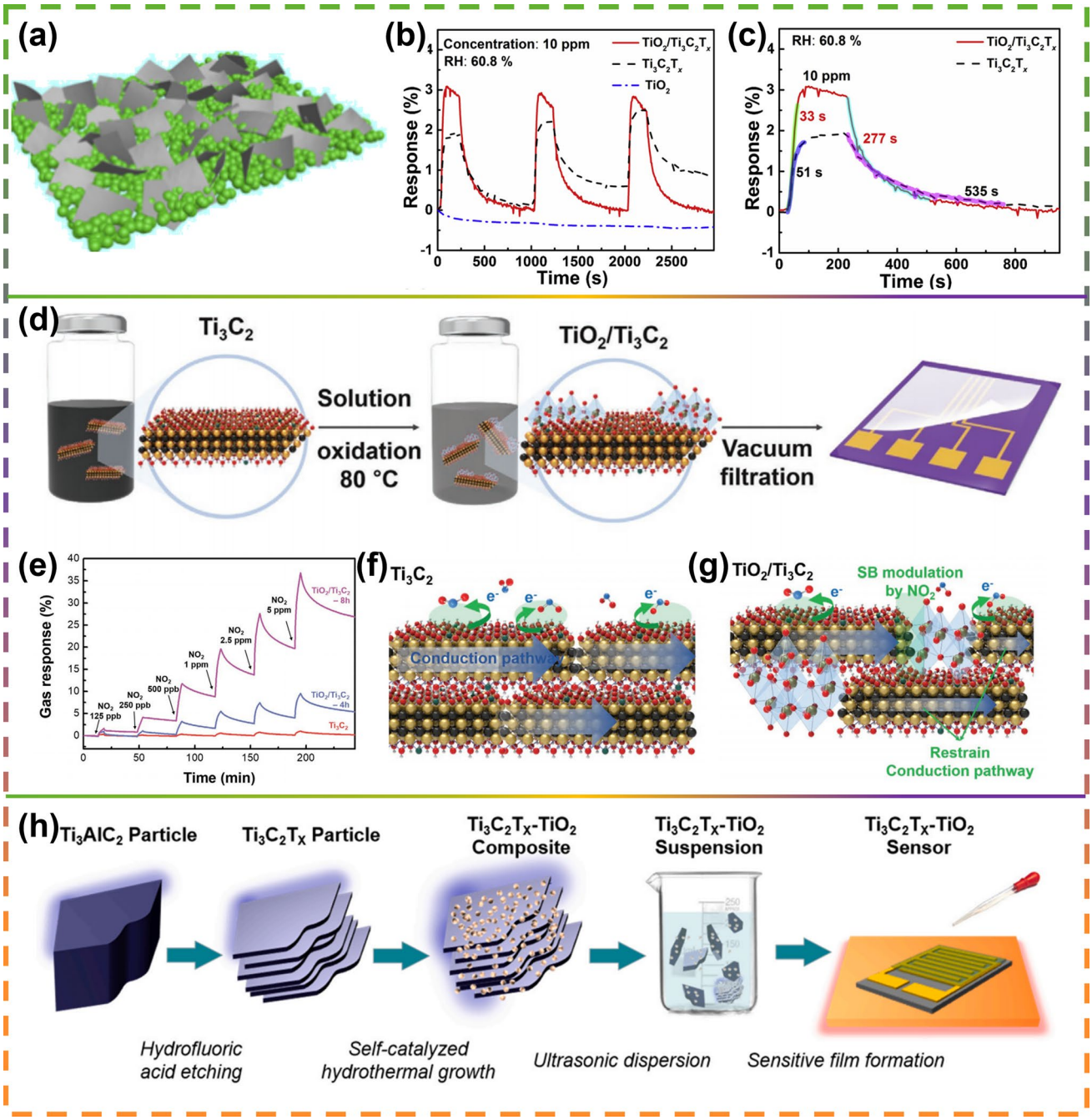

Fig. 7 **a** Structure of $TiO_2/Ti_3C_2T_x$ Gas Sensor. **b** Normalized response recovery curves of the $TiO_2/Ti_3C_2T_x$, $Ti_3C_2T_x$ and TiO_2 gas sensors to 10 ppm NH_3. **c** Response/recovery times of the $Ti_3C_2T_x$ and $TiO_2/Ti_3C_2T_x$ gas sensors. Reproduced with permission from Ref. [144]. **d** A diagram of the composition process of TiO_2/Ti_3C_2 MXene sensor. **e** Experimental real-time gas response curve of TiO_2/Ti_3C_2 depending on NO_2 concentration. **f** and **g** Suspension regime of NO_2 gas by Ti_3C_2 and $TiO_2/TiO_2/Ti_3C_2$ thin films. Reproduced with permission from Ref. [44]. **h** Schematic diagram illustrating the process of the $Ti_3C_2T_x$-TiO_2 nanocomposites preparation and gas sensing device fabrication. Reproduced with permission from Ref. [154]

sensor (1.54% at 1 ppm) with no electrical resistance drift (Fig. 11d) [151].

In addition to this, He et al. [152] successfully synthesized two-dimensional (2D) MXene modified by tin dioxide nanoparticles for gas sensing detection as well by hydrothermal

© The authors https://doi.org/10.1007/s40820-024-01430-4

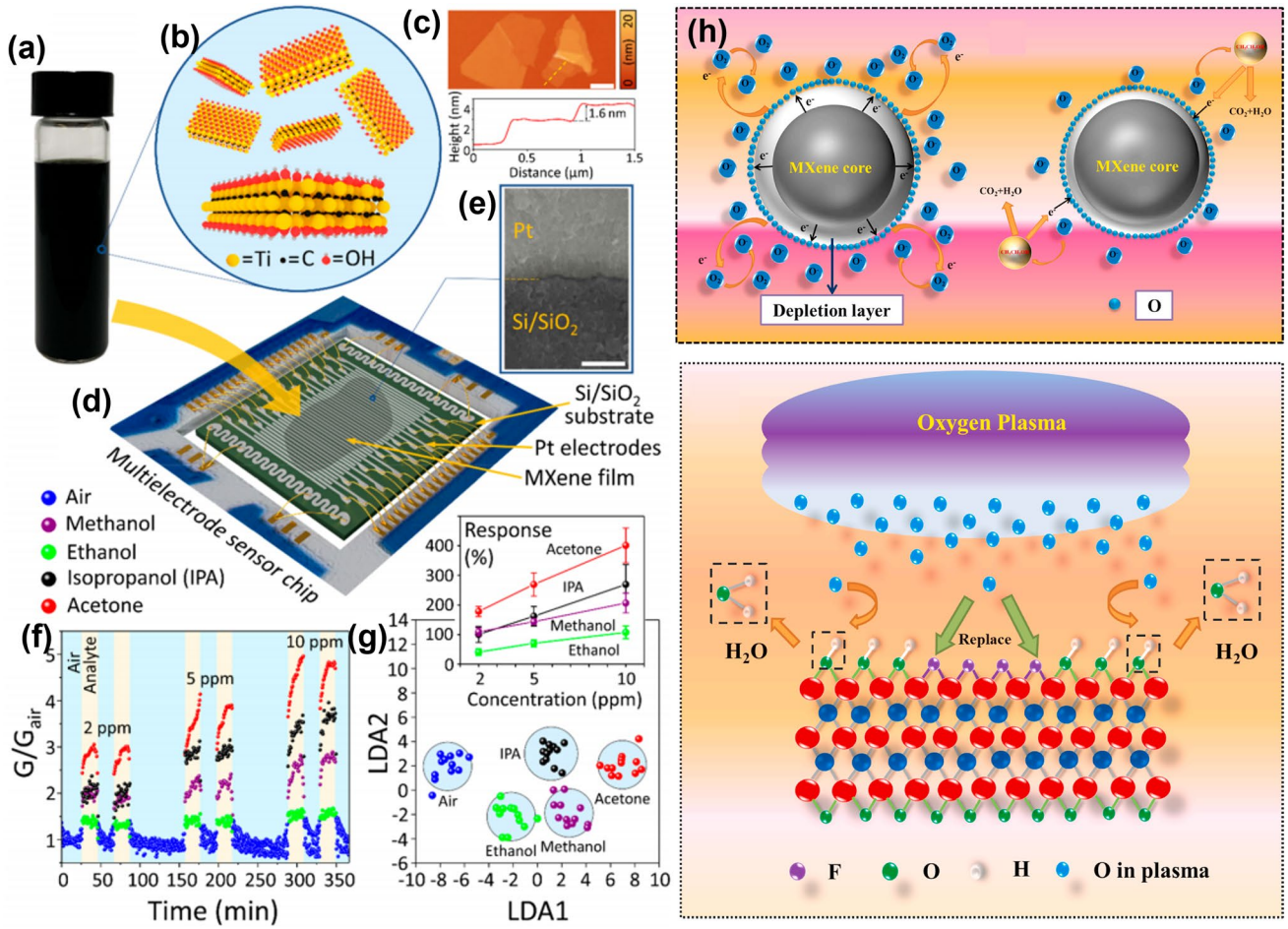

Fig. 8 Characterization of gas sensing in partially aluminized $Ti_3C_2T_x$ MXene films on a multisensor chip. **a** Stabilization of the aqueous solution of layered MXene in photographic form. **b** Diagram of the construction of a single-layer $Ti_3C_2T_x$ MXene sheet. **c** Photographs of an AFM image of a $Ti_3C_2T_x$ MXene flake on Si/SiO_2, the scale bar is 1 μm m. **d** Multi-electrode chip scheme for MXene sheet membrane produced by drop-in casting method. **e** SEM image of the MXene films overlaying the area in contact between the platinum alloy electrode and the Si/SiO_2 backing. Scale bar is 1 μm. **f** MXene partial conductivity G(t) variation, relative to conductivity in air (in dry air at 350 °C with acetone, isopropyl alcohol (IPA), ethanol and methanol dosed sequentially at 2–10 ppm). **g** Illustration: dependence of chemical reactions, $S = \Delta G/Gair$, average of all MXene sensor elements for organic vapor focus on a chip; error bands indicate the fluctuation of resistance of the entire multisensor array. Reproduced with permission from Ref. [148]. **h** Schematic diagram of the possible gas sensing mechanism of $Ti_3C_2T_x$ MXene. Reproduced with permission from Ref [149]

method. Wang et al. [153] successfully synthesized SnO-SnO_2 (p–n junction) and $Ti_3C_2T_x$ MXene nanocomposites for gas sensing by a one-step hydrothermal method. Zinc oxide (ZnO) has long been used as a gas detector. Although it has good response to various gases, high operating temperature limits the widespread application as a gas sensing material. Qui et al. [157] ZnO/$Ti_3C_2T_x$ MXene nanocomposite composed of 2D multilayer MXene and 1D ZnO nanoparticles prepared a room temperature toxic gas sensor (Fig. 12a). The nanocomposite material exhibits enhanced response and recovery behavior to toxic gases, superior to pure $Ti_3C_2T_x$ MXene and pure ZnO. Its gas sensing principle is shown in Fig. 12b. Under the irradiation of the sun, $ZnSO_3$ nanocube and layered $Ti_3C_2T_x$ MXene were synthesized by simple static self-assembly to synthesize $ZnSO_3/Ti_3C_2T_x$ MXene nanocomposites (Fig. 12c). Sima et al. [158] found that the $ZnSO_3/Ti_3C_2T_x$ MXene nanocomposite-based sensor displayed significant selectivity for formaldehyde, with high response (194.7% to 100 ppm and 62.4% to 5 ppm) (Fig. 12d), and rapid response/recovery times (6.2/5.1 s at 100 ppm formaldehyde) (Fig. 12e), and these tests were

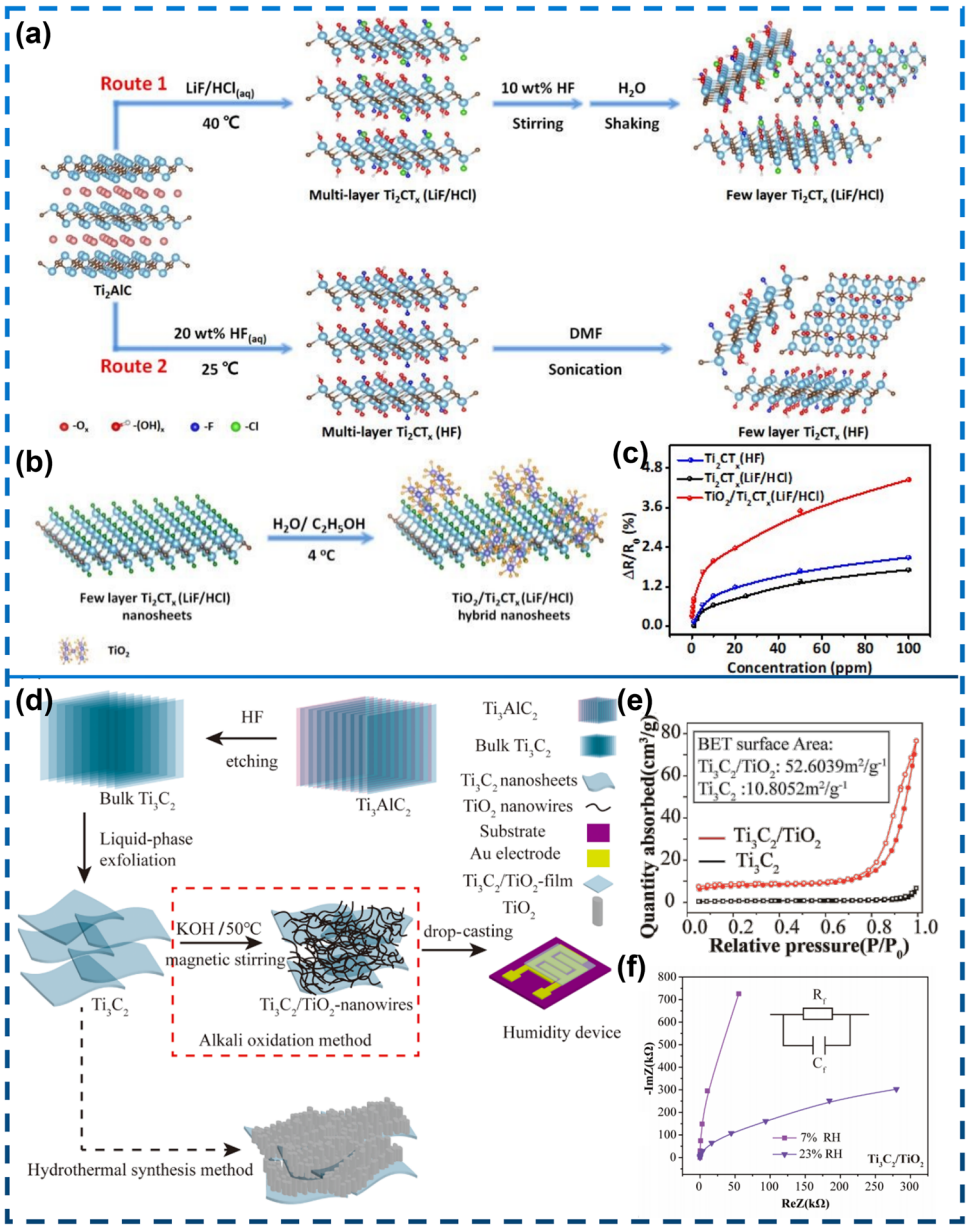

Fig. 9 **a** Preparation process of Ti_2CT_x (LiF/HCl) nanosheets (Route 1) and Ti_2CT_x (HF) nanosheets (Route 2) is schematically shown. **b** Diagram of the fabrication of the TiO_2/Ti_2CT_x (LiF/HCl) blend nanosheets. **c** Regularized resistance changes of each sensor at various NH_3 levels. Reproduced with permission from Ref. [150]. **d** Ti_3C_2/TiO_2-nanowires material preparation process: HF etching, liquid-phase exfoliation, alkali oxidation, and other methods. **e** BET surface area of Ti_3C_2 and Ti_3C_2/TiO_2. **f** Complex impedance plots of Ti_3C_2/TiO_2 composite film at 7%-23% RH. Reproduced with permission from Ref. [159]

conducted at RT. Figure 12f shows the gas sensing scheme of the $ZnSO_3/Ti_3C_2T_x$ MXene laminate.

Different research groups have conducted extensive research on gas sensing performance using pure $Ti_3C_2T_x$ and its complexes with different metal oxides, such as V_2O_5 [45], α-Fe_2O_3 [155], In_2O_3 [156], and $K_2Ti_4O_9$ [160]. Liu [155] successfully prepared heterogeneous composite materials of α-Fe_2O_3 and Ti_3C_2Tx MXene using a simple hydrothermal method (Fig, 13a-c), and characterized their morphology and microstructure through various characterization methods (Fig. 13b–f). The results indicate that a size of approximately 250 nm wide was prepared

© The authors
https://doi.org/10.1007/s40820-024-01430-4

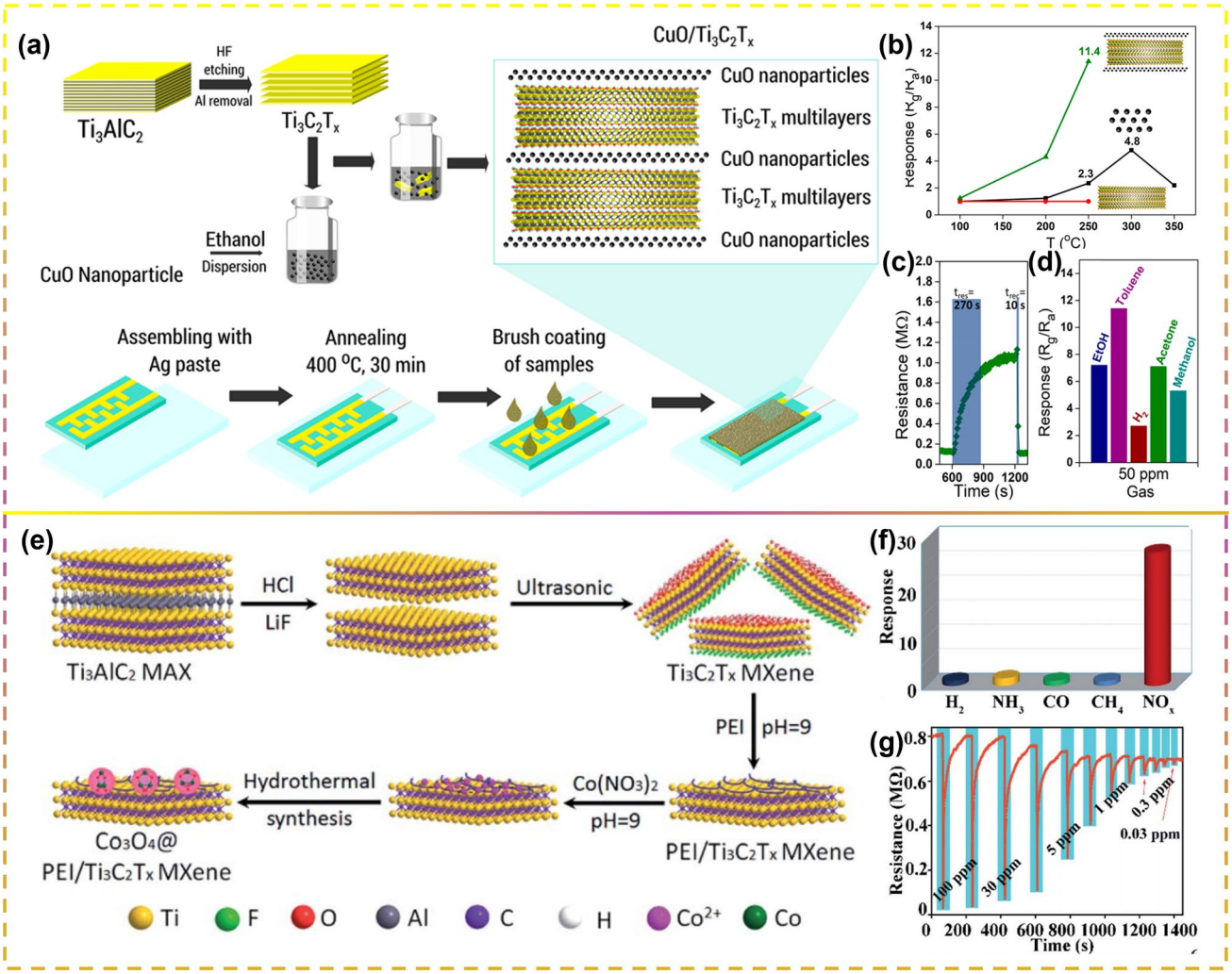

Fig. 10 **a** Schematic Representation of a Facile Preparation of CuO nanoparticles/$Ti_3C_2T_x$ Hybrid Heterostructures and Gas Sensor Device Fabrication. **b** Gas sensing response of CuO, $Ti_3C_2T_x$ MXene, and CuO/$Ti_3C_2T_x$ MXene tested at different working temperatures. **c** Response/recovery times. **d** Selectivity of CuO/$Ti_3C_2T_x$-30 wt% to 50 ppm of tested gas. Reproduced with permission from Ref. [145]. **e** Schematic illustration of the Co_3O_4@PEI/$Ti_3C_2T_x$ MXene composites. **f** CoPM-24 sensor selectivity study under the influence of the presence of various gases at 100 ppm. **g** Momentary feedback of CoPM-24 (Co_3O_4@PEI/$Ti_3C_2T_x$) sensor to 100–0.03 ppm NO_x. Reproduced with permission from Ref. [146]

α-Fe_2O_3 nanocube and uniformly distributed on the surface of $Ti_3C_2T_x$ MXene nanosheets. The results indicate that a size of approximately 250 nm wide was prepared α-Fe_2O_3 nanocube and uniformly distributed on the surface of $Ti_3C_2T_x$ MXene nanosheets. The gas sensitivity test results show that compared with other typical gases, the sensor based on α-Fe_2O_3/$Ti_3C_2T_x$ MXene composite material exhibits excellent selectivity toward acetone, and very favorable response to 5 ppm acetone: 16.6% (Fig. 13g), high rate of response and recovery: 5/5 s (Fig. 13h), excellent linearity, and significant repeatability at room temperature (RT) (Fig. 13i) [160].

Taken together, as shown in Table 3, TiO_2 is the most commonly used metal oxide composition to assist MXenes in detecting reducing gases at room temperature. For the response of NH_3 gas, MXenes, and tungsten tin oxides showed the best response values, but the lower response limit did not change significantly, and the response recovery time needs further investigation [164, 192]. On the other hand, we found that Co_3O_4 and ZnO are suitable support materials for the detection of oxidizing gases using MXenes. In

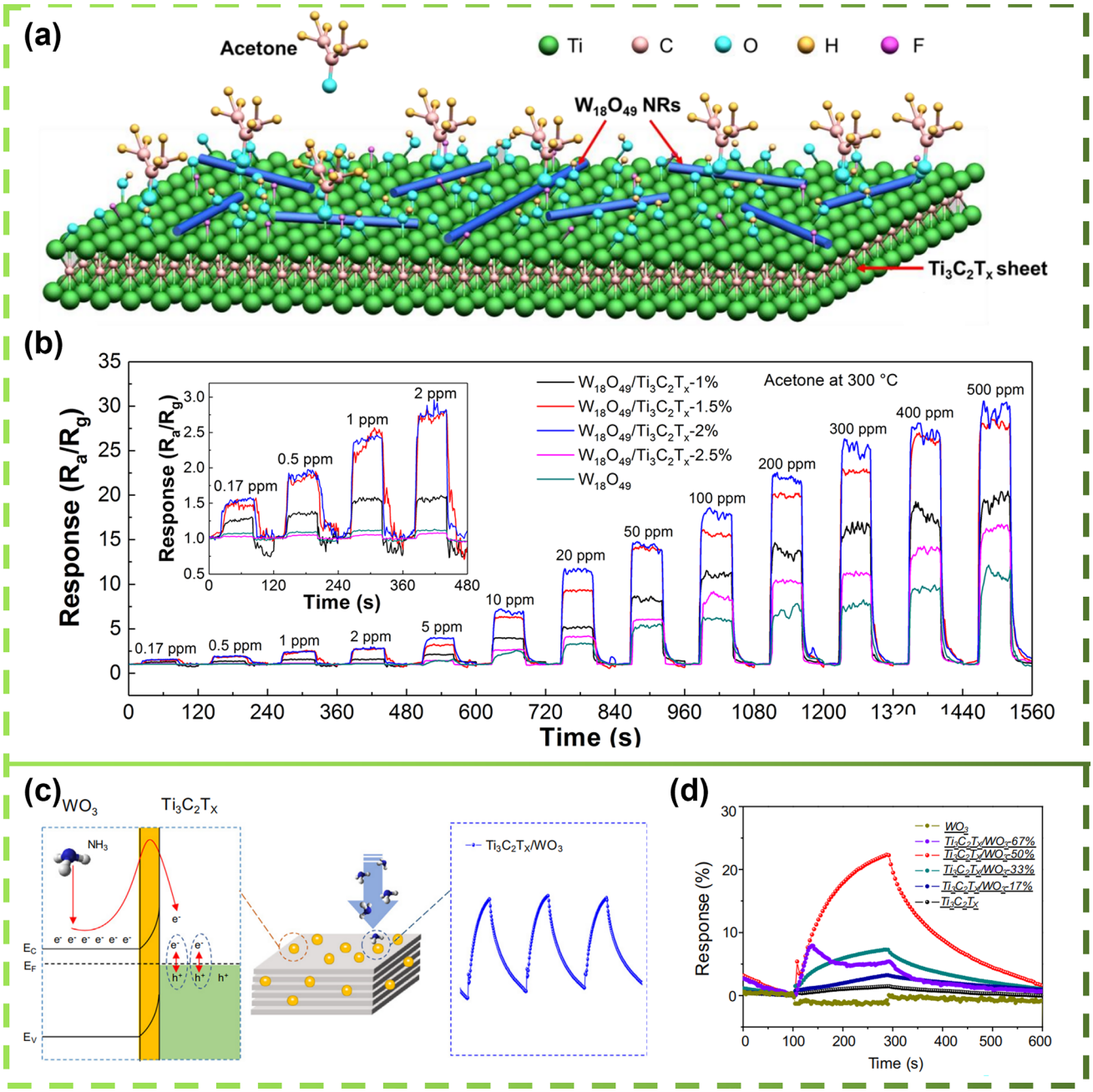

Fig. 11 **a** Image demonstrating the mechanism of acetone sensing by $W_{18}O_{49}/Ti_3C_2T_x$ nanocomposites. **b** Image of instantaneous response curves of $W_{18}O_{49}/Ti_3C_2T_x$-based sensors in the range of acetone concentrations from 0.17 to 500 ppm. Reproduced with permission from Ref. [187]. **c** Mechanisms of sensing of NH_3 by $Ti_3C_2T_x/WO_3$-50% of composites. **d** Different amounts of WO_3 of the composite sensor in response behavior to 1 ppm NH_3 at room temperature. Reproduced with permission from Ref. [151]

the presence of In_2O_3 and α-Fe_2O_3, other reducing volatile organic compounds, such as methanol and acetone, were better perceived, respectively.

4.3 MXene/TMDs

Two-dimensional chalcogenides are two-dimensional materials with unique structures, excellent mechanical, electrical, optical properties, and low energy consumption. It is a

© The authors
https://doi.org/10.1007/s40820-024-01430-4

well-explored sensing application material. However, for gas/VOC sensing, the research on the composite materials of 2D chalcogenides and MXene is still a rarely explored field. So far, there are only two reports on the combination of MXene and sulfides for gas sensing. Firstly, Qui et al. [161] prepared $MoS_2/Ti_3C_2T_x$ heterostructures with interconnected network nanostructures through a simple hydrothermal method (Fig. 14a). The synthesized $MoS_2/Ti_3C_2T_x$ heterostructure exhibits significant lattice matching (Fig. 14b), where vertically arranged MoS_2 nanosheets grow on $Ti_3C_2T_x$ MXene and have a large specific surface area. The obtained gas sensor exhibits very high sensitivity and selectivity to NO_2 gas exposure, reaching up to 25% at 10 ppm, as well as rapid recovery and long-term stability (Fig. 14c, d). Due to the large number of Mo active sites and the conductivity of $Ti_3C_2T_x$ MXene, which can accelerate electron movement and excellent heterojunction interface contact, the presented structure exhibits enhanced NO_2 sensing activity. Secondly, Chen et al. [162] reported on the $Ti_3C_2T_X/WSe_2$ nanohybrid material, which was prepared through simple surface treatment and peel-based

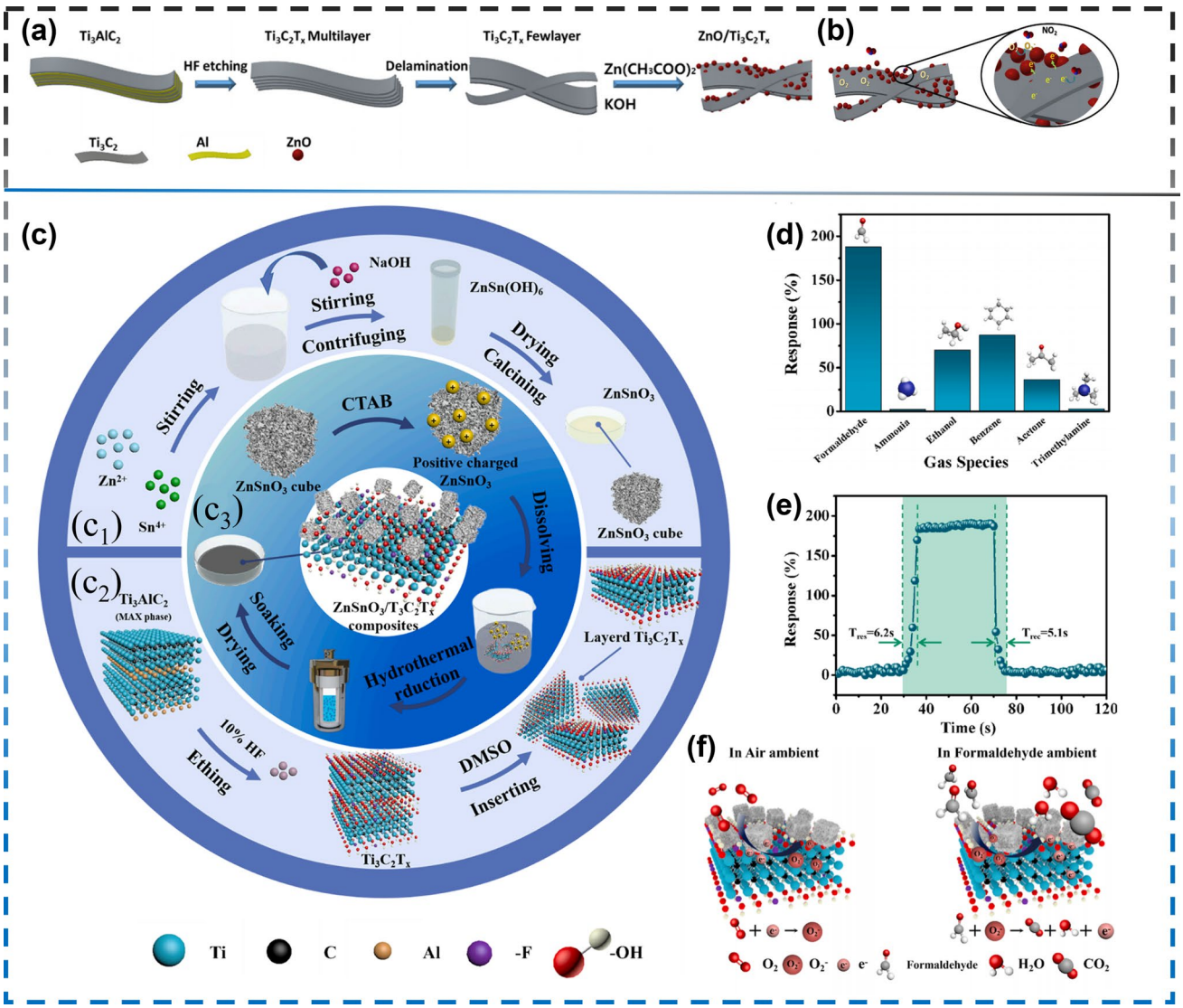

Fig. 12 **a** Schematic synthesis procedure of $ZnO/Ti_3C_2T_x$ heterostructure. **b** Schematic NO_2-sensing reaction mechanism of $ZnO/Ti_3C_2T_x$ nanocomposite. Reproduced with permission from Ref. [157]. **c** Schematic of fabrication process of (c_1) $ZnSnO_3$ nanocube, (c_2) layered $Ti_3C_2T_x$ MXene and (c_3) $ZnSnO_3/Ti_3C_2T_x$ MXene composites. **d** Selective curve of $ZnSnO_3/Ti_3C_2T_x$ MXene composites to 100 ppm different gas at room temperature. **e** Response performance of $ZnSnO_3/Ti_3C_2T_x$ MXene composites to 100 ppm form aldehyde at room temperature. **f** Schematic of gas sensing mechanism of $ZnSnO_3/Ti_3C_2T_x$ MXene composites. Reproduced with permission from Ref. [158]

process (Fig. 14e), and combined as a sensing material into inkjet printing and wireless operation sensors (Fig. 14f). The sensing measurement has excellent repeatability and reproducibility. The energy band diagram of the $Ti_3C_2T_x/WSe_2$ sensor in the presence of ethanol shows n-type sensing behavior and Schottky barrier modulation (Fig. 14g). Compared with sensors made from raw $Ti_3C_2T_x$ and raw WSe_2, the $Ti_3C_2T_x/WSe_2$ hybrid sensor exhibits a 12-fold improvement in ethanol sensitivity, low electrical noise, sound selectivity, and ultra-fast response/recovery characteristics (Fig. 14h). Table 3 summarizes a detailed overview of sensors for MXene and TMDs composite materials.

4.4 MXene/MOF

In recent decades, metal organic frameworks (MOFs) have developed rapidly and their popularity has not decreased, making them a hot topic in the field of materials. However, the conductive MOF obtained by combining MOF and MXene breaks the shackles of MOF materials that are almost non-conductive, perfectly combines the controllable structure of organic materials and the long-term order of inorganic materials, plus the unique high electron mobility, conductive MOF can be described as a favorite, and is also one of the most potential materials in gas sensing applications [163], such as Chang et al. [164] designing and preparing a rod-shaped porphyrin based metal oxide (Co TCP (Fe)) and MXene ($Ti_3C_2T_x$) through hydrogen bonding to

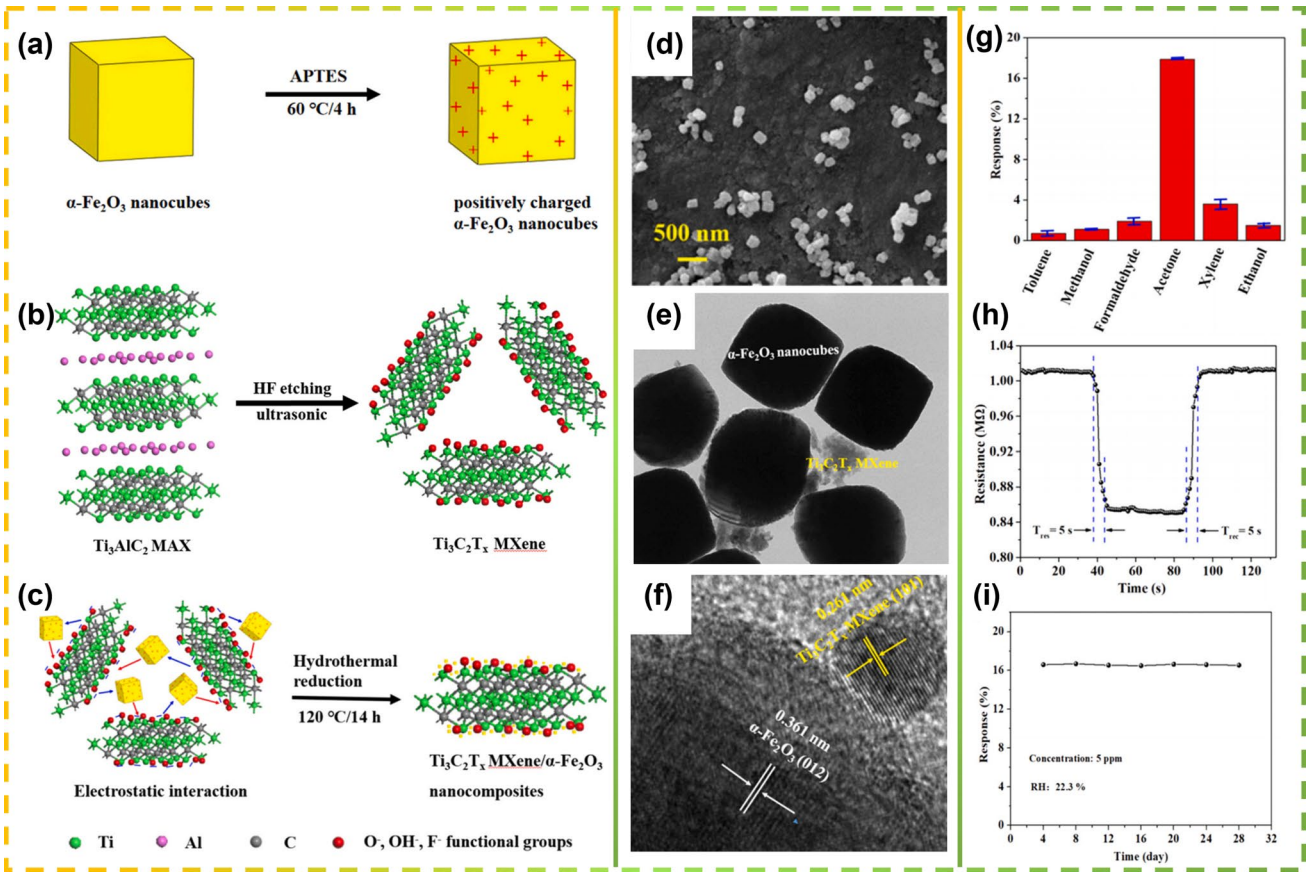

Fig. 13 Illustration of the preparation process of **a** positively charged α-Fe_2O_3 nanocubes, **b** Sheet-like $Ti_3C_2T_x$ MXene and **c** α-$Fe_2O_3/Ti_3C_2T_x$ MXene composites. **d** SEM images of α-$Fe_2O_3/Ti_3C_2T_x$ MXene composites. **e** TEM image. **f** HRTEM image of the α-$Fe_2O_3/Ti_3C_2T_x$ MXene composites. Reproduced with permission from Ref. [155]. **g** Selective property of the sensor based on α-$Fe_2O_3/Ti_3C_2T_x$ MXene composites to 5 ppm of various target gases at room temperature. **h** The real-time resistance measurement of α-$Fe_2O_3/Ti_3C_2T_x$ MXene composite sensor toward acetone vapor at RT. **i** Long-term stability of the α-$Fe_2O_3/Ti_3C_2T_x$ MXene-based sensor for 5 ppm acetone. Reproduced with permission from Ref. [160]

© The authors https://doi.org/10.1007/s40820-024-01430-4

form a chemically resistant NO sensing hybrid (Co-TCPP (Fe)/$Ti_3C_2T_x$) (Fig. 15a). The sensor based on Co TCP (Fe)/$Ti_3C_2T_x$ shows excellent NO sensing performance at room temperature (Fig. 15b), including high response (= 2.0, 10 ppm) (Fig. 15c), reliable repeatability, high selectivity, low actual detection limit (pLOD, 200 ppb), and rapid room temperature NO sensing response/recovery speed (95/15 s, 10 ppm) (Fig. 15d).

4.5 MXene/Polymer

Polymers have excellent flexibility, favorable sensitivity, appropriate electrical conductivity, low cost, a large number of organic groups to interact with the gas on the surface, light weight, and low reaction temperature, making them suitable for gaseous/VOC sensing applications when mixed with MXenes. MXene/polymer composite sensors are used to identify ammonia [101, 103, 165, 166], ethanol [32, 105], methanol [33, 104], acetone [31, 102], and humidity [99, 100, 112, 113] for wear and tear [189–194]. With respect to ammonia identification, the original MXene-based sensor shows excellent NH_3 sensing characteristics, but ammonia has very high adsorption energy and NH_3 is difficult to partition from the MXene screen during recovery, and demonstrates extended recognition time as well as wandering of the baseline resistance. To surmount these limitations, Li et al. [165] developed in situ a flexible chemorepulsive gas sensor based on a hybrid polyaniline (PANI)/$Ti_3C_2T_x$ sensitive layer for tracking ammonia volatilization out of agriculture using self-assembled method in situ (Fig. 16a). The sensor exhibits excellent NH_3 sensing performance over a temperature range of 10–40°C at 20%–80% relative humidity (RH) (sensing response to 10 ppm ammonia peaks at 4.7 at 40% RH, which is almost three times higher than in dry air (~ 1.6)) (Fig. 16b–d). Zhao et al. [105] also used over-PANI, via a low-temperature in situ polymerization method to rationally modified PANI particles coated with $Ti_3C_2T_x$ nanosheets (Fig. 17a, b). This evoked remarkable detection sensitivity, a rapid response/recovery rate and mechanistic stability as well at room temperature. A year later, Zhao et al. [166] also developed room temperature nanocomposites based on 2D MXenes materials and cationic polyacrylamide (CPAM) (Fig. 17c) with high gas responsiveness and flexibility aimed at building high-performance ammonia sensors.

Conductive polymers-3,4-ethylenedioxythiophene (EDOT) and poly(4-styrenesulfonate) (PSS) are also commonly used to composite with MXene. Jin et al. [103] used a dip coating technique to make a gas sensor from the resulting PEDOT:PSS/MXene composite (Fig. 18a). NH_3 at room temperature demonstrated a strong gas response of 36.6% to 100 ppm NH_3 with recovery and response times of 116 and 40 s. Furthermore, the hybrid sensor presented stronger sensitivity performance compared to pure PEDOT:PSS and $Ti_3C_2T_x$ MXene-based sensors, evidencing that the PEDOT:PSS copolymer and $Ti_3C_2T_x$ MXene two-dimensional ingredients have a synergistic effect on each other. In addition to showing a high response to ammonia gas, it also responded well to other gases, e.g., Wang et al. [104] used a 4:1 mixture of PEDOT:PSS and $Ti_3C_2T_x$ to prepare a methanol gas sensor (Fig. 18b, c), where the reaction rate of 5.54 was high for the largest reaction and the second largest reaction tested at room temperature when compared to pure PEDOT:PSS and pure $Ti_3C_2T_x$.

For humidity sensing, composites of polymers with MXene are excellent materials. The synergistic effect of chitosan-modified $Ti_3C_2T_x$ exhibited remarkable performance, enhancing the electrical response to H_2O molecules. Inspired by the structure of onions (Fig. 19a), Li and colleagues [112] synthesized ion-excited MXene/chitosan–quercetin multilayer membranes (MCQMs) using a layering-by-layer assembly approach (Fig, 19b, c) for which strong interactions to the molecules were found (Fig. 19d). The monolayer pair exhibited the highest resistance in MCQMs, with improved conductivity and reproducibility as the number of layers increased, and the sensor exhibited an ultra-high responsiveness (317% at 90% RH), a wide field of detection, and praiseworthy response and recovery speeds (0.75 and 1.6 s at 90% RH) (Fig. 19e–g). For true breathing studies, An et al. [110] described the mechanism of aqueous adsorption of a multilayer component made of MXene microsheets with polyelectrolytes (Fig. 19h) intended for super-fast humidity sensing (Fig. 19i–k), and they showed that MXene/polyelectrolyte multilayers prepared using layer-by-layer (LbL) components exhibited response and recovery times exceeding those of most humidity sensors (Fig. 19l, m).

In addition, comparing all MXene/polymer gas sensing materials in Table 3, it was found that among all reported polymers, PEDOT: PSS and polyaniline were the most

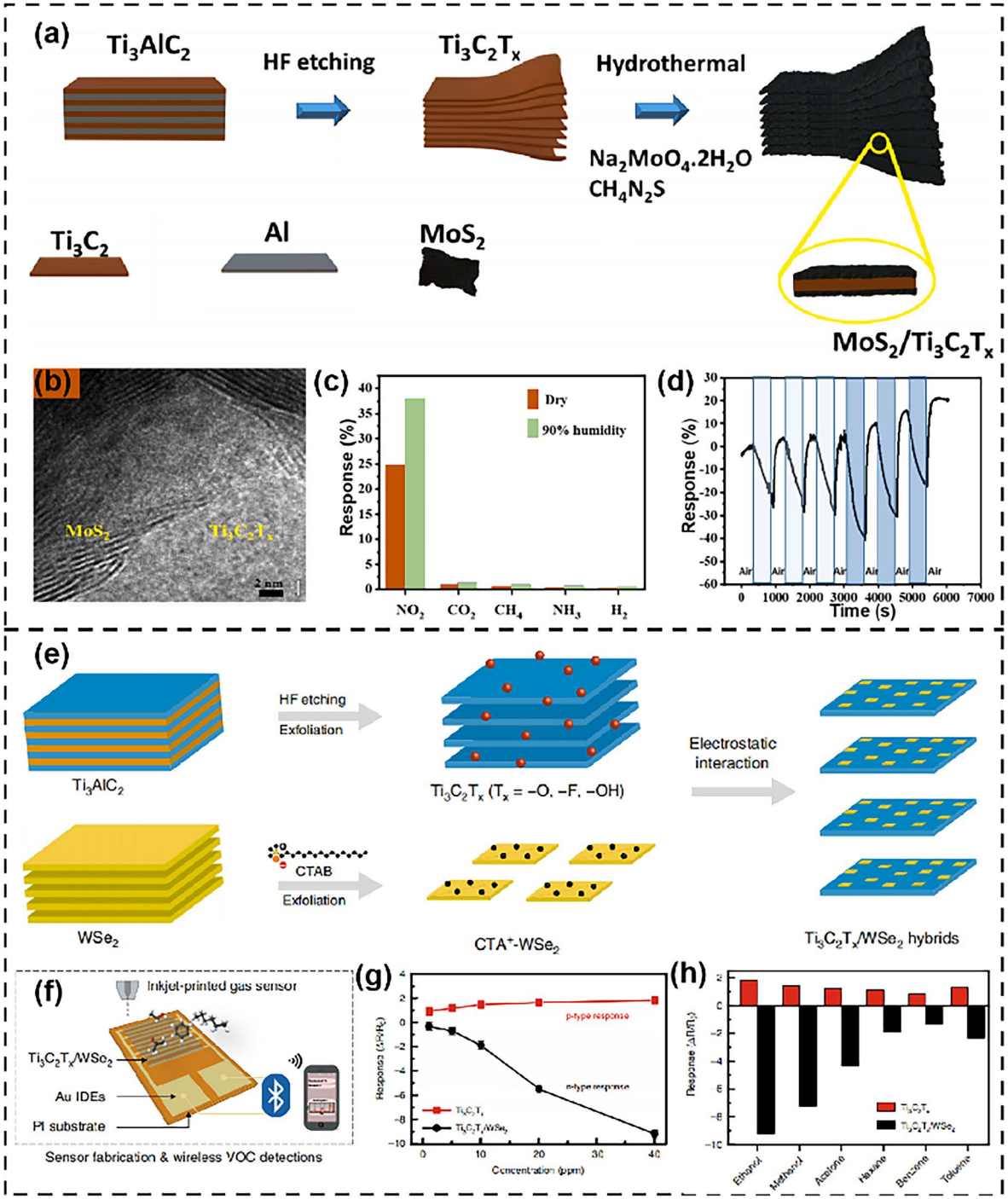

Fig. 14 **a** Schematic illustrating the synthesis process of the $MoS_2/Ti_3C_2T_x$ heterostructure from the Ti_3AlC_2 MAX phase. **b** HRTEM images of the $MoS_2/Ti_3C_2T_x$ heterostructure. **c** Comparison of responses of MT2 sample to various gases at 10 ppm concentration. **d** Cyclic responses of MT2 to 10 and 20 ppm NO_2 gas. Reproduced with permission from Ref. [161]. **e** Schematic illustration of preparation processes for $Ti_3C_2T_x/WSe_2$ nanohybrids. **f** Schematic illustration of inkjet-printed gas sensors in detection of volatile organic compounds with a wireless monitoring system. **g** Comparison of gas response as a function of ethanol gas concentrations for $Ti_3C_2T_x$ and $Ti_3C_2T_x/WSe_2$ sensors. **h** Selectivity test of the $Ti_3C_2T_x$ and $Ti_3C_2T_x/WSe_2$ sensors upon exposure to various VOCs at 40 ppm. Reproduced with permission from Ref. [162]

© The authors
https://doi.org/10.1007/s40820-024-01430-4

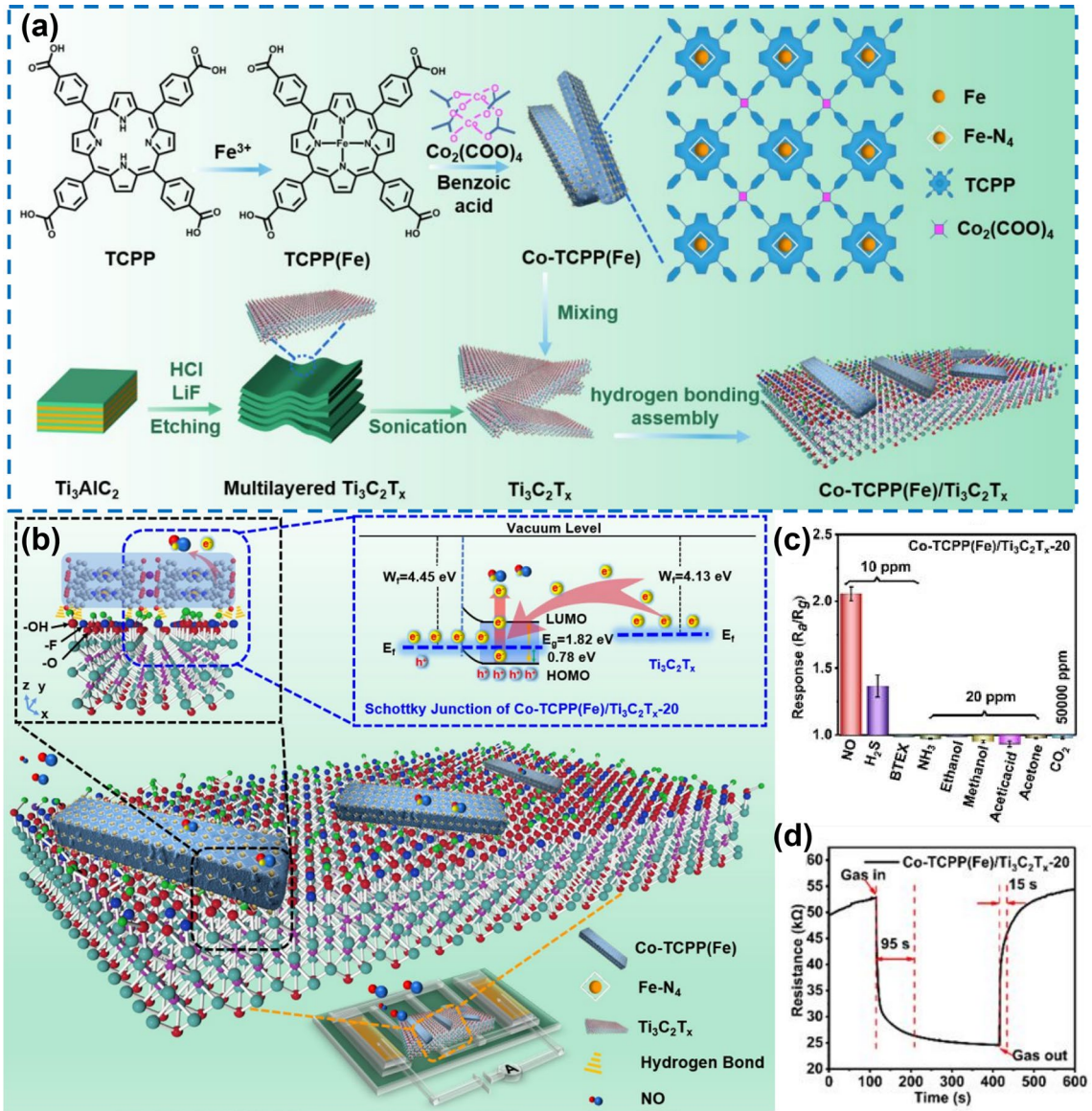

Fig. 15 **a** Synthesis process of Co-TCPP(Fe), $Ti_3C_2T_x$, and Co-TCPP(Fe)/$Ti_3C_2T_x$. **b** Schematic diagram of the sensing mechanism of the Co-TCPP(Fe)/$Ti_3C_2T_x$-20 toward NO. **c** Selectivity of the sensor to various gases at concentrations of 10 and 20 ppm. **d** Real-time response–recovery curve of the Co-TCPP(Fe)/$Ti_3C_2T_x$-20 based sensor toward 10 ppm NO at room temperature. Reproduced with permission from Ref. [164]

suitable for improving NH_3 sensing at room temperature together with MXenes. The biopolymer cellulose composite with MXenes ($Ti_3C_2T_x$/PANI/bacterial cellulose) was the most suitable for humidity sensing [195–208]. The main advantages of polymer doping with MXene are the improved selectivity and sensitivity of MXene, the disadvantages of which are poor stability and more stringent environmental requirements during measurements [148, 209–215].

4.6 Other Materials

Li et al. [111] fabricated a transparent mobile hygrometer using an inkjet printing technique, using a Ti_3C_2/Ag blend as a humidity-sensitive membrane and polydiallyldimethylammonium chloride-based (PDDA) as an adhesive barrier (Fig. 20a). The sensor has ultra-high sensitivity ($106 \pm 800\%$) (Fig. 20d), fast responsiveness (80 ms), and excellent resistance to bending (Fig. 20c, d). Liu et al. [105] reported a vacuum-assisted layer-by-layer assembly

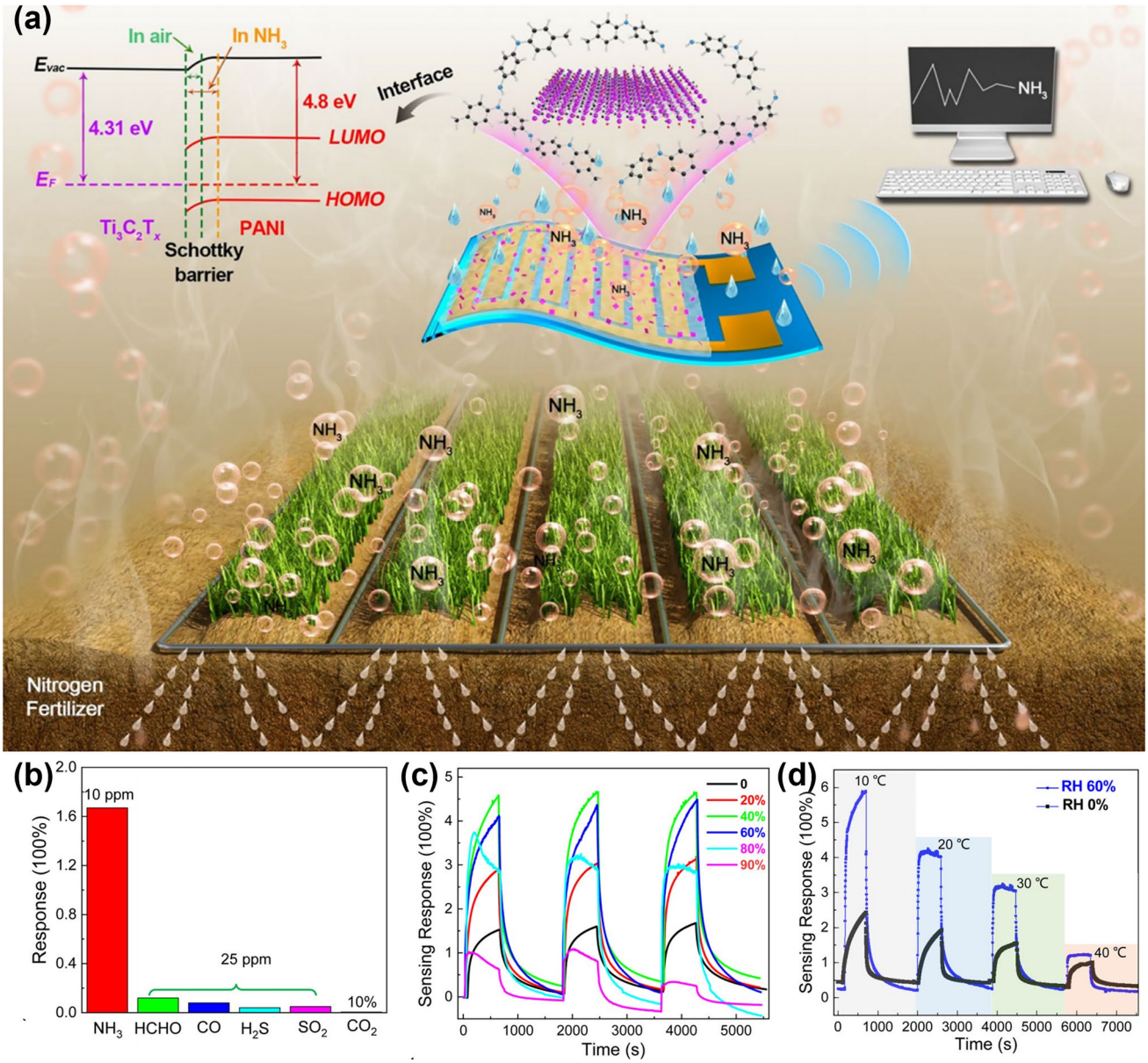

Fig. 16 **a** Application scenarios of PANI/$Ti_3C_2T_x$ hybrid sensitive film-based flexible NH_3 sensor for ammonia volatilization monitoring in agriculture. **b** Selectivity of the hybrid sensor to NH_3 and other interference gases in agricultural fields at room temperature. **c** Moisture dynamic response of the NH_3 sensing performance of PANI/$Ti_3C_2T_x$ hybrid sensitive films. **d** Dynamic sensing response of the hybrid sensor toward 10 ppm NH_3 in the range of 10–40 °C at dry air and 60% RH. Reproduced with permission from Ref. [165]

technique (Fig. 20e) for conformal deposition of conductive materials on textiles (Fig. 20f, g), resulting in a leaf like nanostructure composed of silver nanowires (AgNWs) as high conductivity skeletons (veins) and transition metal carbide/carbon nitride (MXene) nanosheets as thin layers. Having a highly sensitive humidity response (57% RH) (Fig. 20h), Zhu et al. [97] demonstrated a new paper thin-film H_2 sensor using $Ti_3C_2T_x$ MXene nanosheets and palladium colloidal nanoclusters (Pb CNC) as activators. The MXene@Pd CNC paper film is easily prepared through a vacuum filtration process based on a fully colloidal solution (Fig. 21a). The paper film is flexible, lightweight, and has a dense, shiny surface. The obtained MXene@Pd CNC thin-film sensor exhibits moderate H_2 response at room temperature in a flat or curved state (Fig. 21b). Specifically, MXene@Pd CNC thin-film sensor provides a response time

© The authors https://doi.org/10.1007/s40820-024-01430-4

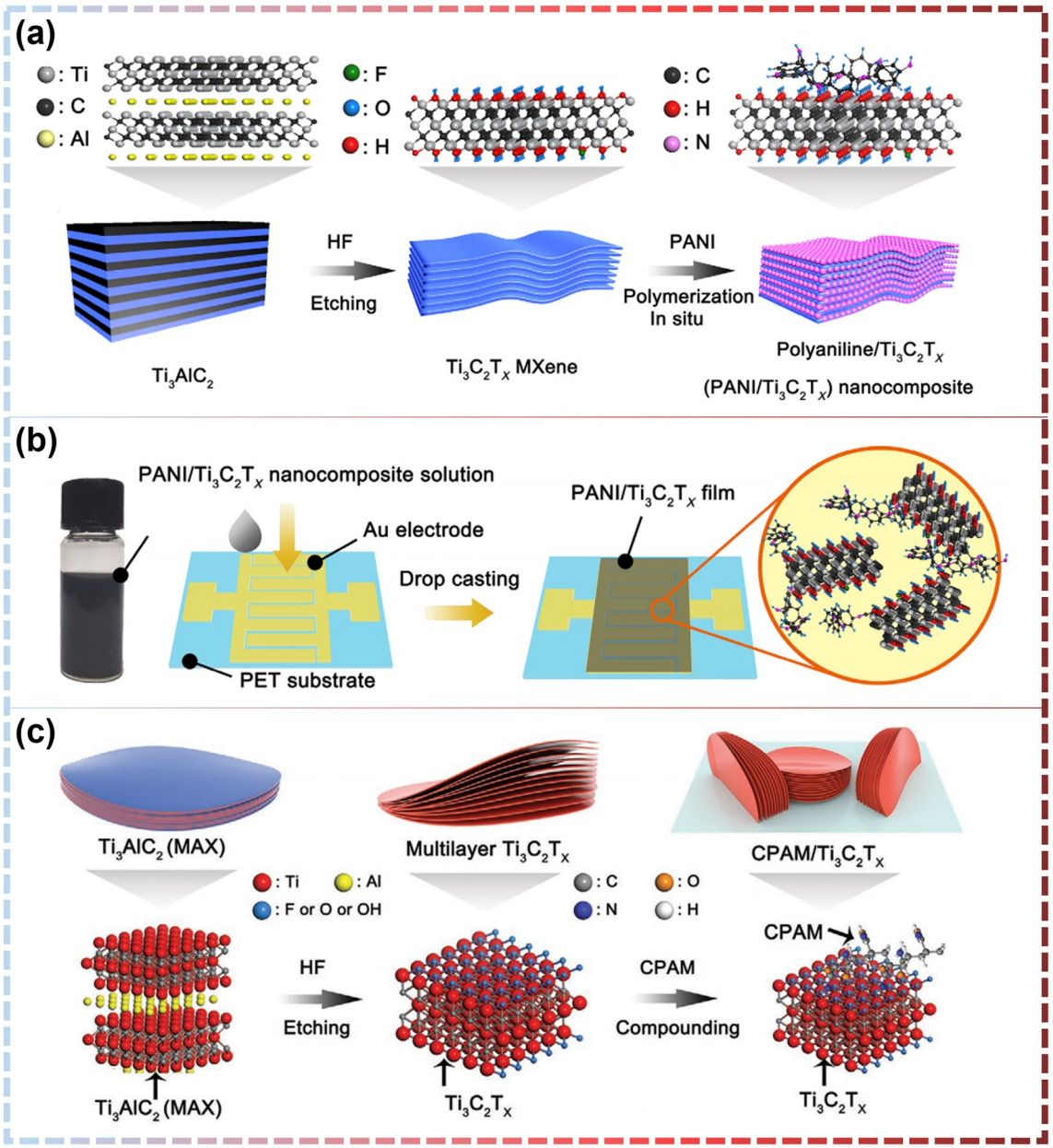

Fig. 17 **a** A diagram of the composite synthesis of PANI/$Ti_3C_2T_x$ nanocomposite, which includes the peeling process of Ti_3AlC_2 and the consolidation process of ANI. **b** Sketch of the Inter-digital polarization of the electrodes shown before and after plating PANI/$Ti_3C_2T_x$ nanocomposites. Reproduced with permission from Ref. [105]. **c** Synthesis scheme of CPAM/$Ti_3C_2T_x$ nanocomposites, including the etching process for Ti_3AlC_2 and composite process of CPAM and $Ti_3C_2T_x$. Reproduced with permission from Ref. [166]

of (32 ± 7)s and a sensitivity of S = (23.0 ± 4.0)% ± 4% H_2 (Fig. 21c). In addition, the MXene@Pd CNC sensor can perform "in situ mode" H_2 detection directly along a paper film of the required size. Intense H_2 entrapment in the ultrafine palladium carbon nanotube lattice alters the work function and leads to MXene's electron codoping, explaining the underlying regime of gas induction (Fig. 21d). Muckleyet et al. [110] reported on ion intercalated MXenes (Ti_3C_2-K and Ti_3C_2-Mg) for humidity sensing (RT). Ion embedding increases the spacing between MXene layers and absorbs H_2O molecules between the layers (Fig. 21e). The conclusion drawn from neutron scattering combined with theoretical calculations is that $K^+$and Mg^{2+} ions cause each ion to embed 2 and 5 H_2O molecules, respectively, indicating

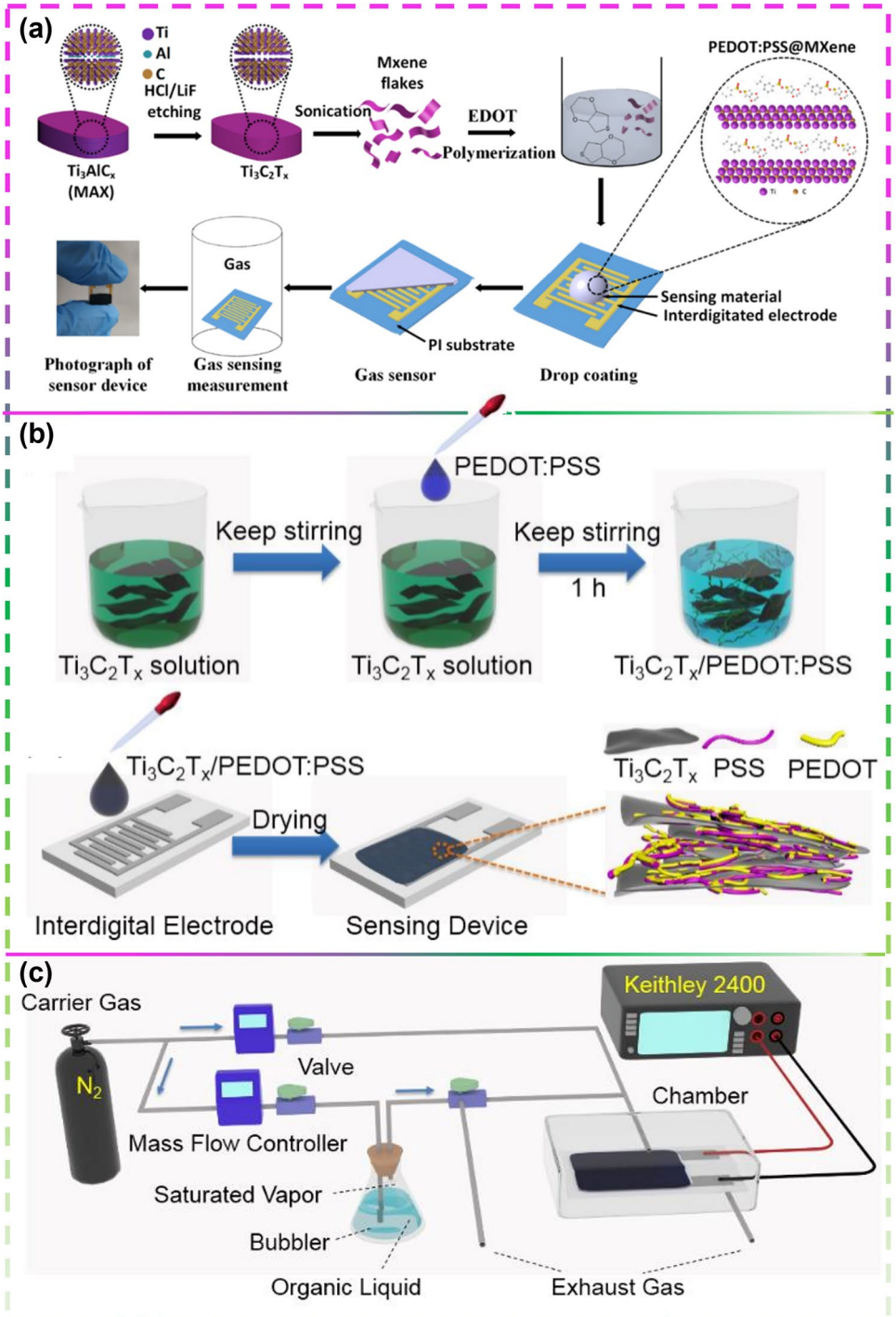

Fig. 18 **a** Schematic Illustration for the Synthesis of PEDOT:PSS/MXene Composites and the Fabrication Process of the Composite-Based Gas Sensor. Reproduced with permission from Ref. [103]. **b** $Ti_3C_2T_x$/PEDOT:PSS profile of material and gas sensor manufacturing. **c** The diagram of the experimental setup. Reproduced with permission from Ref. [104]

© The authors https://doi.org/10.1007/s40820-024-01430-4

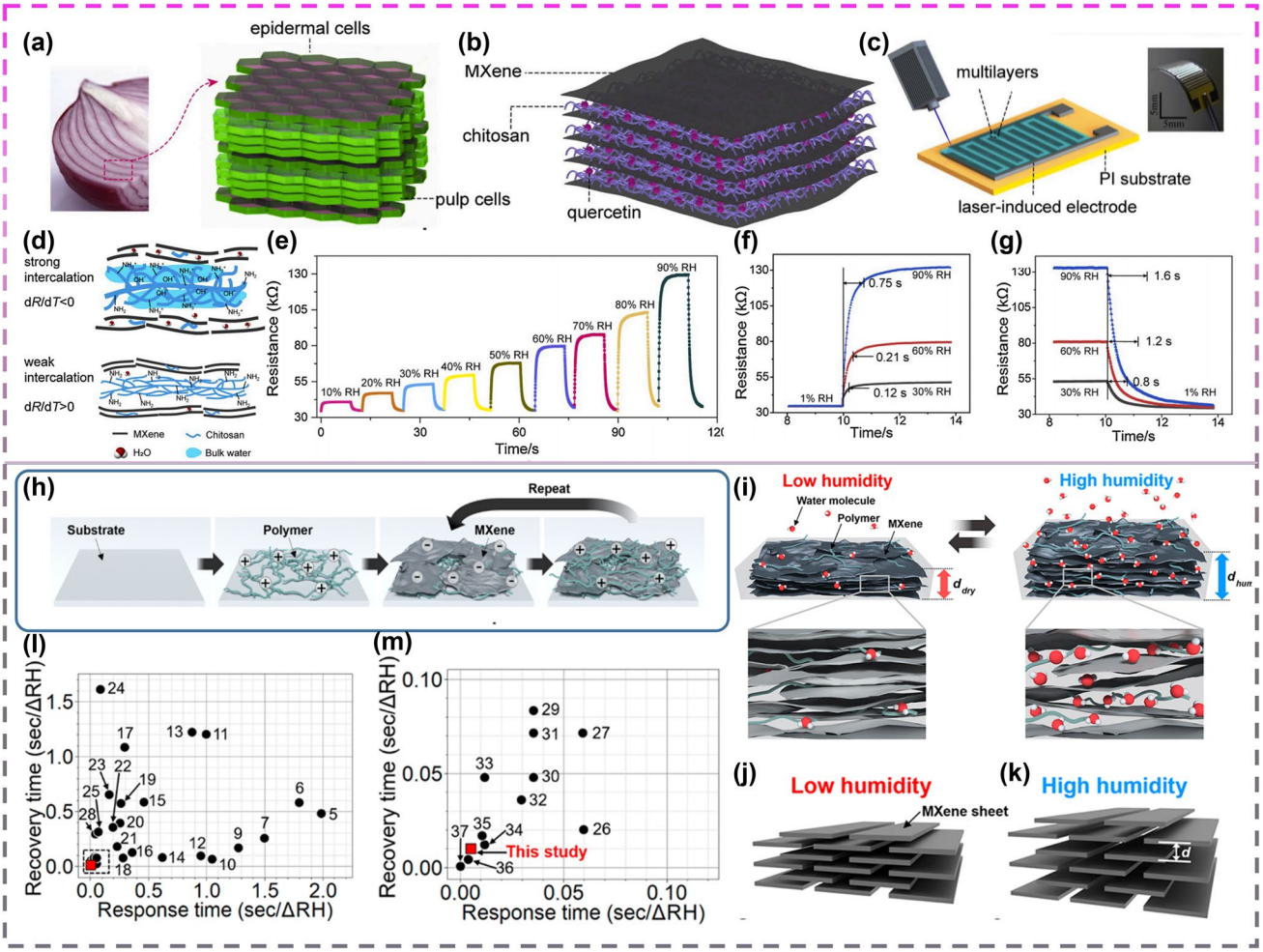

Fig. 19 **a** Photograph of purple onion scale leaves and schematic diagram of the scale leaves. **b** Schematic diagram of the MCQMs composed of MXene flakes and chitosan–quercetin membranes. **c** The humidity sensor based on laser-induced interdigitated electrode upon PI substrate. Inset shows the photograph of the flexible humidity sensor. **d** Chitosan and H_2O intercalation induced by MCQMs. **e** 4-Layer induction response to MCQMs. **f and g** A study of the reaction/recovery time of four layers to MCQM under diverse humidity conditions. Reproduced with permission from Ref. [112]. **h** Schematic of the PDAC/MXene assembly. **i** Schematic illustrations showing the proposed humidity response mechanism of the MXene/polyelectrolyte multilayers. Schematic diagrams of MXene/polyelectrolyte multilayers and the corresponding electrical circuit models for **j** low and **k** high humidity. **l** and **m** Comparison of recovery and response times between the MXene/polyelectrolyte multilayers from this study and other humidity sensors reported in the literature. Reproduced with permission from Ref. [110]

an increase in lattice parameters. They also found that the weight response of MXene to water is 10 times faster than their electrical response, indicating that the expansion/contraction of channels between MXene layers caused by H_2O leads to the capture of H_2O molecules as depletion charge dopants (Fig. 21f–i).

Within other studies, the investigators tried to improve the sampling performance by doping iron molybdate ($Fe_2(MoO_4)_3$) [107], $Ni(OH)_2$ [106] and $Ti_3C_2T_x$ MXene for H_2 (in room temperature), n-butanol (in 120 ℃), and NH_3 (in room temperature) sensing, respectively. In another study, transition metal fluoride oxide ($TiOF_2$) was surface modified on $Ti_3C_2T_x$ and subsequently used as a humidity sensor (Fig. 22a–f). By stabilizing the surface end groups, the MXene films showed improved reaction area, flexibility, and catalytic oxidation (Fig. 22j). In addition, the manufactured sensors exhibit good sensitivity and selectivity when exposed to humid environments [98] (Fig. 22h, i). Table 3 provides a detailed overview of sensors based on MXene nanocomposites. In conclusion, insertion of metallic ions and precious metals is also an effective way to improve the gas sensing performance of the original MXenes [109].

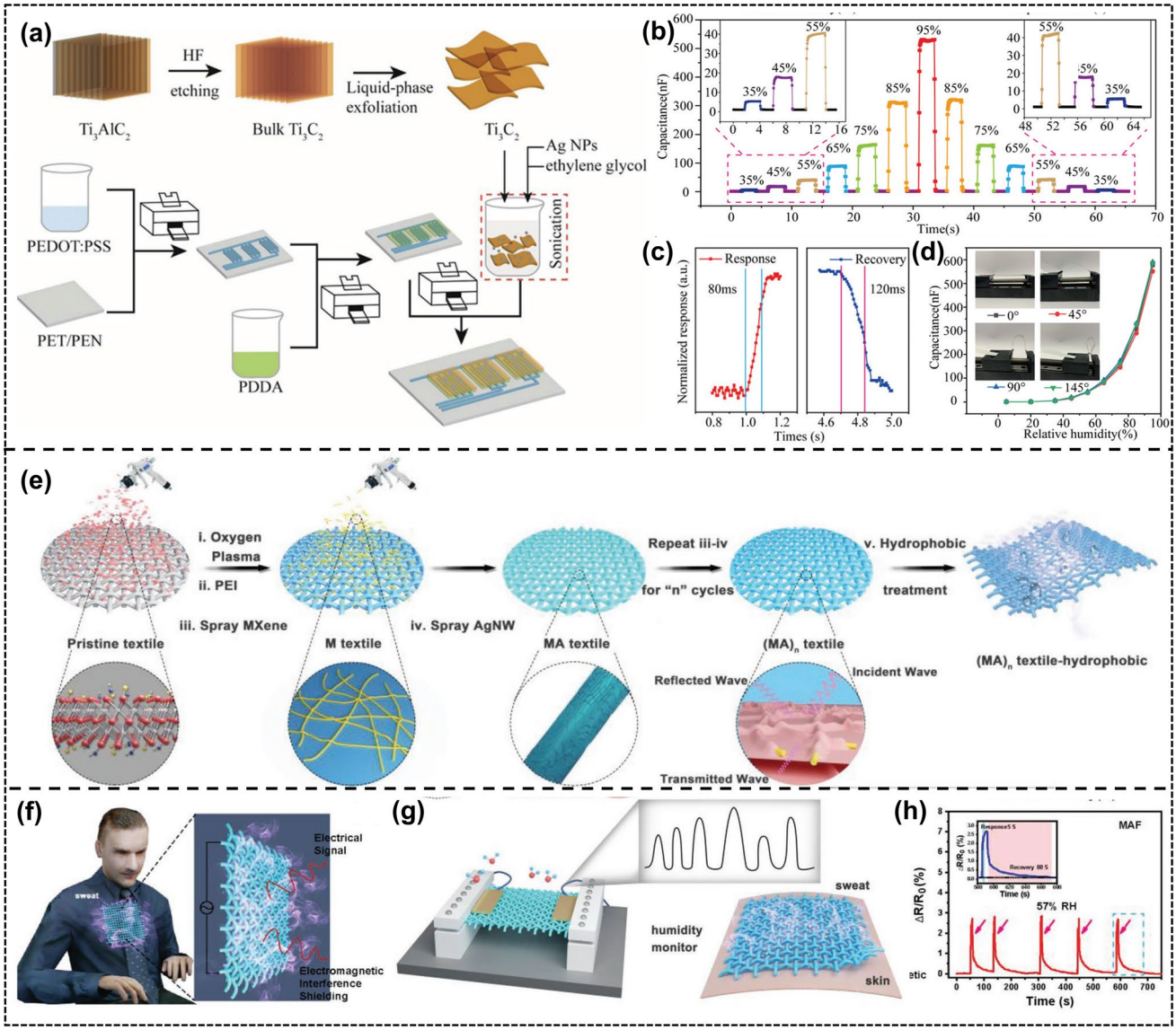

Fig. 20 **a** Flowsheet for the fabrication of Ti_3C_2/Ag-based moisture sensor by inkjet publishing method. **b** Characteristics of the TA2 response and recovery of the sensor exposed to varying relative humidity (RH) conditions. **c** Duration of response and recovery of sensor TA2. **d** Application of sensor TA2 to various curvature measurement performance. (TA2: Ti_3C_2/Ag = 2wt%). Reproduced with permission from Ref. [111]. **e** Schematic illustrating the fabrication of hydrophobic, permeable, and conductive silk textile with a vacuum-assisted layer-by-layer assembly approach. **f** Schematic of the MAF silk detecting sweating humidity. **g** Humidity response of $(MA)_nF$ silk for monitoring human sweating. **h** Sensitivities of electrical resistance change at 57% RH for MAF silk. (MAF: MXene/Ag NWs/POTs). Reproduced with permission from Ref. [108]

The new MXene gas sensor will be the next generation of universal sensors for future wearable electronic devices, with performance comparable to other 2D material sensors. Through Table 3, it can be clearly found that most of the reported 2D MXenes-based composites are suitable for sensing at room temperature. Secondly, MXenes-based composite materials have been tested for sensing different gases/VOCs and have been found to be highly sensitive to ammonia, acetone, ethanol, nitrogen dioxide, methane, and humidity. On the other hand, the application of MXene-based composites in gas sensors has advantages and disadvantages, as shown in Table 4.

© The authors
https://doi.org/10.1007/s40820-024-01430-4

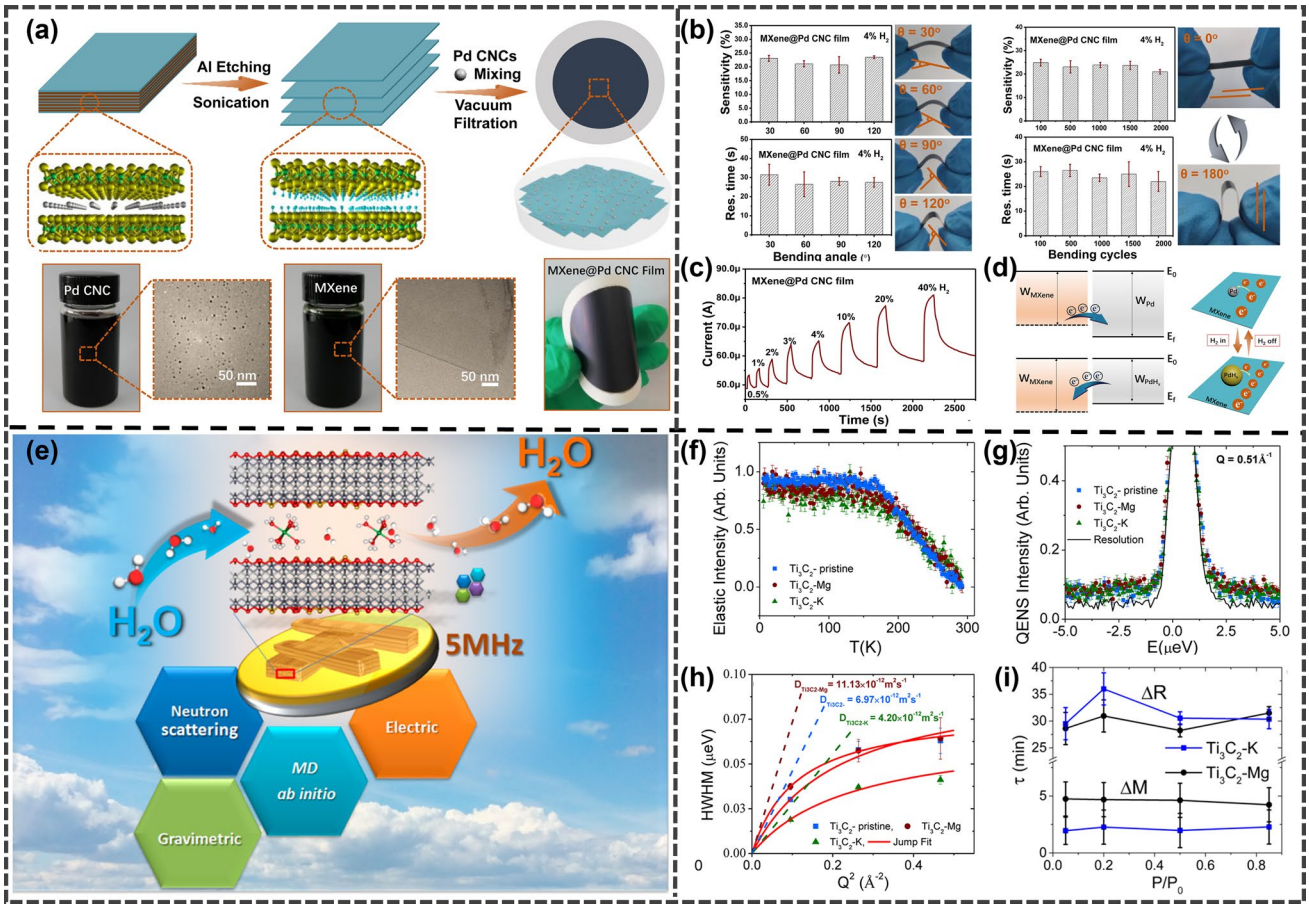

Fig. 21 **a** Diagrams of the manufacturing of MXene and MXene@Pd CNC films and photographs of the completed Pd CNC and MXene suspending solutions. **b** Sensitivities and response times of MXene@Pd CNC film sensor to 4% H_2 (left) and the corresponding flexibility show (right) under different bending angles. Sensitivities and response times of MXene@Pd CNC film sensor to 4% H_2 after n-time bending cycles (left) and one bending cycle show from θ=0° to 180° and back to 0°. **c** MXene@Pd CNC film real-time response/recovery profiles for a wide range of high H_2 compositions (0.5 ~ 40 v/v%). **d** Band diagrams of Pd and MXene before and after being exposed to H_2, and electronic transfer between the surface H_2 sorbed and Pd CNC and MXene. Reproduced with permission from Ref. [97]. **e** Design the structure of MXenes interaction between water vapor and ion insertion. **f** The normalized elastic strength of mature MXene samples measured at 2 K increments over a temperature interval of 20 to 300 K. **g** A representative normalized QENS spectrum was measured at 300 K from the same sample with a representative Q = 0.51 $Å^{-1}$. **h** Dependence of half-width at half-maximum extracted from the model fit on Q^2 Solids lines are jump diffusion model fits. The extracted water diffusion coefficient values are shown. **i** Elastic time constants for the reactions of Δ R and Δ M during H_2O desorption (τ). Reproduced with permission from Ref. [110]

5 Gas Sensing Mechanism of MXenes

5.1 MXenes Surface Adsorption Calculation

It has been theoretically proven that MXenes with semiconductor properties (M_2CO_2, M = Sc, Ti, Zr, Hf) are highly sensitive to NH_3, as shown in Fig. 23a. Xiao et al. [216] calculated and found that after NH_3 was adsorbed as an electron donor on M_2CO_2, charge transfer mainly occurred between the M atom of M_2CO_2 and the N atom of NH_3. When MXene adsorbed NH_3, the charge of NH_3 molecules was transferred to the transition metal atom on the surface of MXene, and the conductivity of Ti_2CO_2 was significantly improved. They also found that desorption of NH_3 can be easily achieved by adjusting the electrons injected into M_2CO_2, making the NH_3 sensor reversible [217]. For example, the lowest unoccupied electronic state (LUES) of Zr_2CO_2 mainly comes from Zr atoms, which means that when an additional electron is introduced into Zr_2CO_2, the electrons will fill the unoccupied electronic orbitals of Zr atoms. Therefore, the injected electrons are mainly distributed on the transition metal, leading to an increase in the metal bond length and adsorption

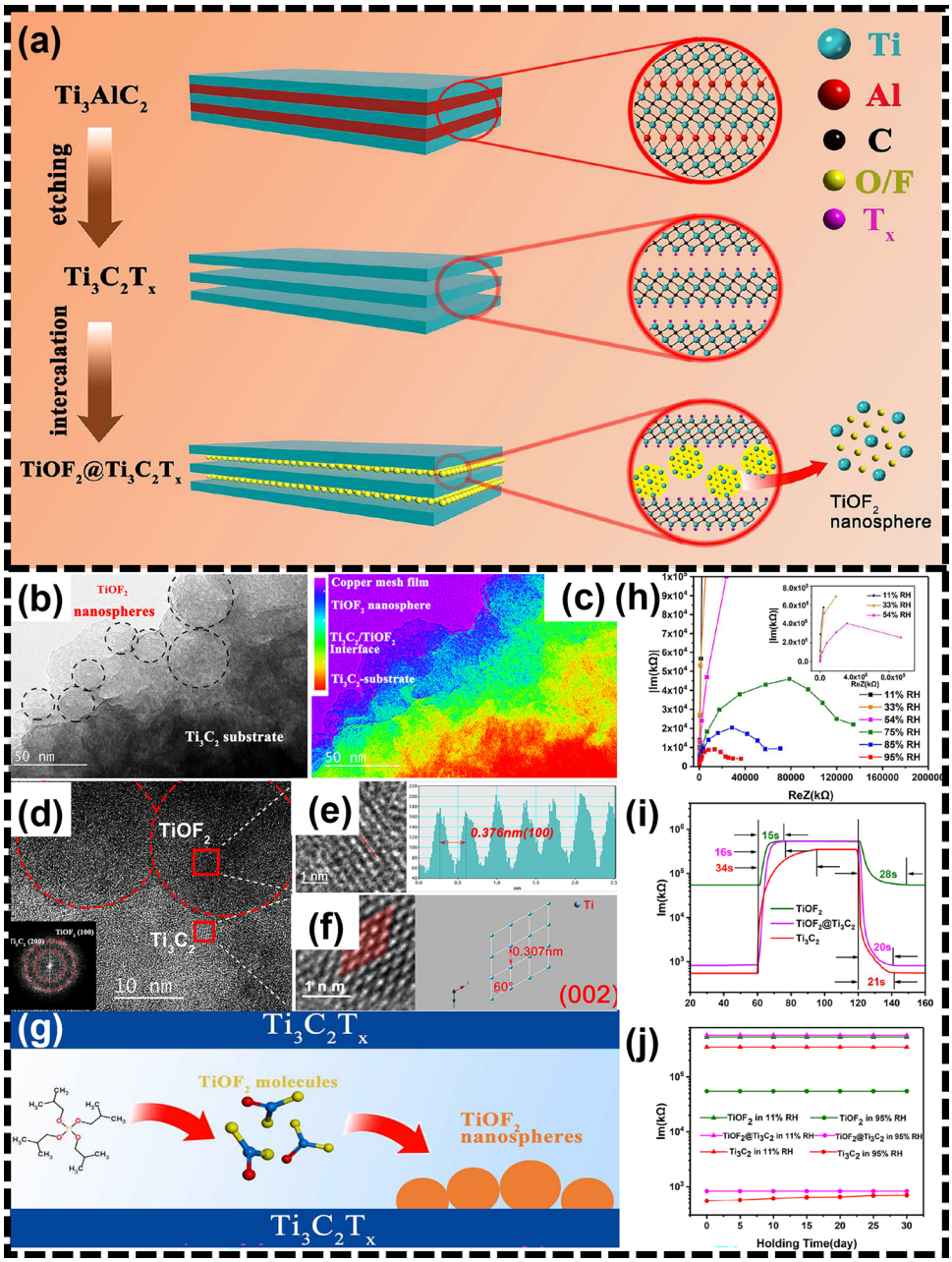

Fig. 22 **a** Scheme for the fabrication of $TiOF_2@Ti_3C_2T_x$. **b** and **c** The cross section of the monolayer of the $TiOF_2@Ti_3C_2T_x$ sheet and the rainbow map to show the composition distribution in situ. **d** TEM image of $TiOF_2$ nanospheres growing on the $Ti_3C_2T_x$ substrate. **e** HRTEM image of $TiOF_2$ nanospheres. **f** HRTEM image of Ti_3C_2 substrate. **g** Scheme for the hydrolysis and adsorption to synthesize $TiOF_2@Ti_3C_2T_x$. **h** Complex impedance property of $TiOF_2@Ti_3C_2T_x$ at the different RH. **i** Response and recovery properties of sensors with $TiOF_2$, $Ti_3C_2T_x$ and $TiOF_2@Ti_3C_2T_x$. **j** Three samples tested for extended stability at variable humidity. Reproduced with permission from Ref. [98]

energy of NH_3-M, resulting in a decrease in the energy of NH_3 adsorption on the MXene surface. The research team [218] also found that the single-molecule layer Sc_2CO_2 has good adsorption strength and obvious charge transfer for SO_2. The transfer of charge from SO_2 to Sc_2CO_2 increases the DOS at the Fermi level of Sc_2CO_2 and the conductivity of Sc_2CO_2. By applying external tensile strain or electric field, high selectivity, high sensitivity, controllable capture, or reversible desorption can be achieved, which predicts that Sc_2CO_2 has good sensing performance for toxic SO_2 gas,

© The authors https://doi.org/10.1007/s40820-024-01430-4

Table 4 Advantages and disadvantages of MXene-based composite gas sensors

MXene-complex	Advantage	Shortcoming
MXene/rGO	The working temperature is room temperature, and the detection limit for various gases is low, with good sensitivity	The response recovery time at room temperature is relatively long, and the corresponding gas sensing mechanism of the composite material is unclear
MXene/metallic oxide	High sensitivity and high response to various VOC gases	The selectivity is poor, the working temperature cannot reach room temperature, and the stability is poor
MXene/TMDs	The reaction temperature is room temperature and has good stability	There is relatively little research, and the gas sensing response of composite materials is relatively low
MXene/MOF	It has high sensitivity in a dry environment and operates at room temperature	There is no gas sensitivity research on VOC gas
MXene/polymer	Composite materials are most suitable for use in humidity gas sensors and operate at room temperature	The minimum limit for detecting gas/VOC/humidity response is relatively high

as shown in Fig. 23b, c. The surface functional groups of MXenes have an undeniable contribution or impact on gas sensing performance. Junkaew et al. [219] used density functional theory (DFT) calculations to investigate the reactivity and selectivity of four O-functionalized MXenes, namely M_2CO_2 (M = Ti, V, Nb, Mo), toward gas molecules. According to the calculated adsorption energy results, among the 11 gas molecules, Ti_2CO_2 and Nb_2CO_2 have stronger adsorption capacity for NH_3, while Mo_2CO_2 and V_2CO_2 are more sensitive to NO. The surface functional groups of $Ti_3C_2T_x$ MXene material are a combination of -F, = O, and -OH. The presence and content changes of these functional groups can achieve selective sensing of gas molecules. For example, Pourfath et al. [220] studied through charge difference calculations that the contribution of surface functional groups to charge transfer is different. Fluorine atoms have a smaller contribution to charge transfer than oxygen atoms. Therefore, there is a strong electrostatic attraction between the lone pair electrons of the O atom in the = O functional group on MXenes and the positively charged part of the exposed hydrogen atom in NH_3 molecules. Therefore, controlling the content of the = O functional group on the MXenes surface can improve the selectivity toward NH_3 molecules. Recently, Naqvi et al. [221] explored several gases (such as CH_4) through DFT calculations.

5.2 First Principles Exploration of MXenes Gas-Sensitive Mechanisms

Maleski et al. [42] used DFT to simulate and calculate the binding energies of acetone and ammonia on $Ti_3C_2T_x$, MoS_2, RGO, and BP to study the sensing mechanism of $Ti_3C_2T_x$ on acetone and NH_3 gases, as shown in Fig. 23d. For the two gases of acetone and ammonia, $Ti_3C_2(OH)_2$ exhibits the strongest binding energy more than twice that of other two-dimensional materials. It is speculated that the superior gas adsorption performance of hydroxyl groups in $Ti_3C_2T_x$ is the main reason for its high sensitivity to acetone and ammonia. This work demonstrates the presence of charge transfer induced by gas adsorption in the gas sensing mechanism of MXenes. In addition, Zhou et al. [216] used $Ti_3C_2T_x$ as a gas sensing material to test CH_4, H_2S, H_2O, NH_3, NO, ethanol, methanol, and acetone gases at room temperature, and found that $Ti_3C_2T_x$ had very high selectivity for NH_3. In order to understand the reason for this high selectivity, they also studied the adsorption behavior, adsorption energy, adsorption geometry, charge transfer, and other aspects using first principles calculation methods. They also confirmed that the charge transfer caused by NH_3 adsorption on $Ti_3C_2T_x$ is the main reason for the change in resistance of $Ti_3C_2T_x$. However, MXenes have metal conductivity and contain interlayer water molecules, which means that gas molecules may interact in a more complex manner than typical charge transfer. Koh et al. [222] demonstrated the swelling effect of gas on $Ti_3C_2T_x$ MXene materials by intercalating $Ti_3C_2T_x$ with Na^+ ions and using in situ XRD technology. After 70 min of ethanol blowing, the (002) peak of $Ti_3C_2T_x$ shifted toward a smaller angle and the interlayer spacing increased by 0.82 Å. After 120 min of N_2 blowing, the adsorbed ethanol was desorbed and the (002) peak of $Ti_3C_2T_x$ recovered toward a larger angle.

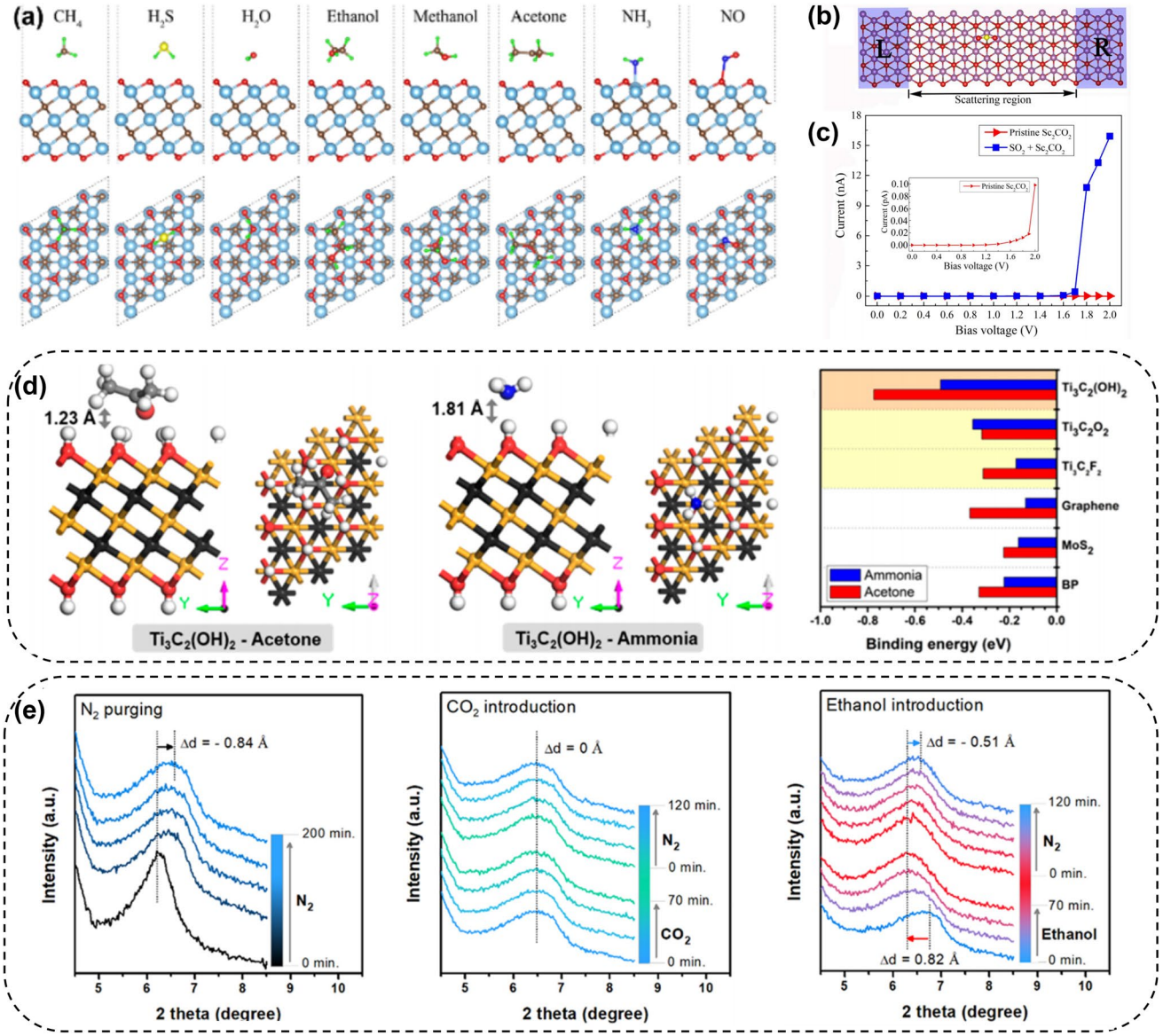

Fig. 23 **a** Side and top views of the most stable configurations of different gas molecules adsorbed on the $Ti_3C_2O_2$ surface. Reproduced with permission from Ref. [216]. **b** Two-probe model of monolayer Sc_2CO_2 sensor for detecting SO_2 molecule. **c** Predicted I-V characteristics of Sc_2CO_2 with SO_2 molecules. Reproduced with permission from Ref. [218]. **d** Density functional theory (DFT) simulation results for gas molecules adsorbed on various 2D materials. Side and top views of the minimum energy configurations for acetone and ammonia on $Ti_3C_2(OH)_2$. Minimum binding energies of acetone and ammonia on $Ti_3C_2(OH)_2$, $Ti_3C_2O_2$, $Ti_3C_2F_2$, graphene, MoS_2, and BP. Reproduced with permission from Ref. [42]. **e** The (002) peak shift of $Ti_3C_2T_2$ film during N_2 purging for 200 min. The (002) peak shift of $Ti_3C_2T_x$ film during introduction of CO_2 (1%) or ethanol (0.1%) for 70 min, followed by N_2 purging for 120 min to purge out target gases. Reproduced with permission from Ref. [222].

The interlayer spacing of $Ti_3C_2T_x$ membrane decreased by 0.51 Å compared to that after ethanol swelling, as shown in Fig. 23e. Therefore, regulating the interlayer distance of $Ti_3C_2T_x$ MXene is also very important for improving the selectivity of gas sensing.

6 Summary and Outlook

Starting from the application of new MXene-based composites in the field of gas sensing, this article briefly introduces the preparation methods of gas sensing devices, the structure of MXene, and the properties related to gas sensing. It

© The authors
https://doi.org/10.1007/s40820-024-01430-4

focuses on the research progress of MXene and graphene, metal oxides, TMDs, MOFs, and polymers in the field of gas sensing, and summarizes the gas sensing mechanism of MXene. However, the development of practical gas sensors based on MXene still faces many challenges:

1. It is necessary to develop green and safe macro preparation methods and surface functional group oriented regulation technologies for MXene. At present, the most mature preparation method for $M_{n+1}X_n$ is liquid-phase chemical etching, usually using ternary $M_{n+1}AX_n$ precursors as starting materials. In fluorinated solutions such as hydrofluoric acid (HF) and fluoride salts ($LiF + HCl$, NH_4HF_2), chemical etching selectively removes the A-layer elements in ternary $M_{n+1}AX_n$, achieving good selective etching effect and obtaining functional group-rich multilayer $M_{n+1}X_nT_x$ materials. On the one hand, MAX phase is usually formed through high-temperature processing of titanium and aluminum, and requires several grinding processes to obtain fine MAX powder. On the other hand, using hydrofluoric acid or fluorinated salts as etching solvents, the highly toxic gases generated during the preparation process seriously endanger human and environmental safety. In addition, the etching capabilities of different solution systems vary, resulting in low two-dimensional yield and difficulty in optimizing the preparation process. This will result in high preparation costs for MXene materials and limit their large-scale application in the gas sensing field. More importantly, the fluorine containing solution reaction system inevitably leads to the random coexistence of three functional groups (=O, -F, -OH) on the surface of $M_{n+1}X_nT_x$, making accurate control extremely difficult. The regulation of functional group states (types and quantities) by changing experimental conditions faces enormous challenges in experiments, and mature and feasible experimental methods for precise regulation of functional groups have not yet been formed, making it difficult to improve selectivity for specific gases through the design of surface functional groups.
2. The variety of MXene material systems still needs to be greatly expanded. Since the discovery of MXene materials in 2011, people's understanding of their structure is still in the initial stage, especially the lack of effective preparation techniques for the types of MXene materials predicted by theory. As a result, MXene currently used in the gas sensing field mainly focuses on two-dimensional $Ti_3C_2T_x$ and its composite materials. For the large number of MXene material families, more innovative preparation methods have been developed to synthesize pure MXene materials with more diverse types. The combination of surface modification, element doping, heterogeneous recombination and other means to design the composition of the material is a technical bottleneck in expanding the application of MXene in the gas sensing field.
3. The interaction mechanism between MXene and gas molecules needs to be further studied. Due to the richer atomic species and combination types of MXene compared to traditional two-dimensional materials such as graphene, the surface adsorption and charge transfer mechanisms in gas-sensitive processes will be more complex. Whether it is oxidizing or reducing, it is observed that all adsorbed gas molecules will cause an increase or decrease in resistance with a high signal-to-noise ratio. At the same time, interlayer expansion also has a significant impact on the conductivity changes and gas response of the material.

At present, research on MXene is still in its infancy, providing a basic building block for gas-sensitive materials. Experimental data and computational predictions indicate that by selecting over 60 sets of available layered ternary carbides and nitrides, stable structures of different types of MXene can be obtained. It is expected that MXene and its composites will have unlimited potential in the field of gas sensing.

Acknowledgements This work was supported by the National Natural Science Foundation of China (No.11375136).

Declarations

Conflicts of Interest The authors declare no conflict of interest. They have no known competing financial interests or personal relationships that could have appeared to influence the work reported in this paper.

Open Access This article is licensed under a Creative Commons Attribution 4.0 International License, which permits use, sharing, adaptation, distribution and reproduction in any medium or format, as long as you give appropriate credit to the original author(s) and the source, provide a link to the Creative Commons licence, and indicate if changes were made. The images or other third party material in this article are included in the article's Creative Commons licence, unless indicated otherwise in a credit line to the material. If material is not included in the article's Creative Commons licence and your intended use is not permitted by statutory regulation or exceeds the permitted use, you will need to obtain permission directly from the copyright holder. To view a copy of this licence, visit http://creativecommons.org/licenses/by/4.0/.

References

1. H. Wang, X. Yuan, G. Zeng, Y. Wu, Y. Liu et al., Three dimensional graphene based materials: Synthesis and applications from energy storage and conversion to electrochemical sensor and environmental remediation. Adv. Colloid Interface Sci. **221**, 41–59 (2015). https://doi.org/10.1016/j.cis.2015.04.005
2. L. Qin, Q. Tao, X. Liu, M. Fahlman, J. Halim et al., Polymer-MXene composite films formed by MXene-facilitated electrochemical polymerization for flexible solid-state microsupercapacitors. Nano Energy **60**, 734–742 (2019). https://doi.org/10.1016/j.nanoen.2019.04.002
3. Y. Zhang, S. Yu, G. Lou, Y. Shen, H. Chen, Review of macroporous materials as electrochemical supercapacitor electrodes. J. Mater. Sci. **52**, 11201–11228 (2017). https://doi.org/10.1007/s10853-017-0955-3
4. L. Zhu, D. Zheng, Z. Wang, X. Zheng, P. Fang et al., A confinement strategy for stabilizing ZIF-derived bifunctional catalysts as a benchmark cathode of flexible all-solid-state zinc-air batteries. Adv. Mater. **30**, e1805268 (2018). https://doi.org/10.1002/adma.201805268
5. H. Tai, Z. Duan, Y. Wang, S. Wang, Y. Jiang, Paper-based sensors for gas, humidity, and strain detections: a review. ACS Appl. Mater. Interfaces **12**, 31037–31053 (2020). https://doi.org/10.1021/acsami.0c06435
6. H. Tai, S. Wang, Z. Duan, Y. Jiang, Evolution of breath analysis based on humidity and gas sensors: Potential and challenges. Sens. Actuat. B Chem. **318**, 128104 (2020). https://doi.org/10.1016/j.snb.2020.128104
7. P. Geng, S. Zheng, H. Tang, R. Zhu, L. Zhang et al., Transition metal sulfides based on graphene for electrochemical energy storage. Adv. Energy Mater. **8**, 1703259 (2018). https://doi.org/10.1002/aenm.201703259
8. V. Sharma, H.L. Kagdada, P.K. Jha, P. Śpiewak, K.J. Kurzydłowski, Thermal transport properties of boron nitride based materials: a review. Renew. Sustain. Energy Rev. **120**, 109622 (2020). https://doi.org/10.1016/j.rser.2019.109622
9. A.C. Bouali, M. Serdechnova, C. Blawert, J. Tedim, M.G.S. Ferreira et al., Layered double hydroxides (LDHs) as functional materials for the corrosion protection of aluminum alloys: a review. Appl. Mater. Today **21**, 100857 (2020). https://doi.org/10.1016/j.apmt.2020.100857
10. A.M. Kuchkaev, S. Lavate, A.M. Kuchkaev, A.V. Sukhov, R. Srivastava et al., Chemical functionalization of 2D black phosphorus toward its applications in energy devices and catalysis: a review. Energy Technol. **9**, 2100581 (2021). https://doi.org/10.1002/ente.202100581
11. D.H. Ho, Y.Y. Choi, S.B. Jo, J.-M. Myoung, J.H. Cho, Sensing with MXenes: progress and prospects. Adv. Mater. **33**, 2005846 (2021). https://doi.org/10.1002/adma.202005846
12. K. Nataf, T.H. Bradley, An economic comparison of battery energy storage to conventional energy efficiency technologies in Colorado manufacturing facilities. Appl. Energy **164**, 133–139 (2016). https://doi.org/10.1016/j.apenergy.2015.11.102
13. H. Zheng, Y. Zeng, H. Zhang, X. Zhao, M. Chen et al., Oxygen vacancy activated Bi_2O_3 nanoflowers as a high-performance anode for rechargeable alkaline battery. J. Power. Sources **433**, 126684 (2019). https://doi.org/10.1016/j.jpowsour.2019.05.090
14. A. Feng, Y. Yu, Y. Wang, F. Jiang, Y. Yu et al., Two-dimensional MXene Ti_3C_2 produced by exfoliation of Ti_3AlC_2. Mater. Des. **114**, 161–166 (2017). https://doi.org/10.1016/j.matdes.2016.10.053
15. T. Bashir, S. Zhou, S. Yang, S.A. Ismail, T. Ali et al., Progress in 3D-MXene electrodes for lithium/sodium/potassium/magnesium/zinc/aluminum-ion batteries. Electrochem. Energy Rev. **6**, 5 (2023). https://doi.org/10.1007/s41918-022-00174-2
16. X. Hui, X. Ge, R. Zhao, Z. Li, L. Yin, Interface chemistry on MXene-based materials for enhanced energy storage and conversion performance. Adv. Funct. Mater. **30**, 2005190 (2020). https://doi.org/10.1002/adfm.202005190
17. A. Iqbal, P. Sambyal, C.M. Koo, 2D MXenes for electromagnetic shielding: a review. Adv. Funct. Mater. **30**, 2000883 (2020). https://doi.org/10.1002/adfm.202000883
18. Q.-N. Zhao, Y.-J. Zhang, Z.-H. Duan, S. Wang, C. Liu et al., A review on $Ti_3C_2T_x$-based nanomaterials: synthesis and applications in gas and humidity sensors. Rare Met. **40**, 1459–1476 (2021). https://doi.org/10.1007/s12598-020-01602-2
19. A. Hermawan, T. Amrillah, A. Riapanitra, W.-J. Ong, S. Yin, Prospects and challenges of MXenes as emerging sensing materials for flexible and wearable breath-based biomarker diagnosis. Adv. Healthc. Mater. **10**, e2100970 (2021). https://doi.org/10.1002/adhm.202100970
20. E. Lee, A. VahidMohammadi, B.C. Prorok, Y.S. Yoon, M. Beidaghi et al., Room temperature gas sensing of two-dimensional titanium carbide (MXene). ACS Appl. Mater. Interfaces **9**, 37184–37190 (2017). https://doi.org/10.1021/acsami.7b11055
21. H. Shi, P. Zhang, Z. Liu, S. Park, M.R. Lohe et al., Ambient-stable two-dimensional titanium carbide (MXene) enabled by iodine etching. Angew. Chem. Int. Ed. **60**, 8689–8693 (2021). https://doi.org/10.1002/anie.202015627
22. Z. Yang, W. Li, G. Zhang, J. Wang, J. Zuo et al., Constructing SbOC bond to improve the alloying reaction reversibility of free-standing Sb_2Se_3 nanorods for potassium-ion batteries. Nano Energy **93**, 106764 (2022). https://doi.org/10.1016/j.nanoen.2021.106764
23. C. Zhang, L. McKeon, M.P. Kremer, S.-H. Park, O. Ronan et al., Additive-free MXene inks and direct printing of micro-supercapacitors. Nat. Commun. **10**, 1795 (2019). https://doi.org/10.1038/s41467-019-09398-1
24. Y. Liang, X. Luo, W. Weng, Z. Hu, Y. Zhang et al., Activated carbon nanotube fiber fabric as a high-performance flexible electrode for solid-state supercapacitors. ACS Appl. Mater. Interfaces **13**, 28433–28441 (2021). https://doi.org/10.1021/acsami.1c02758
25. H. Shan, J. Qin, Y. Ding, H.M.K. Sari, X. Song et al., Controllable heterojunctions with a semicoherent phase boundary boosting the potassium storage of $CoSe_2/FeSe_2$. Adv. Mater.

© The authors https://doi.org/10.1007/s40820-024-01430-4

33, e2102471 (2021). https://doi.org/10.1002/adma.202102471

26. H. Hwang, S. Byun, S. Yuk, S. Kim, S.H. Song et al., High-rate electrospun $Ti_3C_2T_x$ MXene/carbon nanofiber electrodes for flexible supercapacitors. Appl. Surf. Sci. **556**, 149710 (2021). https://doi.org/10.1016/j.apsusc.2021.149710
27. M. Li, J. Lu, K. Luo, Y. Li, K. Chang et al., Element replacement approach by reaction with lewis acidic molten salts to synthesize nanolaminated MAX phases and MXenes. J. Am. Chem. Soc. **141**, 4730–4737 (2019). https://doi.org/10.1021/jacs.9b00574
28. K. Li, X. Wang, X. Wang, M. Liang, V. Nicolosi et al., All-pseudocapacitive asymmetric MXene-carbon-conducting polymer supercapacitors. Nano Energy **75**, 104971 (2020). https://doi.org/10.1016/j.nanoen.2020.104971
29. H.T.M. Hoa, K.J. Lee, H.P. Pham, T.A. Doan, H.H. Nguyen et al., Ammonia gas sensing behavior of hybridization between reduced graphene oxide and gold nanoparticles. J. Nanomater. **2020**, 7680508 (2020). https://doi.org/10.1155/2020/7680508
30. X. Li, Y. Zhao, X. Wang, J. Wang, A.M. Gaskov et al., Reduced graphene oxide (rGO) decorated TiO_2 microspheres for selective room-temperature gas sensors. Sens. Actuat. B Chem. **230**, 330–336 (2016). https://doi.org/10.1016/j.snb.2016.02.069
31. W. Zhang, M. Gong, J. Yang, J. Gu, Zr-MOFs integrated with a guest capturer and a photosensitizer for the simultaneous adsorption and degradation of 4-chlorophenol. Langmuir **37**, 8157–8166 (2021). https://doi.org/10.1021/acs.langmuir.1c00823
32. P. Guo, H. Pan, Selectivity of Ti-doped In_2O_3 ceramics as an ammonia sensor. Sens. Actuat. B Chem. **114**, 762–767 (2006). https://doi.org/10.1016/j.snb.2005.07.040
33. J. Li, Y. Wang, H. Song, Y. Guo, S. Hu et al., Photocatalytic hydrogen under visible light by nitrogen-doped rutile titania graphitic carbon nitride composites: an experimental and theoretical study. Adv. Compos. Hybrid Mater. **6**, 83 (2023). https://doi.org/10.1007/s42114-023-00659-8
34. Y. Wang, T. Guo, Z. Tian, K. Bibi, Y.-Z. Zhang et al., MXenes for energy harvesting. Adv. Mater. **34**, 2108560 (2022). https://doi.org/10.1002/adma.202108560
35. X. He, H. Zhang, X. Zhao, P. Zhang, M. Chen et al., Stabilized molybdenum trioxide nanowires as novel ultrahigh-capacity cathode for rechargeable zinc ion battery. Adv. Sci. **6**, 1900151 (2019). https://doi.org/10.1002/advs.201900151
36. K.C. Divya, J. Østergaard, Battery energy storage technology for power systems—An overview. Electr. Power Syst. Res. **79**, 511–520 (2009). https://doi.org/10.1016/j.epsr.2008.09.017
37. C.J. Zhang, Y. Ma, X. Zhang, S. Abdolhosseinzadeh, H. Sheng et al., Two-dimensional transition metal carbides and nitrides (MXenes): synthesis, properties, and electrochemical energy storage applications. Energy Environ. Mater. **3**, 29–55 (2020). https://doi.org/10.1002/eem2.12058
38. Y. Wang, X. Wang, X. Li, Y. Bai, H. Xiao et al., Scalable fabrication of polyaniline nanodots decorated MXene film electrodes enabled by viscous functional inks for high-energy-density asymmetric supercapacitors. Chem. Eng. J. **405**, 126664 (2021). https://doi.org/10.1016/j.cej.2020.126664
39. X. Xu, Y. Zhang, H. Sun, J. Zhou, F. Yang et al., Progress and perspective: MXene and MXene-based nanomaterials for high-performance energy storage devices. Adv. Electron. Mater. **7**, 2000967 (2021). https://doi.org/10.1002/aelm.202000967
40. F. Wang, X. Wu, X. Yuan, Z. Liu, Y. Zhang et al., Latest advances in supercapacitors: from new electrode materials to novel device designs. Chem. Soc. Rev. **46**, 6816–6854 (2017). https://doi.org/10.1039/C7CS00205J
41. M. Hu, C. Cui, C. Shi, Z.-S. Wu, J. Yang et al., High-energy-density hydrogen-ion-rocking-chair hybrid supercapacitors based on $Ti_3C_2T_x$ MXene and carbon nanotubes mediated by redox active molecule. ACS Nano **13**, 6899–6905 (2019). https://doi.org/10.1021/acsnano.9b01762
42. S.J. Kim, H.J. Koh, C.E. Ren, O. Kwon, K. Maleski et al., Metallic $Ti_3C_2T_x$ MXene gas sensors with ultrahigh signal-to-noise ratio. ACS Nano **12**, 986–993 (2018). https://doi.org/10.1021/acsnano.7b07460
43. S.N. Shuvo, A.M. Ulloa Gomez, A. Mishra, W.Y. Chen, A.M. Dongare et al., Sulfur-doped titanium carbide MXenes for room-temperature gas sensing. ACS Sens. **5**, 2915–2924 (2020). https://doi.org/10.1021/acssensors.0c01287
44. J. Choi, Y.-J. Kim, S.-Y. Cho, K. Park, H. Kang et al., *In situ* formation of multiple Schottky barriers in a Ti_3C_2 MXene film and its application in highly sensitive gas sensors. Adv. Funct. Mater. **30**, 2003998 (2020). https://doi.org/10.1002/adfm.202003998
45. S. Sun, M. Wang, X. Chang, Y. Jiang, D. Zhang et al., $W_{18}O_{49}/Ti_3C_2T_x$ Mxene nanocomposites for highly sensitive acetone gas sensor with low detection limit. Sens. Actuat. B Chem. **304**, 127274 (2020). https://doi.org/10.1016/j.snb.2019.127274
46. H. Qian, H. Ren, Y. Zhang, X. He, W. Li et al., Surface doping vs. bulk doping of cathode materials for lithium-ion batteries: a review. Electrochem. Energy Rev. **5**, 2 (2022). https://doi.org/10.1007/s41918-022-00155-5
47. Y. Li, H. Shao, Z. Lin, J. Lu, L. Liu et al., A general Lewis acidic etching route for preparing MXenes with enhanced electrochemical performance in non-aqueous electrolyte. Nat. Mater. **19**, 894–899 (2020). https://doi.org/10.1038/s41563-020-0657-0
48. D. Zhang, M. Luo, K. Yang, P. Yang, C. Liu et al., Porosity-adjustable MXene film with transverse and longitudinal ion channels for flexible supercapacitors. Microporous Mesoporous Mater. **326**, 111389 (2021). https://doi.org/10.1016/j.micromeso.2021.111389
49. Q. Wang, J. Liu, G. Tian, D. Zhang, Co@N-CNT/MXenes *in situ* grown on carbon nanotube film for multifunctional sensors and flexible supercapacitors. Nanoscale **13**, 14460–14468 (2021). https://doi.org/10.1039/D1NR03641F
50. K. Li, M. Liang, H. Wang, X. Wang, Y. Huang et al., 3D MXene architectures for efficient energy storage and

conversion. Adv. Funct. Mater. **30**, 2000842 (2020). https://doi.org/10.1002/adfm.202000842

51. M.K. Aslam, Y. Niu, M. Xu, MXenes for non-lithium-ion (Na, K, Ca, Mg, and Al) batteries and supercapacitors. Adv. Energy Mater. **11**, 2000681 (2021). https://doi.org/10.1002/aenm.202000681
52. L. Wan, Y. Tang, L. Chen, K. Wang, J. Zhang et al., *In-situ* construction of g-C_3N_4/Mo_2CT_x hybrid for superior lithium storage with significantly improved Coulombic efficiency and cycling stability. Chem. Eng. J. **410**, 128349 (2021). https://doi.org/10.1016/j.cej.2020.128349
53. Z. Yang, L. Jiang, J. Wang, F. Liu, J. He et al., Flexible resistive NO_2 gas sensor of three-dimensional crumpled MXene $Ti_3C_2T_x$/ZnO spheres for room temperature application. Sens. Actuat. B Chem. **326**, 128828 (2021). https://doi.org/10.1016/j.snb.2020.128828
54. V.T. Le, Y. Vasseghian, V.D. Doan, T.T.T. Nguyen, T.T. Thi Vo et al., Flexible and high-sensitivity sensor based on Ti_3C_2-MoS_2 MXene composite for the detection of toxic gases. Chemosphere **291**, 133025 (2022). https://doi.org/10.1016/j.chemosphere.2021.133025
55. L. Li, H. Cao, Z. Liang, Y. Cheng, T. Yin et al., First-principles study of Ti-deficient Ti_3C_2 MXene nanosheets as NH_3 gas sensors. ACS Appl. Nano Mater. **5**, 2470–2475 (2022). https://doi.org/10.1021/acsanm.1c04158
56. B. Sun, F. Qin, L. Jiang, J. Gao, Z. Liu et al., Room-temperature gas sensors based on three-dimensional Co_3O_4/Al_2O_3@$Ti_3C_2T_x$ MXene nanocomposite for highly sensitive NO_x detection. Sens. Actuat. B Chem. **368**, 132206 (2022). https://doi.org/10.1016/j.snb.2022.132206
57. Z. Wang, S. Gao, T. Fei, S. Liu, T. Zhang, Construction of ZnO/SnO_2 heterostructure on reduced graphene oxide for enhanced nitrogen dioxide sensitive performances at room temperature. ACS Sens. **4**, 2048–2057 (2019). https://doi.org/10.1021/acssensors.9b00648
58. X. Zhan, C. Si, J. Zhou, Z. Sun, MXene and MXene-based composites: synthesis, properties and environment-related applications. Nanoscale Horiz. **5**, 235–258 (2020). https://doi.org/10.1039/C9NH00571D
59. Z. Li, D. Guo, D. Wang, M. Sun, H. Sun, Exploration of Metal/Ti_3C_2 MXene-derived composites as anode for high-performance zinc-ion supercapacitor. J. Power. Sources **506**, 230197 (2021). https://doi.org/10.1016/j.jpowsour.2021.230197
60. Y. Li, W. Zhang, X. Yang, J. Zhang, Z. Wang et al., A high-voltage and high-capacity $Ti_3C_2T_x$/$BiCuS_{2.5}$ heterostructure to boost up the energy density and recyclability of zinc-ion-hybrid capacitors. Nano Energy **87**, 106136 (2021). https://doi.org/10.1016/j.nanoen.2021.106136
61. A. VahidMohammadi, W. Liang, M. Mojtabavi, M. Wanunu, M. Beidaghi, 2D titanium and vanadium carbide MXene heterostructures for electrochemical energy storage. Energy Storage Mater. **41**, 554–562 (2021). https://doi.org/10.1016/j.ensm.2021.06.014
62. Y. Gogotsi, What nano can do for energy storage. ACS Nano **8**, 5369–5371 (2014). https://doi.org/10.1021/nn503164x
63. M. Yousaf, H.T.H. Shi, Y. Wang, Y. Chen, Z. Ma et al., Novel pliable electrodes for flexible electrochemical energy storage devices: recent progress and challenges. Adv. Energy Mater. **6**, 1600490 (2016). https://doi.org/10.1002/aenm.201600490
64. L. Wen, F. Li, H.-M. Cheng, Carbon nanotubes and graphene for flexible electrochemical energy storage: from materials to devices. Adv. Mater. **28**, 4306–4337 (2016). https://doi.org/10.1002/adma.201504225
65. Y. Wang, W. Lai, N. Wang, Z. Jiang, X. Wang et al., A reduced graphene oxide/mixed-valence manganese oxide composite electrode for tailorable and surface mountable supercapacitors with high capacitance and super-long life. Energy Environ. Sci. **10**, 941–949 (2017). https://doi.org/10.1039/C6EE03773A
66. B. Ahmed, D.H. Anjum, Y. Gogotsi, H.N. Alshareef, Atomic layer deposition of SnO_2 on MXene for Li-ion battery anodes. Nano Energy **34**, 249–256 (2017). https://doi.org/10.1016/j.nanoen.2017.02.043
67. L. Yang, N. Yi, J. Zhu, Z. Cheng, X. Yin et al., Novel gas sensing platform based on a stretchable laser-induced graphene pattern with self-heating capabilities. J. Mater. Chem. A **8**, 6487–6500 (2020). https://doi.org/10.1039/C9TA07855J
68. Z. Chen, J. Wang, A. Umar, Y. Wang, H. Li et al., Three-dimensional crumpled graphene-based nanosheets with ultrahigh NO_2 gas sensibility. ACS Appl. Mater. Interfaces **9**, 11819–11827 (2017). https://doi.org/10.1021/acsami.7b01229
69. Y. Cheng, Y. Ma, L. Li, M. Zhu, Y. Yue et al., Bioinspired microspines for a high-performance spray $Ti_3C_2T_x$ MXene-based piezoresistive sensor. ACS Nano **14**, 2145–2155 (2020). https://doi.org/10.1021/acsnano.9b08952
70. Y. Yang, Z. Cao, P. He, L. Shi, G. Ding et al., $Ti_3C_2T_x$ MXene-graphene composite films for wearable strain sensors featured with high sensitivity and large range of linear response. Nano Energy **66**, 104134 (2019). https://doi.org/10.1016/j.nanoen.2019.104134
71. D. Sun, M. Wang, Z. Li, G. Fan, L.-Z. Fan et al., Two-dimensional Ti_3C_2 as anode material for Li-ion batteries. Electrochem. Commun. **47**, 80–83 (2014). https://doi.org/10.1016/j.elecom.2014.07.026
72. Y.-X. Zhang, Y.-H. Wang, Nonlinear optical properties of metal nanoparticles: a review. RSC Adv. **7**, 45129–45144 (2017). https://doi.org/10.1039/C7RA07551K
73. S. Alwarappan, N. Nesakumar, D. Sun, T.Y. Hu, C.-Z. Li, 2D metal carbides and nitrides (MXenes) for sensors and biosensors. Biosens. Bioelectron. **205**, 113943 (2022). https://doi.org/10.1016/j.bios.2021.113943
74. K. Zhang, J. Sun, J. Song, C. Gao, Z. Wang et al., Self-healing Ti_3C_2 MXene/PDMS supramolecular elastomers based on small biomolecules modification for wearable sensors. ACS Appl. Mater. Interfaces **12**, 45306–45314 (2020). https://doi.org/10.1021/acsami.0c13653
75. D.H. Ho, Q. Sun, S.Y. Kim, J.T. Han, D.H. Kim et al., Stretchable and multimodal all graphene electronic skin. Adv. Mater. **28**, 2601–2608 (2016). https://doi.org/10.1002/adma.201505739

© The authors https://doi.org/10.1007/s40820-024-01430-4

76. M. Asad, M.H. Sheikhi, Highly sensitive wireless H_2S gas sensors at room temperature based on CuO-SWCNT hybrid nanomaterials. Sens. Actuat. B Chem. **231**, 474–483 (2016). https://doi.org/10.1016/j.snb.2016.03.021
77. W. Li, C. Teng, Y. Sun, L. Cai, J.-L. Xu et al., Sprayed, scalable, wearable, and portable NO_2 sensor array using fully flexible AgNPs-all-carbon nanostructures. ACS Appl. Mater. Interfaces **10**, 34485–34493 (2018). https://doi.org/10.1021/acsami.8b11254
78. H. Yan, M. Zhong, Z. Lv, P. Wan, Stretchable electronic sensors of nanocomposite network films for ultrasensitive chemical vapor sensing. Small **13**, 1701697 (2017). https://doi.org/10.1002/smll.201701697
79. J. Hassinen, J. Kauppila, J. Leiro, A. Määttänen, P. Ihalainen et al., Low-cost reduced graphene oxide-based conductometric nitrogen dioxide-sensitive sensor on paper. Anal. Bioanal. Chem. **405**, 3611–3617 (2013). https://doi.org/10.1007/s00216-013-6805-5
80. A. Abdellah, A. Abdelhalim, F. Loghin, P. Köhler, Z. Ahmad et al., Flexible carbon nanotube based gas sensors fabricated by large-scale spray deposition. IEEE Sens. J. **13**, 4014–4021 (2013). https://doi.org/10.1109/JSEN.2013.2265775
81. J. Lee, W. Shim, E. Lee, J.-S. Noh, W. Lee, Highly mobile palladium thin films on an elastomeric substrate: nanogap-based hydrogen gas sensors. Angew. Chem. Int. Ed. **50**, 5301–5305 (2011). https://doi.org/10.1002/anie.201100054
82. J. Lee, W. Shim, E. Lee, J.S. Noh, W. Lee, Highly mobile palladium thin films on an elastomeric substrate: Nanogap-based hydrogen gas sensors. Angew. Chem. Int. Ed. **123**(23), 5413–5417 (2011). https://doi.org/10.1002/anie.201100054
83. Z. Zhao, G. Huang, Y. Kong, J. Cui, A.A. Solovev et al., Atomic layer deposition for electrochemical energy: from design to industrialization. Electrochem. Energy Rev. **5**, 31 (2022). https://doi.org/10.1007/s41918-022-00146-6
84. J. Zhang, L. Huang, Y. Lin, L. Chen, Z. Zeng et al., Pencil-trace on printed silver interdigitated electrodes for paper-based NO_2 gas sensors. Appl. Phys. Lett. **106**, 143101 (2015). https://doi.org/10.1063/1.4917063
85. J.M. Azzarelli, K.A. Mirica, J.B. Ravnsbæk, T.M. Swager, Wireless gas detection with a smartphone via rf communication. Proc. Natl. Acad. Sci. U.S.A. **111**, 18162–18166 (2014). https://doi.org/10.1073/pnas.1415403111
86. S.H. Lim, B. Radha, J.Y. Chan, M.S. Saifullah, G.U. Kulkarni et al., Flexible palladium-based H_2 sensor with fast response and low leakage detection by nanoimprint lithography. ACS Appl. Mater. Interfaces **5**, 7274–7281 (2013). https://doi.org/10.1021/am401624r
87. N. Tang, C. Zhou, L. Xu, Y. Jiang, H. Qu et al., A fully integrated wireless flexible ammonia sensor fabricated by soft nano-lithography. ACS Sens. **4**, 726–732 (2019). https://doi.org/10.1021/acssensors.8b01690
88. Y. Lin, J. Chen, M.M. Tavakoli, Y. Gao, Y. Zhu et al., Printable fabrication of a fully integrated and self-powered sensor system on plastic substrates. Adv. Mater. **31**, e1804285 (2019). https://doi.org/10.1002/adma.201804285
89. S. Wu, P. Liu, Y. Zhang, H. Zhang, X. Qin, Flexible and conductive nanofiber-structured single yarn sensor for smart wearable devices. Sens. Actuat. B Chem. **252**, 697–705 (2017). https://doi.org/10.1016/j.snb.2017.06.062
90. L.T. Duy, T.Q. Trung, A. Hanif, S. Siddiqui, E. Roh et al., A stretchable and highly sensitive chemical sensor using multilayered network of polyurethane nanofibres with self-assembled reduced graphene oxide. 2D Mater. **4**, 025062 (2017). https://doi.org/10.1088/2053-1583/aa6783
91. N. Kim, S. Choi, D. Yang, J. Bae, J. Park et al., Chemical Highly sensitive and selective hydrogen sulfide and toluene sensors using Pd functionalized WO_3 nanofibers for potential diagnosis of halitosis and lung cancer. Sens. Actuat. B Chem. **193**, 574–581 (2014). https://doi.org/10.1016/j.snb.2013.12.011
92. X. Huang, B. Li, L. Wang, X. Lai, H. Xue et al., Superhydrophilic, underwater superoleophobic, and highly stretchable humidity and chemical vapor sensors for human breath detection. ACS Appl. Mater. Interfaces **11**, 24533–24543 (2019). https://doi.org/10.1021/acsami.9b04304
93. B. Wang, A. Thukral, Z. Xie, L. Liu, X. Zhang et al., Flexible and stretchable metal oxide nanofiber networks for multimodal and monolithically integrated wearable electronics. Nat. Commun. **11**, 2405 (2020). https://doi.org/10.1038/s41467-020-16268-8
94. S.Y. Cho, H. Yu, J. Choi, H. Kang, S. Park et al., Continuous meter-scale synthesis of weavable tunicate cellulose/carbon nanotube fibers for high-performance wearable sensors. ACS Nano **13**, 9332–9341 (2019). https://doi.org/10.1021/acsnano.9b03971
95. S. Guo, D. Yang, S. Zhang, Q. Dong, B. Li et al., Development of a cloud-based epidermal $MoSe_2$ device for hazardous gas sensing. Adv. Funct. Mater. **29**, 1900138 (2019). https://doi.org/10.1002/adfm.201900138
96. C.E. Cava, R.V. Salvatierra, D.C.B. Alves, A.S. Ferlauto, A.J.G. Zarbin et al., Self-assembled films of multi-wall carbon nanotubes used in gas sensors to increase the sensitivity limit for oxygen detection. Carbon **50**, 1953–1958 (2012). https://doi.org/10.1016/j.carbon.2011.12.048
97. J.-W. Kim, Y. Porte, K.Y. Ko, H. Kim, J.-M. Myoung, Micropatternable double-faced ZnO nanoflowers for flexible gas sensor. ACS Appl. Mater. Interfaces **9**, 32876–32886 (2017). https://doi.org/10.1021/acsami.7b09251
98. Z. Zhu, C. Liu, F. Jiang, J. Liu, X. Ma et al., Flexible and lightweight $Ti_3C_2T_x$ MXene@Pd colloidal nanoclusters paper film as novel H_2 sensor. J. Hazard. Mater. **399**, 123054 (2020). https://doi.org/10.1016/j.jhazmat.2020.123054
99. Z. Wang, K. Yu, Y. Feng, R. Qi, J. Ren et al., Stabilizing $Ti_3C_2T_x$-MXenes with $TiOF_2$ nanospheres intercalation to improve hydrogen evolution reaction and humidity-sensing performance. Appl. Surf. Sci. **496**, 143729 (2019). https://doi.org/10.1016/j.apsusc.2019.143729
100. D. Wang, D. Zhang, P. Li, Z. Yang, Q. Mi et al., Electrospinning of flexible poly(vinyl alcohol)/MXene nanofiber-based humidity sensor self-powered by monolayer molybdenum

diselenide piezoelectric nanogenerator. Nano-Micro Lett. **13**, 57 (2021). https://doi.org/10.1007/s40820-020-00580-5

101. H. An, T. Habib, S. Shah, H. Gao, A. Patel et al., Water sorption in MXene/polyelectrolyte multilayers for ultrafast humidity sensing. ACS Appl. Nano Mater. **2**, 948–955 (2019). https://doi.org/10.1021/acsanm.8b02265
102. H. Zhi, X. Zhang, F. Wang, P. Wan, L. Feng, Flexible $Ti_3C_2T_x$ MXene/PANI/bacterial cellulose aerogel for e-skins and gas sensing. ACS Appl. Mater. Interfaces **13**, 45987–45994 (2021). https://doi.org/10.1021/acsami.1c12991
103. Y. Tang, Y. Xu, J. Yang, Y. Song, F. Yin et al., Stretchable and wearable conductometric VOC sensors based on microstructured MXene/polyurethane core-sheath fibers. Sens. Actuat. B Chem. **346**, 130500 (2021). https://doi.org/10.1016/j.snb.2021.130500
104. L. Jin, C. Wu, K. Wei, L. He, H. Gao et al., Polymeric $Ti_3C_2T_x$ MXene composites for room temperature ammonia sensing. ACS Appl. Nano Mater. **3**, 12071–12079 (2020). https://doi.org/10.1021/acsanm.0c02577
105. X. Wang, K. Sun, K. Li, X. Li, Y. Gogotsi, $Ti_3C_2T_x$/PEDOT:PSS hybrid materials for room-temperature methanol sensor. Chin. Chem. Lett. **31**, 1018–1021 (2020). https://doi.org/10.1016/j.cclet.2019.11.031
106. L. Zhao, K. Wang, W. Wei, L. Wang, W. Han, High-performance flexible sensing devices based on polyaniline/MXene nanocomposites. InfoMat **1**, 407–416 (2019). https://doi.org/10.1002/inf2.12032
107. D. Kuang, X. Guo, Z. Zhu, Y. Ding, X. Sun et al., Enhanced room temperature ammonia response of 2D-$Ti_3C_2T_x$ MXene decorated with $Ni(OH)_2$ nanoparticles. Ceram. Int. **47**, 19471–19480 (2021). https://doi.org/10.1016/j.ceramint.2021.03.284
108. S. Zou, J. Gao, L. Liu, Z. Lin, P. Fu et al., Enhanced gas sensing properties at low working temperature of iron molybdate/MXene composite. J. Alloys Compd. **817**, 152785 (2020). https://doi.org/10.1016/j.jallcom.2019.152785
109. L.-X. Liu, W. Chen, H.-B. Zhang, Q.-W. Wang, F. Guan et al., Flexible and multifunctional silk textiles with biomimetic leaf-like MXene/silver nanowire nanostructures for electromagnetic interference shielding, humidity monitoring, and self-derived hydrophobicity. Adv. Funct. Mater. **29**, 1905197 (2019). https://doi.org/10.1002/adfm.201905197
110. W.Y. Chen, S.N. Lai, C.C. Yen, X. Jiang, D. Peroulis et al., Surface functionalization of $Ti_3C_2T_x$ MXene with highly reliable superhydrophobic protection for volatile organic compounds sensing. ACS Nano **14**, 11490–11501 (2020). https://doi.org/10.1021/acsnano.0c03896
111. E.S. Muckley, M. Naguib, H.-W. Wang, L. Vlcek, N.C. Osti et al., Multimodality of structural, electrical, and gravimetric responses of intercalated MXenes to water. ACS Nano **11**, 11118–11126 (2017). https://doi.org/10.1021/acsnano.7b05264
112. N. Li, Y. Jiang, Y. Xiao, B. Meng, C. Xing et al., A fully inkjet-printed transparent humidity sensor based on a Ti_3C_2/Ag hybrid for touchless sensing of finger motion. Nanoscale **11**, 21522–21531 (2019). https://doi.org/10.1039/c9nr06751e
113. X. Li, Y. Lu, Z. Shi, G. Liu, G. Xu et al., Onion-inspired MXene/chitosan-quercetin multilayers: Enhanced response to H_2O molecules for wearable human physiological monitoring. Sens. Actuat. B Chem. **329**, 129209 (2021). https://doi.org/10.1016/j.snb.2020.129209
114. F. Liu, Y. Li, S. Hao, Y. Cheng, Y. Zhan et al., Well-aligned MXene/chitosan films with humidity response for high-performance electromagnetic interference shielding. Carbohydr. Polym. **243**, 116467 (2020). https://doi.org/10.1016/j.carbpol.2020.116467
115. Y. Sun, H. Wang, High-performance, flexible hydrogen sensors that use carbon nanotubes decorated with palladium nanoparticles. Adv. Mater. **19**, 2818–2823 (2007). https://doi.org/10.1002/adma.200602975
116. R. Zhu, M. Desroches, B. Yoon, T.M. Swager, Wireless oxygen sensors enabled by Fe(II)-polymer wrapped carbon nanotubes. ACS Sens. **2**, 1044–1050 (2017). https://doi.org/10.1021/acssensors.7b00327
117. Y. Zheng, H. Li, W. Shen, J. Jian, Wearable electronic nose for human skin odor identification: a preliminary study. Sens. Actuat. A Phys. **285**, 395–405 (2019). https://doi.org/10.1016/j.sna.2018.11.048
118. M. Acuautla, S. Bernardini, L. Gallais, T. Fiorido, L. Patout et al., Ozone flexible sensors fabricated by photolithography and laser ablation processes based on ZnO nanoparticles. Sens. Actuat. B Chem. **203**, 602–611 (2014). https://doi.org/10.1016/j.snb.2014.07.010
119. E. Bihar, Y. Deng, T. Miyake, M. Saadaoui, G.G. Malliaras et al., A Disposable paper Breathalyzer with an alcohol sensing organic electrochemical transistor. Sci. Rep. **6**, 27582 (2016). https://doi.org/10.1038/srep27582
120. N. Nguyen, J.G. Park, S. Zhang, R. Liang, Recent advances on 3D printing technique for thermal-related applications. Adv. Eng. Mater. **20**, 1700876 (2018). https://doi.org/10.1002/adem.201700876
121. K. Crowley, A. Morrin, A. Hernandez, E. O'Malley, P.G. Whitten et al., Fabrication of an ammonia gas sensor using inkjet-printed polyaniline nanoparticles. Talanta **77**, 710–717 (2008). https://doi.org/10.1016/j.talanta.2008.07.022
122. X. Wang, F. Sun, G. Yin, Y. Wang, B. Liu et al., Tactile-sensing based on flexible PVDF nanofibers via electrospinning: a review. Sensors (Basel) **18**, 330 (2018). https://doi.org/10.3390/s18020330
123. Y. Wang, T. Yokota, T. Someya, Electrospun nanofiber-based soft electronics. NPG Asia Mater. **13**, 22 (2021). https://doi.org/10.1038/s41427-020-00267-8
124. T.A. Arica, T. Isık, T. Guner, N. Horzum, M.M. Demir, Advances in electrospun fiber-based flexible nanogenerators for wearable applications. Macromol. Mater. Eng. **306**, 2100143 (2021). https://doi.org/10.1002/mame.202100143
125. C. Linghu, S. Zhang, C. Wang, J. Song, Transfer printing techniques for flexible and stretchable inorganic electronics. NPJ Flex. Electron. **2**, 26 (2018). https://doi.org/10.1038/s41528-018-0037-x
126. P.C. Chen, S. Sukcharoenchoke, K. Ryu, L. Gomez de Arco, A. Badmaev et al., 2, 4, 6-Trinitrotoluene (TNT) chemical

© The authors https://doi.org/10.1007/s40820-024-01430-4

sensing based on aligned single-walled carbon nanotubes and ZnO nanowires. Adv. Mater. **22**, 1900–1904 (2010). https://doi.org/10.1002/adma.200904005

127. A. Carlson, A.M. Bowen, Y. Huang, R.G. Nuzzo, J.A. Rogers, Transfer printing techniques for materials assembly and micro/nanodevice fabrication. Adv. Mater. **24**, 5284–5318 (2012). https://doi.org/10.1002/adma.201201386
128. Y. An, Y. Tian, J. Feng, Y. Qian, MXenes for advanced separator in rechargeable batteries. Mater. Today **57**, 146–179 (2022). https://doi.org/10.1016/j.mattod.2022.06.006
129. B. Anasori, M.R. Lukatskaya, Y. Gogotsi, 2D metal carbides and nitrides (MXenes) for energy storage. Nat. Rev. Mater. **2**, 16098 (2017). https://doi.org/10.1038/natrevmats.2016.98
130. M. Aakyiir, S. Araby, A. Michelmore, Q. Meng, Y. Amer et al., Elastomer nanocomposites containing MXene for mechanical robustness and electrical and thermal conductivity. Nanotechnology **31**, 315715 (2020). https://doi.org/10.1088/1361-6528/ab88eb
131. S. Liu, Z. Wang, S. Zhou, F. Yu, M. Yu et al., Metal-organic-framework-derived hybrid carbon nanocages as a bifunctional electrocatalyst for oxygen reduction and evolution. Adv. Mater. **29**, 1700874 (2017). https://doi.org/10.1002/adma.201700874
132. G.R. Berdiyorov, Effect of surface functionalization on the electronic transport properties of Ti_3C_2 MXene. EPL Europhys. Lett. **111**, 67002 (2015). https://doi.org/10.1209/0295-5075/111/67002
133. C.J. Zhang, B. Anasori, A. Seral-Ascaso, S.H. Park, N. McEvoy et al., Transparent, flexible, and conductive 2D titanium carbide (MXene) films with high volumetric capacitance. Adv. Mater. **29**, 3737–3749 (2017). https://doi.org/10.1002/adma.201702678
134. Z. Wang, H. Kim, H.N. Alshareef, Oxide thin-film electronics using all-MXene electrical contacts. Adv. Mater. **30**, e1706656 (2018). https://doi.org/10.1002/adma.201706656
135. B. Jiang, T. Yang, T. Wang, C. Chen, M. Yang et al., Edge stimulated hydrogen evolution reaction on monodispersed MXene quantum dots. Chem. Eng. J. **442**, 136119 (2022). https://doi.org/10.1016/j.cej.2022.136119
136. M. Khazaei, M. Arai, T. Sasaki, C.-Y. Chung, N.S. Venkataramanan et al., Novel electronic and magnetic properties of two-dimensional transition metal carbides and nitrides. Adv. Funct. Mater. **23**, 2185–2192 (2013). https://doi.org/10.1002/adfm.201202502
137. C. Si, J. Zhou, Z. Sun, Half-metallic ferromagnetism and surface functionalization-induced metal-insulator transition in graphene-like two-dimensional Cr_2C crystals. ACS Appl. Mater. Interfaces **7**, 17510–17515 (2015). https://doi.org/10.1021/acsami.5b05401
138. J. Yang, X. Zhou, X. Luo, S. Zhang, L. Chen Tunable electronic and magnetic properties of $Cr_2M'C_2T_2$ (M' = Ti or V; T = O, OH or F). Appl. Phys. Lett. **109,** 203109 (2016). https://doi.org/10.1063/1.4967983
139. Y. Zhang, Z. Zhou, J. Lan, P. Zhang, Prediction of $Ti_3C_2O_2$ MXene as an effective capturer of formaldehyde. Appl. Surf. Sci. **469**, 770–774 (2019). https://doi.org/10.1016/j.apsusc.2018.11.018
140. S.H. Lee, W. Eom, H. Shin, R.B. Ambade, J.H. Bang et al., Room-temperature, highly durable $Ti_3C_2T_x$ MXene/graphene hybrid fibers for NH_3 gas sensing. ACS Appl. Mater. Interfaces **12**, 10434–10442 (2020). https://doi.org/10.1021/acsami.9b21765
141. M. Liu, Z. Wang, P. Song, Z. Yang, Q. Wang, Flexible MXene/rGO/CuO hybrid aerogels for high performance acetone sensing at room temperature. Sens. Actuat. B Chem. **340**, 129946 (2021). https://doi.org/10.1016/j.snb.2021.129946
142. Y. Wang, Y. Zhou, Y. Wang, Humidity activated ionic-conduction formaldehyde sensing of reduced graphene oxide decorated nitrogen-doped MXene/titanium dioxide composite film. Sens. Actuat. B Chem. **323**, 128695 (2020). https://doi.org/10.1016/j.snb.2020.128695
143. Y. Zhou, Y. Wang, Y. Wang, X. Li, Humidity-enabled ionic conductive trace carbon dioxide sensing of nitrogen-doped $Ti_3C_2T_x$ MXene/polyethyleneimine composite films decorated with reduced graphene oxide nanosheets. Anal. Chem. **92**, 16033–16042 (2020). https://doi.org/10.1021/acs.analchem.0c03664
144. Y. Song, Y. Xu, Q. Guo, Z. Hua, F. Yin et al., MXene-derived TiO_2 nanoparticles intercalating between RGO nanosheets: an assembly for highly sensitive gas detection. ACS Appl. Mater. Interfaces **13**, 39772–39780 (2021). https://doi.org/10.1021/acsami.1c12154
145. H. Tai, Z. Duan, Z. He, X. Li, J. Xu et al., Enhanced ammonia response of $Ti_3C_2T_x$ nanosheets supported by TiO_2 nanoparticles at room temperature. Sens. Actuat. B Chem. **298**, 126874 (2019). https://doi.org/10.1016/j.snb.2019.126874
146. A. Hermawan, B. Zhang, A. Taufik, Y. Asakura, T. Hasegawa et al., CuO nanoparticles/$Ti_3C_2T_x$ MXene hybrid nanocomposites for detection of toluene gas. ACS Appl. Nano Mater. **3**, 4755–4766 (2020). https://doi.org/10.1021/acsanm.0c00749
147. B. Sun, H. Lv, Z. Liu, J. Wang, X. Bai et al., Co_3O_4@PEI/$Ti_3C_2T_x$ MXene nanocomposites for a highly sensitive NO_x gas sensor with a low detection limit. J. Mater. Chem. A **9**, 6335–6344 (2021). https://doi.org/10.1039/d0ta11392a
148. D. Zhang, Q. Mi, D. Wang, T. Li, MXene/Co_3O_4 composite based formaldehyde sensor driven by ZnO/MXene nanowire arrays piezoelectric nanogenerator. Sens. Actuat. B Chem. **339**, 129923 (2021). https://doi.org/10.1016/j.snb.2021.129923
149. H. Pazniak, I.A. Plugin, M.J. Loes, T.M. Inerbaev, I.N. Burmistrov et al., Partially oxidized $Ti_3C_2T_x$ MXenes for fast and selective detection of organic vapors at part-per-million concentrations. ACS Appl. Nano Mater. **3**, 3195–3204 (2020). https://doi.org/10.1021/acsanm.9b02223
150. M. Hou, S. Guo, L. Yang, J. Gao, T. Hu et al., Improvement of gas sensing property for two-dimensional $Ti_3C_2T_x$ treated with oxygen plasma by microwave energy excitation. Ceram. Int. **47**, 7728–7737 (2021). https://doi.org/10.1016/j.ceramint.2020.11.117

151. Q. Sun, J. Wang, X. Wang, J. Dai, X. Wang et al., Treatment-dependent surface chemistry and gas sensing behavior of the thinnest member of titanium carbide MXenes. Nanoscale **12**, 16987–16994 (2020). https://doi.org/10.1039/c9nr08350b
152. X. Guo, Y. Ding, D. Kuang, Z. Wu, X. Sun et al., Enhanced ammonia sensing performance based on MXene-$Ti_3C_2T_x$ multilayer nanoflakes functionalized by tungsten trioxide nanoparticles. J. Colloid Interface Sci. **595**, 6–14 (2021). https://doi.org/10.1016/j.jcis.2021.03.115
153. T. He, W. Liu, T. Lv, M. Ma, Z. Liu et al., MXene/SnO_2 heterojunction based chemical gas sensors. Sens. Actuat. B Chem. **329**, 129275 (2021). https://doi.org/10.1016/j.snb.2020.129275
154. Z. Wang, F. Wang, A. Hermawan, Y. Asakura, T. Hasegawa et al., SnO-SnO_2 modified two-dimensional MXene $Ti_3C_2T_x$ for acetone gas sensor working at room temperature. J. Mater. Sci. Technol. **73**, 128–138 (2021). https://doi.org/10.1016/j.jmst.2020.07.040
155. D. Kuang, L. Wang, X. Guo, Y. She, B. Du et al., Facile hydrothermal synthesis of $Ti_3C_2T_x$-TiO_2 nanocomposites for gaseous volatile organic compounds detection at room temperature. J. Hazard. Mater. **416**, 126171 (2021). https://doi.org/10.1016/j.jhazmat.2021.126171
156. M. Liu, J. Ji, P. Song, M. Liu, Q. Wang, α-Fe_2O_3 nanocubes/$Ti_3C_2T_x$ MXene composites for improvement of acetone sensing performance at room temperature. Sens. Actuat. B Chem. **349**, 130782 (2021). https://doi.org/10.1016/j.snb.2021.130782
157. M. Liu, Z. Wang, P. Song, Z. Yang, Q. Wang, In_2O_3 nanocubes/$Ti_3C_2T_x$ MXene composites for enhanced methanol gas sensing properties at room temperature. Ceram. Int. **47**, 23028–23037 (2021). https://doi.org/10.1016/j.ceramint.2021.05.016
158. Q.T.H. Ta, D. Thakur, J.S. Noh, Enhanced gas sensing performance of ZnO/$Ti_3C_2T_x$ MXene nanocomposite. Micromachines **13**, 1710 (2022). https://doi.org/10.3390/mi13101710
159. Z. Sima, P. Song, Y. Ding, Z. Lu, Q. Wang, $ZnSnO_3$ nanocubes/$Ti_3C_2T_x$ MXene composites for enhanced formaldehyde gas sensing properties at room temperature. Appl. Surf. Sci. **598**, 153861 (2022). https://doi.org/10.1016/j.apsusc.2022.153861
160. N. Li, Y. Jiang, C. Zhou, Y. Xiao, B. Meng et al., High-performance humidity sensor based on urchin-like composite of Ti_3C_2 MXene-derived TiO_2 nanowires. ACS Appl. Mater. Interfaces **11**, 38116–38125 (2019). https://doi.org/10.1021/acsami.9b12168
161. J. Wu, P. Lu, J. Dai, C. Zheng, T. Zhang et al., High performance humidity sensing property of $Ti_3C_2T_x$ MXene-derived $Ti_3C_2T_x$/$K_2Ti_4O_9$ composites. Sens. Actuat. B Chem. **326**, 128969 (2021). https://doi.org/10.1016/j.snb.2020.128969
162. Q. Thanh Hoai Ta, N. NgocTri, J.-S. Noh, Improved NO_2 gas sensing performance of 2D MoS_2/$Ti_3C_2T_x$ MXene nanocomposite. Appl. Surf. Sci. **604**, 154624 (2022). https://doi.org/10.1016/j.apsusc.2022.154624
163. W.Y. Chen, X. Jiang, S.N. Lai, D. Peroulis, L. Stanciu, Nanohybrids of a MXene and transition metal dichalcogenide for selective detection of volatile organic compounds. Nat. Commun. **11**, 1302 (2020). https://doi.org/10.1038/s41467-020-15092-4
164. D. Wang, D. Zhang, Y. Yang, Q. Mi, J. Zhang et al., Multifunctional latex/polytetrafluoroethylene-based triboelectric nanogenerator for self-powered organ-like MXene/metal-organic framework-derived CuO nanohybrid ammonia sensor. ACS Nano **15**, 2911–2919 (2021). https://doi.org/10.1021/acsnano.0c09015
165. Y. Chang, M. Chen, Z. Fu, R. Lu, Y. Gao et al., Building porphyrin-based MOFs on MXenes for ppb-level NO sensing. J. Mater. Chem. A **11**, 6966–6977 (2023). https://doi.org/10.1039/d3ta00072a
166. X. Li, J. Xu, Y. Jiang, Z. He, B. Liu et al., Toward agricultural ammonia volatilization monitoring: a flexible polyaniline/$Ti_3C_2T_x$ hybrid sensitive films based gas sensor. Sens. Actuat. B Chem. **316**, 128144 (2020). https://doi.org/10.1016/j.snb.2020.128144
167. L. Zhao, Y. Zheng, K. Wang, C. Lv, W. Wei et al., Highly stable cross-linked cationic polyacrylamide/$Ti_3C_2T_x$ MXene nanocomposites for flexible ammonia-recognition devices. Adv. Mater. Technol. **5**, 2000248 (2020). https://doi.org/10.1002/admt.202000248
168. O. Mashtalir, M.R. Lukatskaya, A.I. Kolesnikov, E. Raymundo-Piñero, M. Naguib et al., The effect of hydrazine intercalation on the structure and capacitance of 2D titanium carbide (MXene). Nanoscale **8**, 9128–9133 (2016). https://doi.org/10.1039/C6NR01462C
169. Z. Ling, C.E. Ren, M.-Q. Zhao, J. Yang, J.M. Giammarco et al., Flexible and conductive MXene films and nanocomposites with high capacitance. Proc. Natl. Acad. Sci. U.S.A. **111**, 16676–16681 (2014). https://doi.org/10.1073/pnas.1414215111
170. C. Hu, F. Shen, D. Zhu, H. Zhang, J. Xue et al., Characteristics of Ti_3C_2X–chitosan films with enhanced mechanical properties. Front. Energy Res. **4**, 41 (2017). https://doi.org/10.3389/fenrg.2016.00041
171. K. Wang, Y. Zhou, W. Xu, D. Huang, Z. Wang et al., Fabrication and thermal stability of two-dimensional carbide Ti_3C_2 nanosheets. Ceram. Int. **42**, 8419–8424 (2016). https://doi.org/10.1016/j.ceramint.2016.02.059
172. J.-H. Chen, C. Jang, S.M. Xiao, M.S. Ishigami, Fuhrer, Intrinsic and extrinsic performance limits of graphene devices on SiO_2. Nat. Nanotechnol. **3**, 206–209 (2008). https://doi.org/10.1038/nnano.2008.58
173. J. Wang, Z. Wu, K. Hu, X. Chen, H. Yin, High conductivity graphene-like MoS_2/polyaniline nanocomposites and its application in supercapacitor. J. Alloys Compd. **619**, 38–43 (2015). https://doi.org/10.1016/j.jallcom.2014.09.008
174. M. Mariano, O. Mashtalir, F.Q. Antonio, W.-H. Ryu, B. Deng et al., Solution-processed titanium carbide MXene films examined as highly transparent conductors. Nanoscale **8**, 16371–16378 (2016). https://doi.org/10.1039/C6NR03682A

© The authors https://doi.org/10.1007/s40820-024-01430-4

175. Y. Wang, Y. Li, Z. Qiu, X. Wu, P. Zhou et al., Fe_3O_4@Ti_3C_2 MXene hybrids with ultrahigh volumetric capacity as an anode material for lithium-ion batteries. J. Mater. Chem. A **6**, 11189–11197 (2018). https://doi.org/10.1039/C8TA00122G
176. K. Hantanasirisakul, M.Q. Zhao, P. Urbankowski, J. Halim, B. Anasori et al., Fabrication of $Ti_3C_2T_x$ MXene transparent thin films with tunable optoelectronic properties. Adv. Electron. Mater. **2**, 1600050 (2016). https://doi.org/10.1002/aelm.201600050
177. A.D. Dillon, M.J. Ghidiu, A.L. Krick, J. Griggs, S.J. May et al., Highly conductive optical quality solution-processed films of 2D titanium carbide. Adv. Funct. Mater. **26**, 4162–4168 (2016). https://doi.org/10.1002/adfm.201600357
178. V.N. Borysiuk, V.N. Mochalin, Y. Gogotsi, Molecular dynamic study of the mechanical properties of two-dimensional titanium carbides Ti(n+1)C(n) (MXenes). Nanotechnology **26**, 265705 (2015). https://doi.org/10.1088/0957-4484/26/26/265705
179. M. Alhabeb, K. Maleski, T.S. Mathis, A. Sarycheva, C.B. Hatter et al., Selective etching of silicon from Ti_3SiC_2 (MAX) to obtain 2D titanium carbide (MXene). Angew. Chem. Int. Ed. **57**, 5444–5448 (2018). https://doi.org/10.1002/anie.201802232
180. X.-H. Zha, Q. Huang, J. He, H. He, J. Zhai et al., The thermal and electrical properties of the promising semiconductor MXene Hf_2CO_2. Sci. Rep. **6**, 27971 (2016). https://doi.org/10.1038/srep27971
181. S. Uzun, M. Han, C.J. Strobel, K. Hantanasirisakul, A. Goad et al., Highly conductive and scalable $Ti_3C_2T_x$-coated fabrics for efficient electromagnetic interference shielding. Carbon **174**, 382–389 (2021). https://doi.org/10.1016/j.carbon.2020.12.021
182. J. Pang, R.G. Mendes, A. Bachmatiuk, L. Zhao, H.Q. Ta et al., Applications of 2D MXenes in energy conversion and storage systems. Chem. Soc. Rev. **48**, 72–133 (2019). https://doi.org/10.1039/C8CS00324F
183. K. Huang, Z. Li, J. Lin, G. Han, P. Huang, Correction: Two-dimensional transition metal carbides and nitrides (MXenes) for biomedical applications. Chem. Soc. Rev. **47**, 6889 (2018). https://doi.org/10.1039/C8CS90090F
184. D. Xiong, X. Li, Z. Bai, S. Lu, Recent advances in layered $Ti_3C_2T_x$ MXene for electrochemical energy storage. Small **14**, e1703419 (2018). https://doi.org/10.1002/smll.201703419
185. A. Lipatov, M.J. Loes, H. Lu, J. Dai, P. Patoka et al., Quasi-1D TiS_3 nanoribbons: mechanical exfoliation and thickness-dependent Raman spectroscopy. ACS Nano **12**, 12713–12720 (2018). https://doi.org/10.1021/acsnano.8b07703
186. S.A.M. Chachuli, M.N. Hamidon, M. Ertugrul, M.S. Mamat, O. Coban et al., Effects of MWCNTs/graphene nanoflakes/MXene addition to TiO_2 thick film on hydrogen gas sensing. J. Alloys Compd. **882**, 160671 (2021). https://doi.org/10.1016/j.jallcom.2021.160671
187. P.-G. Su, S.-L. Peng, Fabrication and NO_2 gas-sensing properties of reduced graphene oxide/WO_3 nanocomposite films. Talanta **132**, 398–405 (2015). https://doi.org/10.1016/j.talanta.2014.09.034
188. H. Naderi, S. Hajati, M. Ghaedi, K. Dashtian, M.M. Sabzehmeidani, Sensitive, selective and rapid ammonia-sensing by gold nanoparticle-sensitized V_2O_5/$CuWO_4$ heterojunctions for exhaled breath analysis. Appl. Surf. Sci. **501**, 144270 (2020). https://doi.org/10.1016/j.apsusc.2019.144270
189. T. Xu, J. Wei, P. He, J. Wu, N. Chen et al., CuS-doped Ti_3C_2 MXene nanosheets for highly efficient adsorption of elemental mercury in flue gas. Energy Fuels **36**, 2503–2514 (2022). https://doi.org/10.1021/acs.energyfuels.1c03705
190. J. Kim, J. You, E. Kim, Flexible conductive polymer patterns from vapor polymerizable and photo-cross-linkable EDOT. Macromolecules **43**, 2322–2327 (2010). https://doi.org/10.1021/ma9025306
191. L. Qin, Z. Ding, M. Hanif, J. Jiang, L. Liu et al., Poly(3,4-dioxythiophene) soft nano-network with a compatible ion transporting channel for improved electrochromic performance. Polym. Chem. **7**, 6954–6963 (2016). https://doi.org/10.1039/C6PY01642A
192. S.R. Forrest, The path to ubiquitous and low-cost organic electronic appliances on plastic. Nature **428**, 911–918 (2004). https://doi.org/10.1038/nature02498
193. L. Qin, J. Xu, B. Lu, Y. Lu, X. Duan et al., Synthesis and electrochromic properties of polyacrylate functionalized poly(3,4-ethylenedioxythiophene) network films. J. Mater. Chem. **22**, 18345–18353 (2012). https://doi.org/10.1039/C2JM32457A
194. Y. Shi, L. Peng, Y. Ding, Y. Zhao, G. Yu, Nanostructured conductive polymers for advanced energy storage. Chem. Soc. Rev. **44**, 6684–6696 (2015). https://doi.org/10.1039/C5CS00362H
195. C. Reese, M. Roberts, M.-M. Ling, Z. Bao, Organic thin film transistors. Mater. Today **7**, 20–27 (2004). https://doi.org/10.1016/S1369-7021(04)00398-0
196. A. Ali, P.K. Shen, Nonprecious metal's graphene-supported electrocatalysts for hydrogen evolution reaction: Fundamentals to applications. Carbon Energy **2**, 99–121 (2020). https://doi.org/10.1002/cey2.26
197. H.F. Zhang, J.Y. Xuan, Q. Zhang, M.L. Sun, F.C. Jia, AStrategies and challenges for enhancing performance of MXene-based gas sensors: a review. Rare Met. **41**, 3976–3999 (2022). https://doi.org/10.1007/s12598-022-02087-x
198. M.S. Bhargava Reddy, S. Kailasa, B.C.G. Marupalli, K.K. Sadasivuni, S. Aich, A family of 2D-MXenes: synthesis, properties, and gas sensing applications. ACS Sens. **7**, 2132–2163 (2022). https://doi.org/10.1021/acssensors.2c01046
199. J. Li, X. Chen, X. Zhu, Y. Jiang, X. Chang et al., Two-dimensional transition metal MXene-based gas sensors: a review. Chin. Chem. Lett. **35**, 108286 (2024). https://doi.org/10.1016/j.cclet.2023.108286
200. E. Mostafavi, S. Iravani, MXene-graphene composites: a perspective on biomedical potentials. Nano-Micro Lett. **14**, 130 (2022). https://doi.org/10.1007/s40820-022-00880-y
201. S. He, Y. Gui, Y. Wang, J. Yang, A self-powered β-$Ni(OH)_2$/MXene based ethanol sensor driven by an enhanced triboelectric nanogenerator based on β-$Ni(OH)_2$@PVDF at room

temperature. Nano Energy **107**, 108132 (2023). https://doi.org/10.1016/j.nanoen.2022.108132

202. X. Wang, L. Gong, Z. Li, Y. Yin, D. Zhang, A room temperature ammonia gas sensor based on cerium oxide/MXene and self-powered by a freestanding-mode triboelectric nanogenerator and its multifunctional monitoring application. J. Mater. Chem. A **11**, 7690–7701 (2023). https://doi.org/10.1039/d2ta07917h
203. S. Sardana, H. Kaur, B. Arora, D.K. Aswal, A. Mahajan, Self-powered monitoring of ammonia using an MXene/TiO_2/cellulose nanofiber heterojunction-based sensor driven by an electrospun triboelectric nanogenerator. ACS Sens. **7**, 312–321 (2022). https://doi.org/10.1021/acssensors.1c02388
204. S. Sardana, A. Mahajan, Edge-site-enriched $Ti_3C_2T_x$ MXene/MoS_2 nanosheet heterostructures for self-powered breath and environmental monitoring. ACS Appl. Nano Mater. **6**, 469–481 (2023). https://doi.org/10.1021/acsanm.2c04581
205. R. Saini, A. Mahajan, R.K. Bedi, D.K. Aswal, Room temperature detection of amine vapours using copper phthalocyanine based thin films. Phys. Status Solidi A **209**, 1245–1250 (2012). https://doi.org/10.1002/pssa.201127569
206. R. Saini, A. Mahajan, R.K. Bedi, D.K. Aswal, A.K. Debnath, Phthalocyanine based nanowires and nanoflowers as highly sensitive room temperature Cl_2 sensors. RSC Adv. **4**, 15945–15951 (2014). https://doi.org/10.1039/C3RA47002D
207. K.K. Khun, A. Mahajan, R.K. Bedi, Surfactant assisted growth of nanostructured tin oxide films for gas sensing applications. Electron. Mater. Lett. **7**, 303–308 (2011). https://doi.org/10.1007/s13391-011-0140-9
208. D. Wang, D. Zhang, M. Tang, H. Zhang, T. Sun et al., Ethylene chlorotrifluoroethylene/hydrogel-based liquid-solid triboelectric nanogenerator driven self-powered MXene-based sensor system for marine environmental monitoring. Nano Energy **100**, 107509 (2022). https://doi.org/10.1016/j.nanoen.2022.107509
209. J. Yu, Q. He, G. Yang, W. Zhou, Z. Shao et al., Recent advances and prospective in ruthenium-based materials for electrochemical water splitting. ACS Catal. **9**, 9973–10011 (2019). https://doi.org/10.1021/acscatal.9b02457
210. C. Yang, D. Zhang, D. Wang, H. Luan, X. Chen et al., *In situ* polymerized MXene/polypyrrole/hydroxyethyl cellulose-based flexible strain sensor enabled by machine learning for handwriting recognition. ACS Appl. Mater. Interfaces **15**, 5811–5821 (2023). https://doi.org/10.1021/acsami.2c18989
211. D. Wang, D. Zhang, M. Tang, H. Zhang, F. Chen et al., Rotating triboelectric-electromagnetic nanogenerator driven by tires for self-powered MXene-based flexible wearable electronics. Chem. Eng. J. **446**, 136914 (2022). https://doi.org/10.1016/j.cej.2022.136914
212. W. Lin, Z. Hui, A.O. Govorov, M. Ouyang, Hierarchical synthesis of non-centrosymmetric hybrid nanostructures and enabled plasmon-driven photocatalysis. Nat. Commun. **5**, 4792 (2014). https://doi.org/10.1038/ncomms5792
213. D. Zhang, S. Yu, X. Wang, J. Huang, W. Pan et al., UV illumination-enhanced ultrasensitive ammonia gas sensor based on (001)TiO_2/MXene heterostructure for food spoilage detection. J. Hazard. Mater. **423**, 127160 (2022). https://doi.org/10.1016/j.jhazmat.2021.127160
214. M.C. Tang, Z.J. Wang, D.Y. Wang, R.Y. Mao, H. Zhang et al., Construction of LaF_3 QD-modified SnS_2 nanorod composites for ultrasensitive detection of H_2S. ChemElectroChem **11**(18), 9942–9954 (2023). https://doi.org/10.1039/d2ta08496a
215. M. Tang, D. Zhang, Q. Chen, Z. Wang, D. Wang et al., Heterostructure construction of SnS_2 Debye nanowires modified with ZnO nanorods for chemiresistive H_2S detection in sulfur hexafluoride decomposition products. Sens. Actuat. B Chem. **390**, 133952 (2023). https://doi.org/10.1016/j.snb.2023.133952
216. Y. Wang, Y. Wang, Y. Kuai, M. Jian, "Visualization" gas—gas sensors based on high performance novel MXenes materials. Small **20**, 2305250 (2024). https://doi.org/10.1002/smll.202305250
217. M. Wu, M. He, Q. Hu, Q. Wu, G. Sun et al., Ti_3C_2 MXene-based sensors with high selectivity for NH_3 detection at room temperature. ACS Sens. **4**, 2763–2770 (2019). https://doi.org/10.1021/acssensors.9b01308
218. B. Xiao, Y.-C. Li, X.-F. Yu, J.-B. Cheng, MXenes: Reusable materials for NH_3 sensor or capturer by controlling the charge injection. Sens. Actuat. B Chem. **235**, 103–109 (2016). https://doi.org/10.1016/j.snb.2016.05.062
219. S. Ma, D. Yuan, Z. Jiao, T. Wang, X. Dai, Monolayer Sc_2CO_2: a promising candidate as a SO_2 gas sensor or capturer. J. Phys. Chem. C **121**, 24077–24084 (2017). https://doi.org/10.1021/acs.jpcc.7b07921
220. A. Junkaew, R. Arróyave, Enhancement of the selectivity of MXenes (M_2C, M = Ti, V, Nb, Mo) *via* oxygen-functionalization: promising materials for gas-sensing and-separation. Phys. Chem. Chem. Phys. **20**, 6073–6082 (2018). https://doi.org/10.1039/C7CP08622A
221. P. Khakbaz, M. Moshayedi, S. Hajian, M. Soleimani, B.B. Narakathu et al., Titanium carbide MXene as NH_3 sensor: realistic first-principles study. J. Phys. Chem. C **123**, 29794–29803 (2019). https://doi.org/10.1021/acs.jpcc.9b09823
222. S.R. Naqvi, V. Shukla, N.K. Jena, W. Luo, R. Ahuja, Exploring two-dimensional M_2NS_2 (M = Ti, V) MXenes based gas sensors for air pollutants. Appl. Mater. Today **19**, 100574 (2020). https://doi.org/10.1016/j.apmt.2020.100574
223. H.J. Koh, S.J. Kim, K. Maleski, S.Y. Cho, Y.J. Kim et al., Enhanced selectivity of MXene gas sensors through metal ion intercalation: *in situ* X-ray diffraction study. ACS Sens. **4**, 1365–1372 (2019). https://doi.org/10.1021/acssensors.9b00310

© The authors https://doi.org/10.1007/s40820-024-01430-4